

Alma Mater Studiorum – Università di Bologna

DOTTORATO DI RICERCA IN

CHIMICA

Ciclo XXX

Settore Concorsuale di afferenza: 03/C2

Settore Scientifico disciplinare: CHIM/04

**CARBON FIBER REINFORCED POLYMERS: MATRIX
MODIFICATIONS AND REUSE OF CARBON FIBERS
RECOVERED BY PYROLYSIS**

Presentata da: Emanuele D'Angelo

Coordinatore Dottorato

Prof. Aldo Roda

Supervisore

Dr. Tiziana Benelli

Co-supervisori

Prof. Loris Giorgini

Dr. Laura Mazzocchetti

Esame finale anno 2018

ABSTRACT

Due to their extraordinary properties, Carbon Fiber Reinforced Polymers (CFRPs) are used in a growing number of fields (automotive, military, aircraft, aerospace, wind turbines, sport, civil infrastructure and leisure). Since the matrix in CFRPs is polymer-based, these composites have poor resistance to fire; additionally, when exposed to high temperatures, they can burn or lose their thermo-mechanical stability. Moreover, the recent huge and continuous development of CFRPs opened the question related to their disposal and total dependence on fossil resources. This thesis focussed on epoxy-based CFRPs. In more detail, commercial epoxy resins have been modified and replaced with bio-based alternatives, and short recycled carbon fibers composites have been produced.

Two new bentonite-based organoclays were prepared with low cost reactants and mild reactions conditions and used to modify the flame behaviour of a commercial epoxy resin. The epoxy-modified resin flame behaviour was evaluated by cone-calorimeter and some significant improvements with just a 3 %wt loading level of organoclay were obtained. Furthermore, the possibility to recover and reuse carbon fibers by pyrolysis of CFRPs waste was studied: a validation of the recycling conditions and the treatments required to reuse recycled carbon fibers were assessed in order to obtain clean fibers and promote fiber/matrix adhesion in epoxy composites. Recycled carbon fiber were then used in a lab-scale composite manufacturing process and comparable mechanical properties for virgin and recycled short carbon fiber composites were achieved when an optimized coupled pyrolysis/oxidative process to CFRPs waste is applied. Finally, more sustainable CFRPs have been produced and characterized coupling highly bio-based epoxy systems, appropriately modified and optimized, and recycled carbon fibers. This latter work represents the first attempt aimed at replacing petroleum- BPA-based epoxy resins and high cost short virgin carbon fibers in the future CFRPs manufacturing processes.

INDEX

Overview	1
Chapter 1	3
<i>Polymeric composite and nanocomposite materials.....</i>	3
1.1. Composite materials	3
1.2. Carbon fiber reinforced polymers (CFRPs).....	7
1.2.1. Polymer matrixes	8
<i>Epoxy resins.....</i>	<i>10</i>
1.2.2. Carbon fiber	12
<i>Carbon fibers manufacturing</i>	<i>14</i>
1.2.3. CFRP manufacturing processes	17
1.3. Polymer nanocomposite materials.....	22
1.3.1. Nanoclay	24
1.3.2. Nano-oxides	26
1.3.3. Carbon-nanomaterials: graphene and nanotubes	27
1.3.4. Other nanoparticles	28
1.3.5. Common flame retardant epoxy resin nanocomposites	29
1.4. Recycling of CFRPs	31
1.4.1. Mechanical recycling	33
1.4.2. Pyrolysis.....	33
1.4.3. Fluidised bed	34
1.4.4. Solvolysis.....	34
Chapter 2	36
<i>New nitrogen-rich heterocycles for organo-modified bentonites as flame retardant fillers in epoxy resin nanocomposites*</i>	36

2.1. Introduction	36
2.1.1. Polymer combustion and flame retardancy	40
2.1.2. Cone-calorimeter	42
2.2. Experimental	44
<i>Materials</i>	44
<i>Synthesis of 6-(4-butylphenyl)-1,3,5-triazine-2,4-diamine 3 (BFTDA)</i>	44
<i>Synthesis of 11-amino-N-(pyridine-2yl)undecanamide 8 (APUA)</i>	45
<i>Synthesis of 11-[(tert-butoxycarbonyl)amino]undecanoic acid 5</i>	45
<i>Synthesis of tert-butyl (11-oxo-11-(pyridin-2-ylamino)undecyl)carbamate 7</i>	46
<i>Synthesis of 11-amino-N-(pyridin-2-yl)undecanamide 8</i>	46
<i>Preparation of BENTO-APUA and BENTO-BFTDA organoclays</i>	47
<i>Preparation of BENTO-APUA and BENTO-BFTDA epoxy nanocomposites</i>	47
<i>Characterization</i>	48
2.3. Results and Discussion	49
<i>Synthesis and characterization of Pristine Bentonite and Organoclays</i>	49
2.4. Conclusions	61
Chapter 3	63
<i>Synthesis and characterization of highly bio-based epoxy resins derived from aromatic lignin derived diols for polymer composites</i>	63
3.1. Introduction	63
3.2. Experimental	67
<i>Materials</i>	67
<i>Synthesis of Diglycidyl Ether of Vanillyl alcohol (DGEVA) and Gastrodigenin (DGEVD)</i>	67
<i>Preparation of cured-epoxy resins samples</i>	69
<i>Characterization</i>	70
3.3. Results and Discussion	71

<i>Synthesis and characterization of epoxy resins</i>	71
<i>Preparation and characterization of cured-epoxy resins</i>	72
3.4. Conclusions	80
Chapter 4	82
<i>Validation of carbon fibers recycling by pyro-gasification: the influence of gasification conditions to obtain clean fibers and promote fiber/matrix adhesion in epoxy composites*</i>	82
4.1. Introduction	82
4.2. Experimental	85
<i>Pyrolysis of CFRPs: the case of a pilot bench-scale plan</i> ⁶³	85
<i>Materials</i>	87
<i>Post-Pyrolysis gasification treatments</i>	87
<i>Chopped Carbon Fiber Reinforced Polymers (Re-CCFRPs) Production</i>	88
<i>Methods</i>	88
4.3. Results and discussion	89
<i>Gasification treatments and characterization of carbon fibers</i>	89
<i>Composites production and characterization</i>	98
4.4. Conclusions	104
Chapter 5	106
Toward more sustainable high-performance CFRPs by coupling bio-based epoxy resins and recycled carbon fibers.	106
5.1. Introduction	106
5.2. Experimental	109
<i>Materials</i>	109
<i>Preparation of Vi-SCFRPs and Re-SCFRPs</i>	109
<i>Characterization</i>	112
5.3. Results and discussion	113

<i>Bio-based composites production and characterization</i>	113
5.4. Conclusions	121
Chapter 6	123
Conclusions and future works	123
<i>On epoxy resin modification with improved flame behaviour (Chapter 2)</i>	123
<i>On bio-based epoxy curing agent modification (Chapter 3)</i>	124
<i>On reuse of carbon fibers recovered by pyrolysis and their reuse (Chapter 4)</i> ..	125
<i>On reusing recycled carbon fibers with highly bio-based epoxy resins (Chapter 5)</i>	126
Bibliography	128

Overview

The subject of carbon fiber reinforced polymers (CFRPs) is truly inter- and multidisciplinary matter: it would be an impossible task to cover it from all the viewpoints. In this thesis will be presented some different works on CFRPs and their components. Due to their extraordinary mechanical properties, high specific strength and specific stiffness, associated with lightweight, the CFRPs are used in a growing number of fields (automotive, military, aircraft, aerospace, wind turbines, sport, civil infrastructure and leisure). Since the matrix in CFRPs is polymer-based, these composites have poor resistance to fire and, when exposed to high temperatures, can burn or lose their thermo-mechanical stability. The recent huge and continuous development of CFRPs opened the question related to their disposal and total dependence on fossil resources. Because of their heterogeneous compositions, it is very difficult to separate carbon fibers from composites' polymer matrix, in particular, in thermoset CFRPs where the matrix cannot easily be separated, recovered and recycled by remelting and remoulding. Furthermore, due to the high performance required for a CFRPs matrix, bio-based resins cannot easily satisfy these requirements.

Most of the data presented in this PhD thesis are related to epoxy-based CFRPs and their main issues. In particular, with the aim of studying and/or improving some CFRPs properties, this thesis is focused on the following topics:

- the modification of a commercial epoxy resin in order to improve the flame behaviour of the final material;
- the reuse of carbon fibers recovered by pyrolysis:
- the production of bio-based epoxy resins and their use as matrix in CFRPs

Within this framework, *Chapter 1* gives a comprehensive background about composite and nanocomposite polymer materials, with particular attention to the CFRPs and their components and recycling processes.

Chapter 2 reports the experimental data of a commercial epoxy resin modified with two new bentonite-based organoclay, highlighting the flame behaviour improvements obtained by cone calorimeter analysis. This chapter is adapted from two published works^{1,2}.

The important issue related to CFRPs disposal and their recycle is discussed in *Chapters 4*: the scientific data of a reliable way to recover and reuse carbon fibers by pyrolysis are presented. This work was submitted to a peer-reviewed journal, *Composites Part A*.

Chapters 3 and *Chapter 5* show the project carried out in collaboration with Professor Stanzione during a period of research spent at Rowan University (Glassboro-NJ USA) as visiting PhD student. This work was spilt in two not consecutive chapters to provide a certain continuity in the discussed topics.

Chapter 3 deals with the thermo-mechanical properties of two bio-based epoxy prepolymers, crosslinked with an aromatic curing agent in order to obtain suitable epoxy resins for the CFRPs manufacturing. In *Chapter 5*, these modified epoxy resin were used as polymer matrix for the production of more sustainable CFRPs with recycled carbon fibers.

Finally, *Chapter 6* summarizes the single conclusions and future works of each chapter.

Chapter 1

Polymeric composite and nanocomposite materials

1.1. Composite materials

A composite material is made by combining two or more materials to give better properties than those of the individual components used alone. These new multifunctional materials have unprecedented mechanical and physical properties, which can be tailored to meet the requirements of a particular application. They offer several advantages over traditional engineering materials such as low density, high specific stiffness and strength, high corrosion and fatigue resistance, good dimensional stability³. These unique characteristics and the design flexibility provide new class of materials with design opportunities not possible with conventional monolithic (unreinforced) materials. An illustrative comparison between some aluminium and steel properties and the composite materials ones is shown in Figure 1.

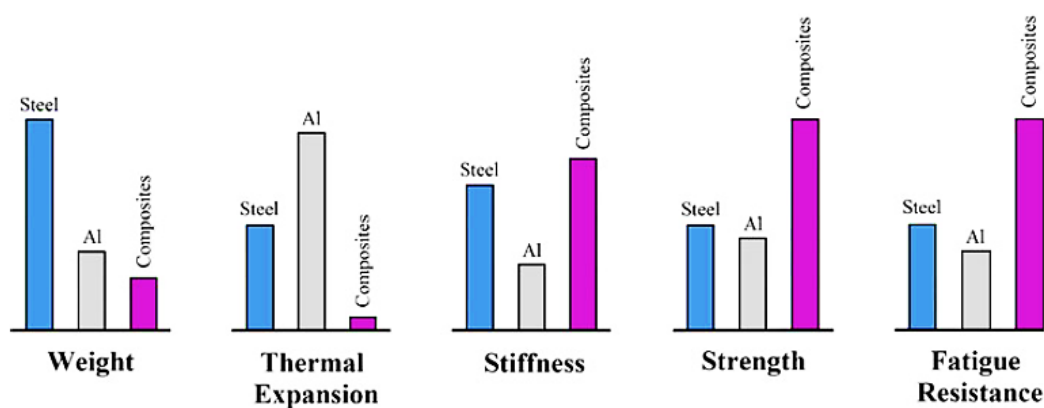


Figure 1. Comparison between conventional monolithic materials and composite materials⁴.

The concept of composites was not invented by human beings: nature is full of examples wherein the idea of composite materials is used. Wood is a fibrous composite: cellulose fibers in a lignin matrix. The cellulose fibers have high tensile strength but are very flexible

(i.e., low stiffness), while the lignin matrix joins the fibers and furnishes the stiffness. Bone is yet another example of a natural composite that supports the weight of various members of the body: it is made from a hard but brittle material, the hydroxyapatite, and a soft and flexible material, the collagen⁴.

People have been making composites for many thousands of years. One early example is mud bricks. Mud can be dried out into a brick shape to give a building material. It is strong if you try to squash it (it has good compressive strength) but it breaks quite easily if you try to bend it (it has poor tensile strength). Straw seems very strong if you try to stretch it, but you can crumple it up easily. By mixing mud and straw together, it is possible to make bricks that are resistant to both squeezing and tearing and make excellent building blocks. Although the ancient peoples were used to mix the straw with the mud to get a more resistant and less fragile bricks, the large-scale use of composite materials started during World War II (late 1940s and early 1950s) with marine and aerospace military applications. Then, the increasing demand for materials that are stiffer and stronger yet lighter in fields as diverse as aerospace, automotive, boating, sporting goods, energy, infrastructure, consumer and more, naturally led to a resurgence of the ancient concept of combining different materials in an integral-composite material to satisfy the user requirements.

Returning on the composite's definition, combining two or more materials does not always allow for getting a composite material: examples are metallic alloys, copolymers, additives, minerals and all the substances that are not pure; in this way, the most of the materials available on the market would be considered a composite. Technically, in a composite material, each material retains its separate chemical, physical, and mechanical properties: the two distinct materials, usually belonging to different materials' categories (metals, polymers or ceramics), can always be identified and separated from one another; the result is a heterogeneous material consisting of distinct and combined phases in various proportions and shapes. For these reasons, in a composite it is possible to distinguish a **matrix**, a **reinforcement** and a matrix-reinforcing **interface**.

The **matrix** is the continuous phase that provides rigidity and shape to the artefact and influences several functions in a composite structure, most of which are vital to the satisfactory performance of the structure. A matrix material keeps the reinforcement phase together and transfers the external load to it, providing at the same time, protection against chemical attacks, mechanical damage (wear) and environmental factors. The

reinforcement is instead the internal and discontinuous fraction of the object; it is typically in the form of long fibers, short fibers, particles or nanomaterials such as nanofibers, or nanoparticles, and exhibits some properties far superior to those of the matrix. The reinforcement carries the load (in a structural composite, 70 to 90% of the load is carried by the reinforcement), provides stiffness, strength, thermal stability, and other structural properties in the composites. Finally, the **interface** consists of the bond between the reinforcement and matrix and the immediate region adjacent to this bond. The interface, usually considered to be of zero thickness for analysis purposes, contributes to determining the overall physical and mechanical properties of the composite, and plays a key role in explaining and maintaining them. In fact, a good adhesion or wetting of the matrix to the reinforcement is always required for that synergic effect between matrix and reinforcement. The matrix-reinforcement adhesion, when not sufficient, can be promoted by the use of a third component applied in a very thin layer, often of atomic thickness, or by physical or chemical treatments that make the surface of the reinforcement more compatible with the matrix. Other substances are sometimes used to improve specific properties. For example, composites may also contain fillers, additives, core materials or surface finishes designed to improve the manufacturing process, appearance and performance of the final product.

There are many different types of composite materials in use today. The most common composites are made with strong fibers held together in a matrix. Particles or flakes are also used as reinforcements but they are not as effective as fibers. Composites are usually classified by the type of material used for the matrix. The three primary categories of composites are Metal Matrix Composites (MMCs), Ceramic Matrix Composites (CMCs) and Polymer matrix composites (PMCs).

At this time, PMCs are by far the most widely used type of composites. Non-polymer matrix materials occupy only around 20% of the whole global composite market⁵. This is mainly because these material combinations are frequently applied to individual niche applications (e.g. aerospace) and a particularly high price is paid for such special solutions. The use of PMCs instead is no longer limited to niche applications: due to their flexible design, the presence of PMCs is in almost every industrial sector such as aerospace, architecture, automotive, transportation, energy, infrastructure, marine, military, sports and recreation. In addition, the development of new high-volume and improved composites manufacturing processes, such as compression molding (SMC) or resin transfer molding

(RTM), have caused unlimited product development opportunities and a drop in their final price.

Polymer matrices generally are relatively weak, low-stiffness, viscoelastic materials, mainly if compared to metals and ceramics. The strength and stiffness of PMCs come primarily from the reinforcement: in fact, PMCs are almost exclusively manufactured using fibrous reinforcing materials, principally glass, carbon and aramid (Kevlar) fibers. Other high-performance fibers such as boron, silicon carbide, basalt and alumina fibers are relatively new and they only have become commercial in recent years.

Table 1. Typical properties of some conventional and polymer composites materials³.

Material	Density (ρ) (g/cc)	Tensile Modulus (E) (GPa)	Tensile Strength (σ) (GPa)	Specific Modulus (E/ ρ)	Specific Strength (σ/ρ)	Max. Service Temp. (°C)
Metals						
Cast iron, grade 20	7.0	100	0.14	14.3	0.02	230–300
Steel, AISI 1045 hot rolled	7.8	205	0.57	26.3	0.073	500–650
Aluminum 2024-T4	2.7	73	0.45	27.0	0.17	150–250
Aluminum 6061-T6	2.7	69	0.27	25.5	0.10	150–250
Plastics						
Nylon 6/6	1.15	2.9	0.082	2.52	0.071	75–100
Polypropylene	0.9	1.4	0.033	1.55	0.037	50–80
Epoxy	1.25	3.5	0.069	2.8	0.055	80–215
Phenolic	1.35	3.0	0.006	2.22	0.004	70–120
Ceramics						
Alumina	3.8	350	0.17	92.1	0.045	1425–1540
MgO	3.6	205	0.06	56.9	0.017	900–1000
Short fiber composites						
Glass-filled epoxy (35%)	1.90	25	0.30	8.26	0.16	80–200
Glass-filled polyester (35%)	2.00	15.7	0.13	7.25	0.065	80–125
Glass-filled nylon (35%)	1.62	14.5	0.20	8.95	0.12	75–110
Glass-filled nylon (60%)	1.95	21.8	0.29	11.18	0.149	75–110
Unidirectional composites						
S-glass/epoxy (45%)	1.81	39.5	0.87	21.8	0.48	80–215
Carbon/epoxy (61%)	1.59	142	1.73	89.3	1.08	80–215
Kevlar/epoxy (53%)	1.35	63.6	1.1	47.1	0.81	80–215

Many fiber-reinforced polymers offer a combination of strength and modulus that are either comparable to or better than many traditional metallic materials. Because of their low density, the strength–weight ratios and modulus–weight ratios of these composite materials are markedly superior to those of metallic materials (Table 1). For these reasons, fiber reinforced polymers have emerged as a major class of structural materials and are either used or being considered for use as substitution for metals in many weight-critical applications and where an high service temperature is not required.

Glass fiber reinforced polymers (GRPs) represent the largest class of PMCs and still dominate the composites market accounting for approximately 95 % of its total volume. Nevertheless, carbon fiber reinforced polymers (CFRPs) are the most important structural composites and currently represent the most relevant segment of the whole composite market^{4,5}. Most of the data presented in this work will be related to PMCs and in particular, on CFRPs.

1.2. Carbon fiber reinforced polymers (CFRPs)

CFRPs are made from a polymer matrix that is reinforced with synthetic carbon fibers. As discussed before, the matrix protects the fibers from environmental and external damage, transfers the load between the fibers and give the shape to the final composite. The fibers, in turn, provide strength and stiffness to reinforce the matrix and help it to resist cracks and fractures. An illustrative scheme on how it is made a CFRP as well as some commercial examples of its various components, are shown in Figure 2.

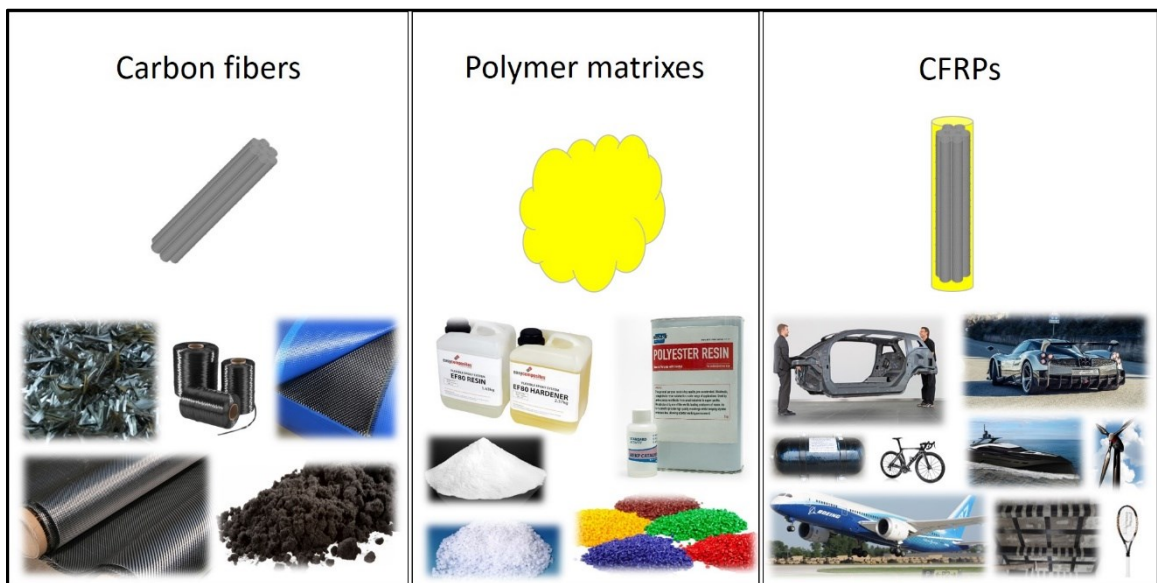


Figure 2. Schematic representation of CFRPs components (on top) and the actual materials ones (on the bottom).

The most important advantages and disadvantages of using CFRPs are listed below. As explained in the next subparagraphs, most of them derive from both carbon fibers and polymer matrixes properties.

Advantages:

- Low density (1,5-1,8 Kg/m³) 70% lighter than steel and 40% percent lighter than aluminum
- Low coefficient of thermal expansion (CTE)
- High ultimate strength
- High elastic moduli
- High corrosion resistance
- High design flexibility

Disadvantages:

- High manufacturing cost
- High scraps production
- Expensive landfilling costs
- Waste and scraps disposal issues
- Problematic recycling of end of life materials
- Aging effects
- Poor properties at temperature above 100-200 °C
- Flammability
- Excellent thermal insulation properties and slow burn-through

1.2.1. Polymer matrixes

The CFRP matrix selection depends on chemical, thermal, mechanical electrical, flammability, environmental, cost and production requirements. The matrix determines the service temperature of the final composite as well as the manufacturing process parameters³. Polymers are structurally much more complex than metals or ceramics, but they are cheap enough and can be easily processed. In contrast, they have lower strength and modulus and lower use temperature limits. One of the key issues in polymer matrix selection is the maximum service temperature: the elastic and strength properties of polymers in fact decrease quickly with increasing temperature. In particular, polymers suffer significant losses in both strength and stiffness above their glass transition temperatures (T_g); for instance, their moduli are reduced by as much as five orders of magnitude. Then, for high-performance composites, the polymer matrix T_g value must be

higher than the composite maximum use temperature. In addition, polymers are viscoelastic materials; this means for example that, when a constant load is applied, the deformation grows continuously with time and, the slower is the application of the load, the larger will be it. There are two major classes of polymers used as matrix materials in CFRPs: thermosets and thermoplastics.

Thermoplastic polymers can be heat-softened, melted, and reshaped (or postformed) as many times as desired. They are usually solid at room temperature and can be divided into two main classes: amorphous and semi-crystalline. As the temperature is increased, both amorphous and semi-crystalline thermoplastics achieve highly viscous liquid states above their T_g or melting point (T_m). Thermoplastics have high impact strength, high ultimate strain and short manufacturing times; they can also be repaired for thermo-welding or solvents, produced in various forms (powder, pellets, grains, etc.) and stored for long periods. Low- and high-density polyethylene (LD/HDPE), polystyrene (PS), polyamides (PA6, PA66), polycarbonate (PC), polyethylene terephthalate (PET), polymethyl methacrylate (PMMA), acrylonitrile-butadiene-styrene (ABS), polyethersulfone (PES), polyetherimide (PEI) and polyether etherketone (PEEK) are some common examples of thermoplastic matrixes. Because of their high melt or solution viscosities, incorporation of continuous fibers into a thermoplastic matrix is very difficult; they are more commonly used with short fiber-reinforced composites that are injection-molded.

Thermoset materials once formed cannot be remelted or reformed; they decompose on heating producing char and finally burn at very high temperatures. The molecules are chemically joined together by cross-links, forming a rigid, three-dimensional network structure. Cross-linking makes sliding of molecules past one another difficult, making the polymer strong and rigid. The higher the number of cross-linkings, the more rigid, thermally stable and resistant to solvents and corrosive environments will be the material. The starting materials used in the polymerization of a thermoset polymer are usually low-molecular-weight liquid chemicals with very low viscosities, consisting of monomers or pre-polymers often named resins; multifunctional crosslinking agents, commercially known as curing agents or hardeners are added as well. The polymerization process that occurs during the cross-linking is also called curing process or simply curing or cure. The most common resin materials used in thermoset composites are epoxy, polyester, vinylester, phenolics, cyanate esters, bismaleimides, and polyimides.

Since the viscosity of the polymer at the time of fiber incorporation is very low, thermoset resins provide easy processability and better fiber impregnation without the aid of either high temperature or pressure. Thermosets offer greater thermal and dimensional stability, less creep and stress relaxation, better rigidity, excellent adhesion to a wide variety of reinforcements and higher electrical, chemical, and solvent resistance than thermoplastics. Nevertheless, thermoset polymers present some disadvantages: limited storage life of their components at room temperature before the cure, long fabrication time in the mold, low strain-to-failure. Finally when the cure occurs, their parts cannot be remolded, and any scrap or end of life material cannot be straightforwardly recycled. In §1.2.3, the important issue related to CFRPs disposal and their recycle will be discussed.

At this time, thermosets matrix systems still dominate the global CFRPs market with around 71.5% (approx. US \$9,46 billion)⁵. Due to their easy processability and superior mechanical properties, many types of composite manufacturing processes have been developed to produce the type of structure desired. A brief description of the most important processing that are relevant for CFRPs are presented in this chapter.

Epoxy resins

Among thermosetting matrixes, epoxy resins find applications in a wide range of CFRPs parts and structures. An epoxy resin is made of low molecular weight polymers or molecules that contains two or more epoxide groups in its chemical structure. An epoxy group (a three-membered ring of two carbon atoms and one oxygen atom), can simply react with nucleophile organic compounds containing amino or acid groups. The epoxy ring has an anomalous reactivity when it is compared with other cyclic ethers: the highly tensioned bond angles and the polarization of the C-C and the C-O bonds, in fact, make the epoxy ring very reactive to the attack of electron-donor groups as reported in Figure 3⁶.

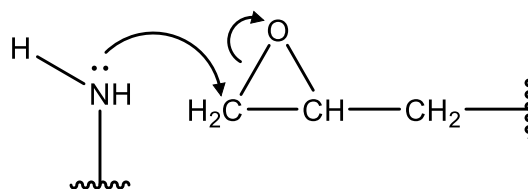


Figure 3. Epoxy ring opening mechanism.

The commercial epoxy precursors consist of aliphatic, cycloaliphatic or aromatic molecules; these are commercialized with a wide range of molecular weights, ranging from

hundreds to tens of thousands of Dalton, depending on the resin final use. One of the most commonly used epoxy resins is the diglycidyl ether of bisphenol A (DGEBA) produced by reaction of epichlorhydrin with bisphenol A (Figure 4).

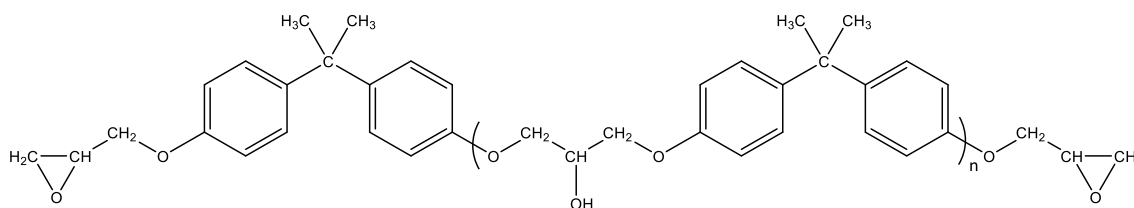


Figure 4. Molecular structure of a generic diglycidyl ether of bisphenol A (DGEBA).

The polymerization (curing) reaction to transform the precursors to a high performance solid material is initiated by adding small amounts of curing agents, which allow the different chains to cross-link each other in a 3D network and finally form a solid epoxy resin. Common commercial curing agents or hardeners include aliphatic or aromatic secondary and tertiary diamine or anhydrides.

Epoxy resins are widely used because of their versatility, high mechanical properties, high corrosion resistance, low shrinkage, excellent resistance to chemicals and solvents, excellent adhesion to a wide variety of fillers, fibers, and other substrates and absence of volatile matters during cure. Epoxy resins are also favoured for their simple cure process that can be achieved at any temperature between 5 to 180°C, depending on the type of curative and accelerators used. Cure rates can be controlled through proper selection of hardeners and/or catalysts. Each hardener provides different cure characteristics and different properties to the final material. Epoxy-based composites provide good performance at room and elevated temperatures: they can operate well up to temperatures of 90 to 180°C. The operating temperature is always below the glass transition temperature, which is high for brittle epoxies (up to 240°C) and lower for toughened epoxies (between 60 and 185°C)⁷. Some important characteristics of epoxy resins typically used as CFRP matrixes are reported in Table 2⁴.

Table 2. CFRPs epoxy resins typical properties⁴.

Density, ρ (g/cm ³)	Strength, σ (MPa)	Modulus, E (GPa)	Poisson's ratio, ν	CTE, α (10 ⁻⁶ K ⁻¹)	Cure shrinkage (%)	Use Temp. (°C)
1.2-1.3	50-125	2-4	0.2-0.33	50-100	1-5	90-180

Epoxy resins are commercialized in liquid, solid, and semi-solid forms. Liquid epoxies are compatible with the most common CFRPs manufacturing processes (see §1.2.3), like hand lay-up, filament winding, pultrusion, RTM and other processes with various reinforcing fibers. Semi-solid epoxies can be found in prepregs (see §1.2.3) for vacuum bagging and autoclave processes. Solid epoxy resins are eventually used for bonding purposes, mainly in the preparation of powder paints. Epoxies are more expensive than polyester and vinylesters and are therefore not used in cost-sensitive markets unless specific performance is needed.

1.2.2. Carbon fiber

Carbon fibers are black, thin, synthetic filaments made of 90% or greater of carbon atoms. They typically have a diameter between 5 and 10 μm and the highest strength and stiffness of all the reinforcement fibers; their extraordinary properties include lightweight (1.7-2.2 g/cm^3 vs. 8.1 g/cm^3 for traditional steel), good fatigue resistance, electrical conductivity, chemical inertness, and low coefficient of thermal expansion^{3,7,8}. Owing to the extreme fragility of these small-diameter filaments, numerous parallel filaments are typically grouped together into bundle having different number of filaments or tow size. The term tow count refers to the number of untwisted filaments per bundle and is often expressed with nomenclature such as 1K, 5K, 24K and so on, where the letter K designates the number 1,000; thus, 24K describes a carbon fiber having 24,000 filaments per bundle. Carbon fibers are available in many standard continuous or discontinuous forms. Continuous tow is the basic form of carbon fiber that allows to obtain discontinuous chopped fibers, woven fabrics, multidirectional fabrics, stapled, woven or knitted three-dimensional preforms³. As the other fibers, carbon fibers have a length that is much greater than its diameter. The length-to-diameter (l/d) ratio is known as the aspect ratio and can vary greatly. Continuous fibers have long aspect ratios, while discontinuous fibers have short aspect ratios. Continuous-fiber composites normally have a preferred orientation, while discontinuous fibers generally have a random orientation.

There are dozens of different kinds of commercial trademarked carbon fibers, and new ones are continually being developed; due to their variety of tensile modulus, (from 20 GPa to 1000 GPa) and strength (from 1000 MPa to 7000 MPa), they are often classified according to these two important mechanical properties as reported in Figure 5⁷.

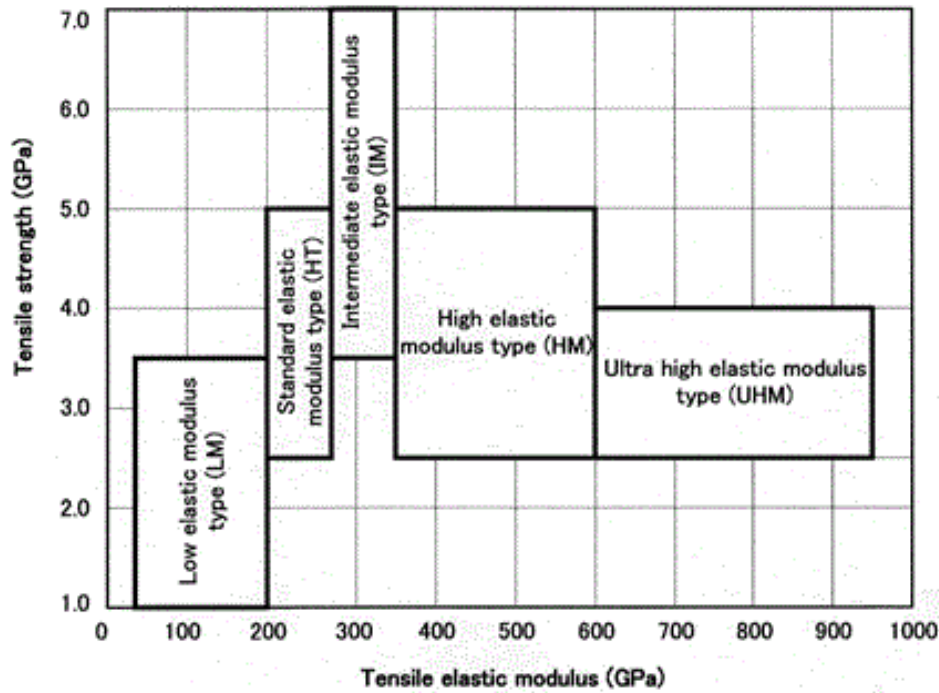


Figure 5. Classification of carbon fibers according to their tensile modulus and strength values⁷.

Some of the limitations of carbon fibers are their low shock resistance (due to their high rigidity, high fragility), as well as susceptibility to chemical attack in the presence of oxygen and other oxidizing compounds at temperatures higher than 400°C. Galvanic corrosion will take place if carbon fiber composites are in electrical contact with metals, due to their good electrical resistance.

Structurally, carbon fibers contain a blend of amorphous and graphitic carbon⁸. Their high tensile modulus derives from the graphitic form, in which carbon atoms are arranged in a crystallographic structure of parallel hexagonal planes like in the graphite. The strong covalent bonds between carbon atoms in the layer plane result in an extremely high modulus while the weak van der Waals-type bonds between the adjacent layers result in a lower modulus in that direction. Thus, these graphite crystal alignments make the carbon fibers incredibly strong for their size and give them significant anisotropic properties^{4,9}. In a carbon fiber, the graphitic lamellar structures are aligned along the fiber axis; however, in the transverse direction, the alignment can be either circumferential, radial, random, or a combination of these arrangements (Figure 6). Depending on which of these arrangements exists, some properties such as modulus, coefficient of thermal expansion can be different. If the arrangement is circumferential, the fiber is said to be circumferentially orthotropic; if radial, the fiber is radially orthotropic and if random, the fiber is transversely isotropic. In commercial fibers, a two-zone structure with

circumferential arrangement in the skin and either radial or random arrangement in the core is commonly observed (Figure 6 d and e).

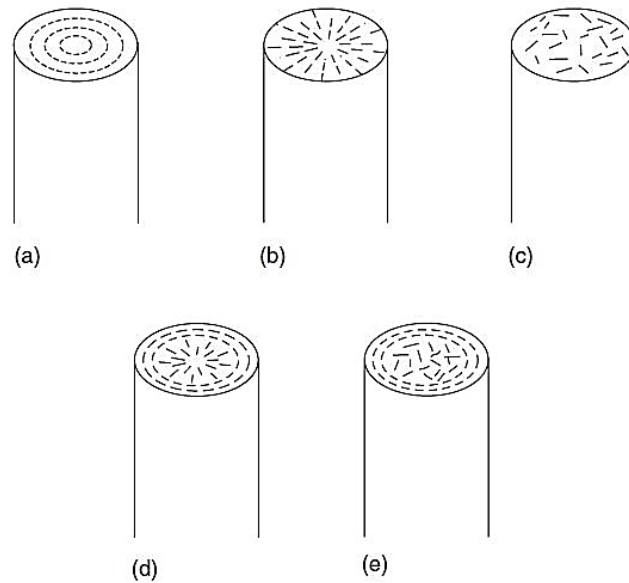


Figure 6. Arrangement of graphite crystals in a direction transverse to the fiber axis: (a) circumferential, (b) radial, (c) random, (d) radial-circumferential, and (e) random-circumferential⁸.

Carbon fibers manufacturing

Thomas Edison made the first carbon fibers on record in 1879 when he carbonized cotton thread to produce a filament for a light bulb. However, large-scale production of carbon fibers had to wait until the late 1950's, when cloth and felt from carbonized rayon were commercialized. In the 1960's, workers in Japan and in the UK developed high-strength carbon fibers with Young's modulus of about 170-600 GPa from polyacrylonitrile fibers (PAN). At about the same time, pitch-based fibers saw their start in Japan and the U.S. Since then, developments in the technology of carbon fibers have occurred in rapid strides⁹.

The properties of carbon fibers depend on the raw material and the process used for its manufacture. Two main organic precursors are used: textile polyacrylonitrile fibers or pitch fibers obtained by spinning purified petroleum or coal tar pitch. All the carbon fiber manufacturing processes have the goal of obtaining fibers with different graphite structure arrangements and improving the orientation of graphitic crystals. Pitch-based carbon fibers are produced in the same way as PAN-based fibers but pitch is more difficult to spin and the resultant fiber is more difficult to handle. The essential steps that transform the organic precursors to carbon fibers are the following:

1. A **stabilization or oxidation** step, which prevents the fiber from melting in the subsequent high-temperature treatments (200-300°C under air).
2. A **carbonization** step, which removes most non-carbon elements (250-1000°C under inert atmosphere).
3. A **graphitization** step, which improves the mechanical properties of carbon fiber (1000-2500°C under inert atmosphere).
4. A **surface treatment** step, generally using air, carbon dioxide, ozone, sodium hypochlorite, nitric acid or electrolytic coatings, which adds oxygen atoms to the surface as well as etches and roughens it, giving the fibers better chemical and mechanical bonding properties.
5. A **sizing** step, which protects from damage during winding or weaving and improving the matrices compatibility (epoxy, polyester, nylon, urethane are used like coating materials).
6. Finally a **winding** step, during which the fibers are wound in bobbins and twisted into yarns of various sizes.

In all processes, the precursor is stretched at some stage of pyrolysis to obtain the high degree of alignment of graphitic basal planes. Rigorous controls, applied during all these steps, preserve the fiber integrity from any fracture. A schematic representation of the PAN and pitch manufacturing processes is shown in Figure 7.

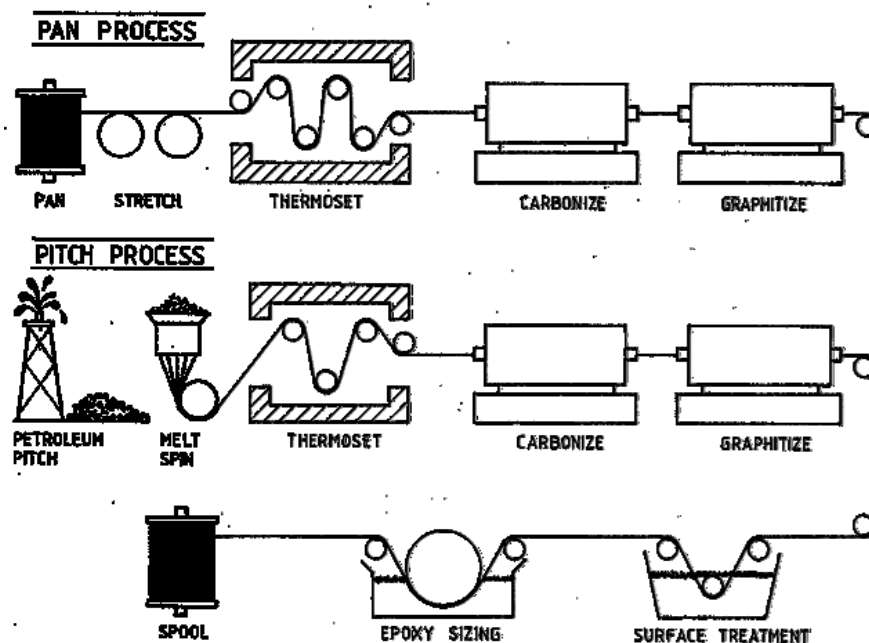
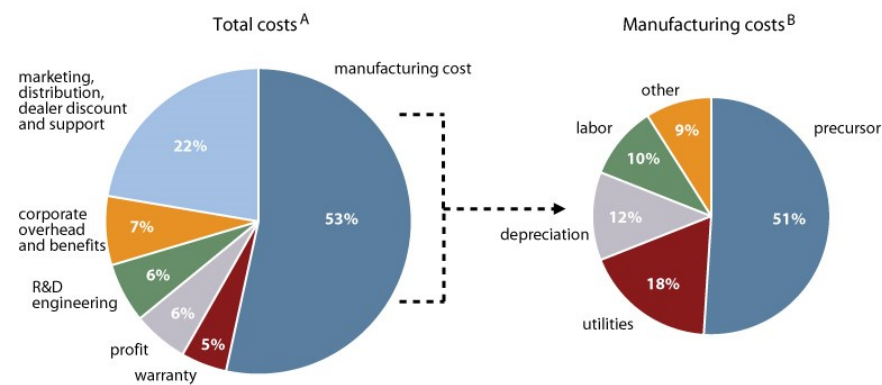


Figure 7. PAN and pitch-based carbon fibers manufacturing processes flow diagrams⁸.

Nowadays, the PAN-based carbon fibers are definitely the most common; they dominate the carbon fiber market due to its cost-effectiveness and the quality of the fiber produced: more than 90% of the carbon fibers produced are made from PAN¹⁰. The pitch-based carbon fibers are more fragile and sensible to surface defects than the PAN-based ones: because of their intrinsic graphitic structure, their tensile strength is about one-half and their compressive strength is about one-third^{2-5,8}. Standard modulus carbon fiber with a modulus of 200-280 GPa and a strength of 2500-5000 MPa has 80%–90% of total market today¹⁰. In general, the low-modulus fibers have lower density, lower cost, higher tensile and compressive strengths, and higher tensile strains-to-failure than the high-modulus fibers. The cost of carbon fibers varies in function of the strength and stiffness properties as well as the tow sizes. Fibers with high stiffness and strength properties cost more. The higher the tow size, the lower the cost will be. For example, 24K tow costs less than 6K tow.

The whole fabrication method for the production of carbon fibers is slow and capital intensive. Currently, the prices of carbon fibers range from \$20 to \$130/Kg^{3,10}. The cost of carbon fiber is strictly related to manufacturing and the raw material costs: about the 50% of the final price depends on the manufacturing process and about the 50% of this cost is due to the precursor cost. For illustration, a carbon fiber cost breakdown is reported in Figure 8.



Carbon fiber manufacturing costs through a standard manufacturing process^B

	precursors	stabilization & oxidation	carbonization/ graphitization	surface treatment	spooling & packaging
baseline cost per pound	\$5.04	\$1.54	\$2.32	\$0.37	\$0.61
baseline cost per pound, high volume	\$4.64	\$0.99	\$1.48	\$0.33	\$0.41

Figure 8. Carbon fiber cost breakdown¹². Note that 1kg ≈ 2.2 pounds.

The PAN-based precursor costs around \$3 to \$6/Kg but its yield in carbon fibers is almost 50% of the original weight. Pitch based precursors have an insignificant cost by themselves, but processing and purifying them to the fiber form are very expensive; however, pitch precursors allow for making very ultra-high modulus (UHM) carbon fibers^{3,4}. All carbon fiber manufacturers in the market place have their own in-house polymerization and precursor spinning capabilities. The exact composition of each precursor as well as the manufacturing process differs from one company to another and are generally considered a trade secret covered by intellectual property. If the carbon fiber can be purchased in the open market directly from carbon fiber manufacturers or other distribution channels, the precursors are not available for purchase because the carbon fiber manufacturers retain in-house their own precursor for intra-company activities. Consequently, there are only about 15 carbon fiber manufacturers in the world, which alone the top 5 already achieve the 69.3% of the worldwide carbon fiber capacity^{5,10}. In brief, the manufactures are still free to add any value at the conclusion of the carbon fiber manufacturing process and control their final prize.

1.2.3. CFRP manufacturing processes

There are many processing methods for CFRPs with thermoset and thermoplastic matrix materials. The choice of manufacturing process depends on the type of matrix and fibers, the temperature required to form the part and to cure the matrix, and the cost-effectiveness of the process. This last one is largely influenced by the rate of production, the production volume, and adequacy of a manufacturing process to produce the type of structure desired^{7,8}.

Today, many techniques, originally developed for making glass fiber reinforced polymer matrix composites, are used with carbon fiber, and new others are constantly developed. Most of these are referred to thermosetting matrixes, the most common in the CFRPs manufacturing. Thermoplastics soften on heating, and therefore melt flow techniques of forming can be used. Such techniques include injection molding, extrusion, and thermoforming; these well-known techniques in the thermoplastic manufacturing do not be discussed in this work. More attention will be given instead to the main current manufacturing processes for thermosetting CFRPs.

As said before, thermosets harden on curing. Curing or cross-linking occurs in thermosets by adding appropriate curing or catalytic agents and by the application of heat and pressure

for a programmed length of time. The length of time required to properly cure a part is called the cure cycle⁸. Processing of thermoset CFRPs involves the following general steps:

- fiber placement
- impregnation with the resin system
- consolidation by elimination of excess resin, air and volatile
- polymerization or cure of the polymer matrix
- demolding and/or finishing operations

Each operation has significant impact on the cost, production rate, quality, and performance of the final product; often some of these steps may be combined or accomplished in different ways to improve the process cost-effectiveness. There are several manufacturing processes for CFRPs with thermoset matrix materials and each one has intrinsic advantages and limitations that affect the structural and material design.

The early and still reliable manufacturing process for CFRPs were very slow and labour-intensive like the hand lay-up technique; others like compression molding, pultrusion, filament winding and resin transfer molding (RTM) can support mass production rates and allow producing composite parts with different and complex shapes. In recent years, due to the introduction of automation, fast-curing resins, new fiber forms and high-resolution quality control tools, the manufacturing technology for CFRPs has made tremendous progresses. Many techniques have been improved and new ones developed with the aim to reduce the cycle time to less than minutes such as the high-pressure resin transfer molding process (HP-RTM).

Before discussing about the most relevant manufacturing processes for thermosetting CFRPs, **prepreg**, a very common material used for the CFRPs manufacturing, is described. The term prepreg is a short form of preimpregnated fibers. A prepreg is a resin-impregnated fiber, fabric, or mat in flat form, which is stored for later use in hand lay-up or molding operations³. The amount of polymer matrix is predetermined and uniformly distributed on the fiber tape and partially cured or thickened. The fibers can be arranged in a unidirectional tape, a woven fabric, or random chopped fiber sheets. Unidirectional fiber-reinforced epoxy prepreps are manufactured by pulling a row of uniformly spaced (collimated) fibers through a resin bath containing catalyzed epoxy resin dissolved in an appropriate solvent; instead woven fabric prepreps and random chopped fiber are made by

preimpregnating with resin via a hot melt process or by solution treatment. Preimpregnated fibers are then passed through a chamber in which heat is applied in a controlled manner to advance the curing reaction to a B-stage. A B-stage cured resin is a system wherein the reaction between the resin and the curing agent/hardener is in a partially cured stage; in this way, when the prepregs are then reheated at elevated temperatures, the cross-linking can be completed and the system fully cured. Therefore, at the end of B-staging, uncured prepreg with various types of drape and tack are obtained. Tack is the stickiness of uncured prepregs and is required for easy laying and processing; drape is the ability of prepreg to take the shape of a contoured surface. Consequently, the prepreg sheet is backed up with a polyethylene release film or waxed paper and wound around a take-up roll.

Epoxy is the primary matrix material in prepreg sheets, although other thermoset and thermoplastic polymers have also been used. The resin content in commercially available prepregs is between 30% and 50% by weight; the width of prepreg sheets may vary from less than 25 mm to 1.5 m and their thicknesses are normally in the range of 0.13–0.25 mm. Since the resin is partially cured, prepregs have a limited shelf life. The normal shelf life (storage time before molding) for epoxy prepregs is 6–8 days at room temperature (22–25 °C); however, it can be prolonged up to 6 months or more if stored at -18 °C. The backup material (release film) is generally hand-separated from the prepreg sheet just before it is placed in the mold to manufacture the composite part. Prepregs provide consistent properties as well as consistent fiber/resin mix and complete wet-out. They eliminate the need for weighing and mixing resin, curing agent and catalyst. Various types of drape and tack are provided with prepregs to meet various application needs. Prepregs are generally used for autoclave molding, compression molding, and automatic lay-up processes. Once the prepregs are laid on a tool, it is cured in the presence of pressure and temperature to obtain the final product.

The most common CFRP manufacturing processes are briefly described below:

- **Hand lay-up.** The hand lay-up technique, also called **wet lay-up**, is the simplest and most widely used manufacturing process because it requires a minimum investment in equipment. Fibers can be laid onto a mold by hand and the resin is sprayed or brushed on. When the resin and fibers (chopped) are sprayed together onto the mold surface through a chopper gun, the process is called **spray up**. In both cases, the deposited layers are densified with rollers. Curing may be done at

room temperature or at a moderately high temperature in an oven; accelerators and catalysts are commonly used. This process is used to make both large and small items, including boats, storage tanks, tubs, pools, furniture showers, aircraft and truck parts etc. Production volume per mold is low, so often multiple molds are used. This manufacturing process are very labour intensive and requires skilled workers.

- **Filament Winding.** This process is primarily used for hollow, generally circular or oval sectioned components, such as pipes and tanks. Fiber tows are passed through a resin bath before being wound onto a mandrel in a variety of orientations, controlled by the fiber feeding mechanism, and rate of rotation of the mandrel. Filament winding is highly automated and does not require an expensive intermediate product form such as a fabric or prepreg. High-volume parts in a cost-effective manner can be obtained with this manufacturing technique.
- **Autoclave Molding.** It is also called **prepreg lay-up** or **vacuum bagging** process. In this process, prepregs are cut, laid down in the desired fiber orientation on a tool, and then vacuum bagged. The tooling for the prepreg lay-up process is an open mold on which unidirectional or bidirectional prepregs are laid in the desired fiber orientation and sequence. A uniform pressure is applied to the laminate by a flexible bag, which is perfectly sealed to the tool and improves consolidation of the fibers and removal of the excess resin, air, and volatiles from the matrix. After vacuum bagging, the composite with the mold is put inside an oven or **autoclave** and then heat and pressure are applied for curing and consolidation of the part. The cure cycle depends on the type of resin material and the thickness and geometry of the part; it normally takes from about 6 to 48 hours. Prepreg lay-up process is widely used in high performance aerospace and automotive parts and complex geometries; it also represents the only choice for large parts exceeding the size of available presses. Autoclave-molded parts have low porosity, a smooth paintable surface, and excellent strength properties. However, this process is very labour intensive, requires high capital investment for the autoclave and is not suitable for high-volume production applications.
- **Compression Molding.** Compression molding is used for transforming sheet-molding compounds (SMC) into low-thickness finished products in matched molds. It is very popular in the automotive industry because of its high volume capabilities. A hydraulic press, using heat and a relatively high pressure, is used to

cure the fibers and resin by closing the male and female halves of the mold. Cycle times are shorter than they are for autoclave molding, but this process likewise requires high-cost prepreg. The principal advantage of compression molding is its ability to produce parts of complex geometry in short periods of time. Sheet molding compound is lower cost but also lower strength than continuous tow product forms. Because of the excellent surface finish, compression molding products are appropriate for paintable parts such as automotive body panels.

- **Resin Transfer Molding (RTM).** In RTM, several layers of dry fiber preforms or fabrics are placed in the bottom half of a two-part mold, the mold is closed, and a catalyzed liquid resin is injected into the mold via a centrally located sprue. The parts are cured with heat and pressure in low-tonnage presses. Injecting pressure from 10 to 20 bars and cycle time of 30 to 60 minutes are very common in the RTM process. The RTM process can produce large continuous/discontinuous fiber-reinforced composites with complicated shapes and relatively short cycle times, without the use of expensive prepregs. However, RTM does not achieve the same surface finish, porosity, or strength as autoclave or compression molding. The RTM process is suitable for making small- to large-sized structures in small- to medium-volume quantities and is largely used in automotive, aerospace, sporting goods, and consumer product applications. RTM has a very low tooling cost and simple mold clamping requirements. When vacuum is used in addition to the resin injection system to pull the liquid resin into the fiber preform, the process is known as Vacuum- Assisted RTM (**VARTM**).
- **High-pressure resin transfer molding (HP-RTM).** HP-RTM process is a very new process developed by the combination of high-pressure technology and the conventional RTM process. For the production of HP-RTM components, a preform made of a textile reinforcement material is required. Such preforms are manufactured using a fully automated process. Textiles in the form of fabrics or mats are unreel from a roll on to a cutting machine and the plies are cut to size as required for the component to be produced. The cut plies are then joined to form a layered package and subsequently fed into the forming unit or draping station; thermoplastic or thermosetting binders can be used to bond and keep the preform shape. After that, the consolidated preform is automatically placed into the RTM mould inside a press with a press force up to 3600 tonnes and a very low-viscosity, reactive resin is injected into the cavity at high pressure (up to 150 bar in the

mixing head and from 30 to 120 bar inside the mold, depending on part size and geometry). HP-RTM process ensures very short cycle times (less than 10 minutes) and offers cost saving benefits of automation: high productivity, energy-efficient press technology, self-cleaning high-pressure mixing heads as well as low porosity and excellent surface qualities final products. HP-RTM is already used in series production of structural CFRP parts in BMW's i3 and i8 model.

The significant process steps, intermediate products, and approximate unit prices in the value chain that transform crude oil into carbon fiber and finally CFRP is shown in Figure 9¹⁰.

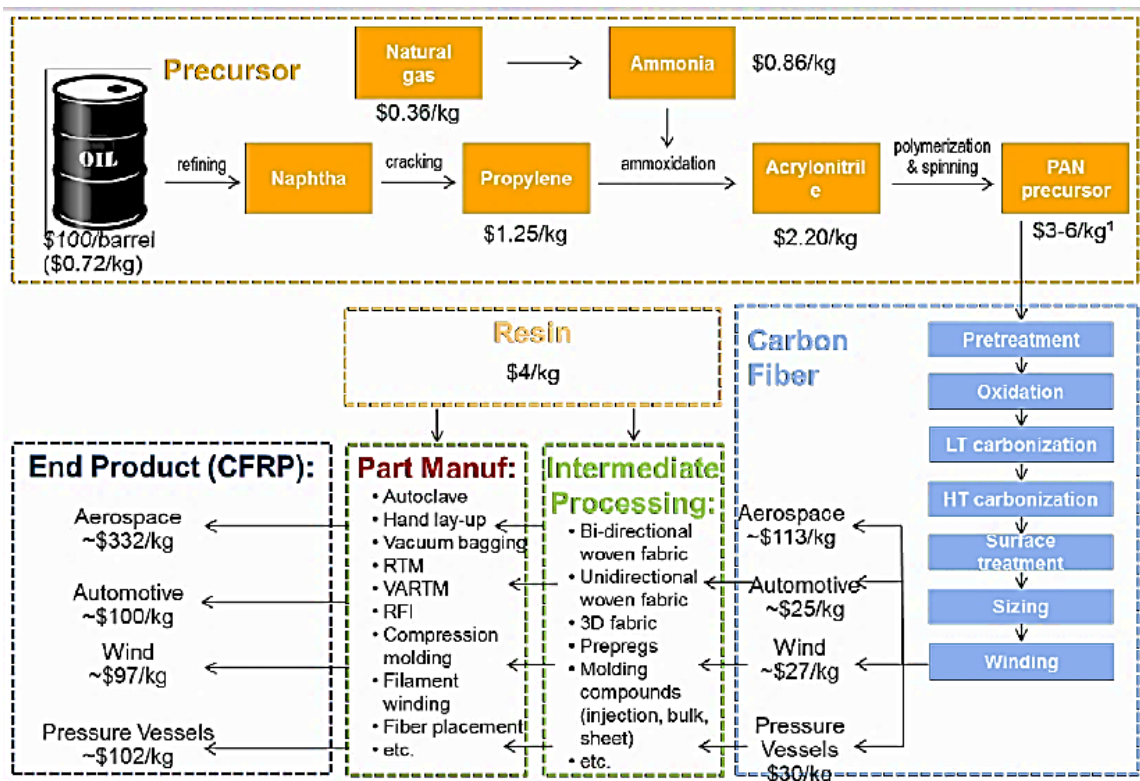


Figure 9. Carbon fiber and CFRPs value chain¹⁰.

1.3. Polymer nanocomposite materials

Polymer nanocomposites are polymer matrix composites in which the reinforcement has at least one of its dimensions in the nanometre range, typically less than 100 nm (1 nanometre = 10^{-9} m). Nowadays, new nanotechnology developments have been pushing the interest in nanostructured or nanocomposite materials obtainable by adding nanometric fillers to improve a particular property of the material¹³. These composites show great potential not only in terms of superior mechanical properties, but also in terms of superior thermal, electrical, optical, and other properties, and, in general, at relatively low-

reinforcement volume fractions; there are circumstances where nanocomposites can show properties not expected with larger scale particulate reinforcements. Consequently, polymer matrix based nanocomposites have generated a significant amount of attention in the recent literature ^{8,13,14}. The transition from microparticles to nanoparticles yields dramatic changes in physical properties. In particular, nanoscale materials have a large surface area for a given volume. In the case of particles and fibers, the surface area per unit volume is inversely proportional to the material's diameter, thus, the smaller the diameter, the greater the surface area per unit volume¹³. For the layered material, instead, the surface area/volume is dominated, especially for nanomaterials, by the thickness. As a result, a change in particle diameter, layer thickness, or fibrous material diameter from the micrometer to nanometer range, can affect the surface area-to-volume ratio by three orders of magnitude.

The uniform dispersion of these nanoparticles provides a greater interfacial interaction with the polymer matrix and they can be incorporated in addition to traditional fillers and additives, and eventually traditional reinforcement fibers such as glass or carbon; common loading rates in polymer matrix range from less than 1% to 10% wt. Nanoscale materials can be catalogued based on their shape and number of dimensions that falls in the order of nanometres (Figure 10):

- *0D zero-dimensional*, no dimension exceeds 100 nm (SiO₂ or TiO₂ particles, fullerenes and other zero-dimensional clusters);
- *1D mono-dimensional*, a dimension greater than the nanometer scale (carbon nanotubes, molecular clusters);
- *2D bi-dimensional*, typical of flat structure materials and thickness of some nanometres (graphene, fillosylates);
- *3D three-dimensional* where all sizes exceed the nanometer scale, typical of crystalline systems (diamond, graphite, metals) and aggregate structures.

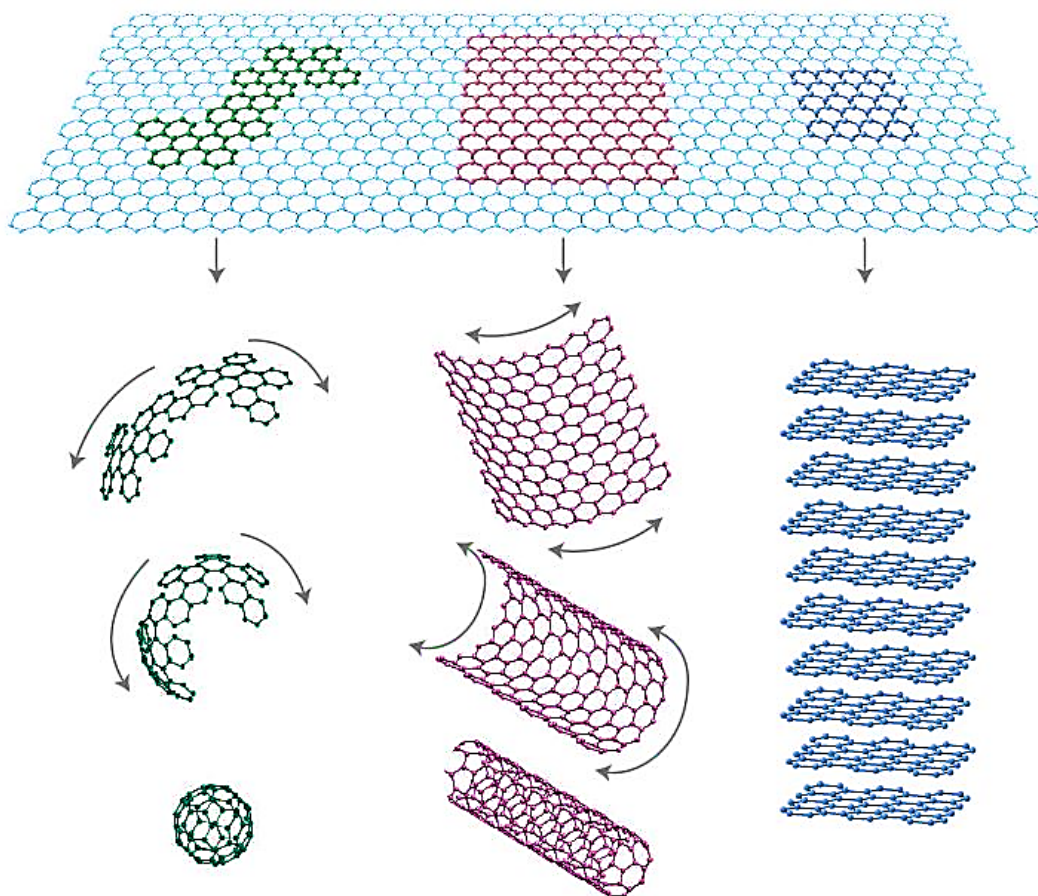


Figure 10. Graphene is a 2D building material for carbon materials of all other dimensionalities. It can be wrapped up into 0D buckyballs, rolled into 1D nanotubes or stacked into 3D graphite¹⁵.

Nowadays, various nanofillers are studied and even more others are discovered; materials like nanoclays, nano-oxides, nanofibers, graphene, carbon nanotubes, carbon nanofibers, polyhedral oligosilsesquioxanes (POSS) etc. are already used with polymer matrixes. However, nanoclays are the most commonly used commercial additive for the preparation of nanocomposites; carbon nanofibers, carbon nanotubes, POSS and the others start gaining commercial interest but their cost/performance and processability characteristics make very difficult finding commercial applications.

1.3.1. Nanoclay

Nanoclays are nanoparticles of layered magnesium aluminium silicates¹⁴. Depending on chemical structure and nanoparticle morphology, nanoclays are organized into several classes such as montmorillonite, bentonite, kaolinite, hectorite, and halloysite. These layered silicates commonly used in nanocomposites belong to the structural family known as the 2:1 phyllosilicates; due their natural abundance, they have very low cost if compered to all the other nanofillers. Their crystal lattice consists of two-dimensional layers where a

central octahedral sheet of alumina or magnesia is fused to two external silica tetrahedron by the tip so that the oxygen ions of the octahedral sheet do also belong to the tetrahedral sheets¹⁴. These layers organize themselves to form stacks with a regular van der Waals gap in between them called the interlayer or the gallery. The layer thickness is around 1 nm and the lateral dimensions of these layers may vary from 300 Å to several microns and even larger depending on the particular silicate. Isomorphic substitution within the layers (for example, Al^{3+} replaced by Mg^{2+} or by Fe^{2+} , or Mg^{2+} replaced by Li^+) generates negative charges that are counterbalanced by alkali or alkaline earth cations, usually Na^+ , situated in the interlayer (Figure 11).

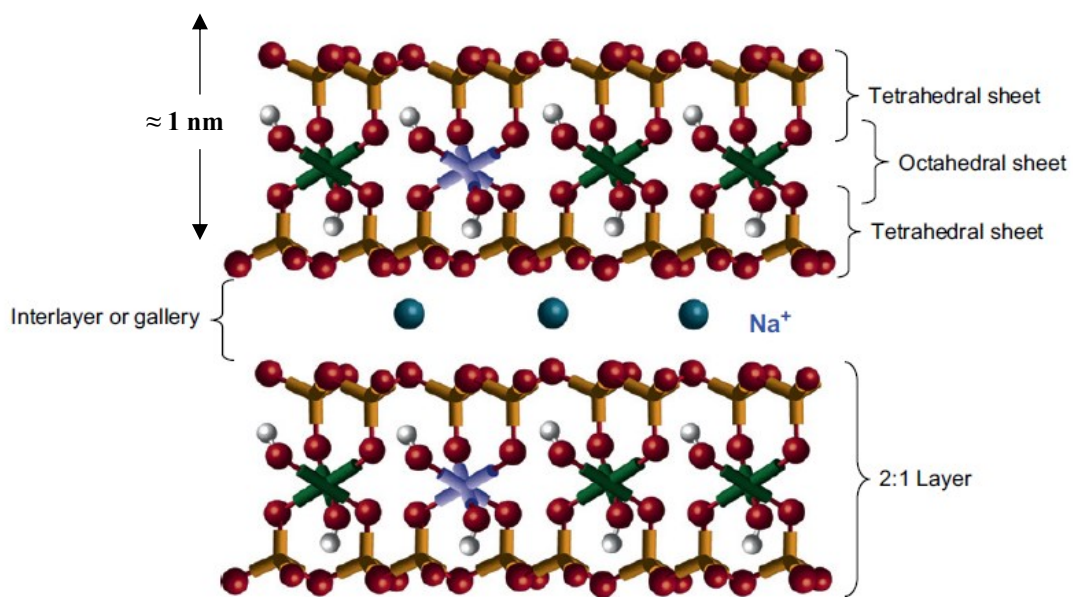


Figure 11. Structure of sodium montmorillonite¹⁴.

Hydration of these cations causes the galleries to expand and the clay to swell; indeed, these platelets can be fully dispersed in water and an aspect ratio as high as 1000 for fully dispersed individual layers can be obtained. The interlayer cations can be replaced via ion exchange reactions with various organic cations such as quaternary alkylammonium cations or cationic surfactants, in order to render the normally hydrophilic silicate surface more organophilic. The surface modification of the clays lowers the surface energy of the silicate surface and increase the interlayer gallery space. Hence, organosilicates, also known as organoclays, are much more compatible with most thermoplastic and thermosetting engineering plastics. Additionally, the organic cations may contain various functional groups that react with the polymer to improve adhesion between the inorganic phase and the matrix^{14,16}.

Polymer layered silicate (PLS) nanocomposites exhibit enhanced properties at very low filler level, usually inferior to 5 wt.%, such as increased Young's modulus and storage modulus, increase in thermal stability and gas barrier properties and good flame retardancy¹⁷⁻¹⁹. In addition, because of the length scale involved that minimizes scattering, nanocomposites are usually transparent^{20,21}. Polymer nanocomposites reinforced with nanoclays particles are already commercially viable: the Toyota researchers first used clay/nylon 6 composites for timing belt covers in 1990 and major automakers have started making use of nanocomposites in their autos.

1.3.2. Nano-oxides

Many nano-oxide particles have attracted the interest of researchers in polymer nanocomposite manufacturing. Nano-oxides like metals oxides and nanosilica are spherical particles with diameter in the range of 20-300 nm. The most common are derived from titanium dioxide, alumina and silica^{22,23}. A brief overview is reported below.

- *Anatase* (one of the tetragonal crystal forms of titanium dioxide) is commonly used as spherical particles with diameter around 20 nm for its photocatalytic properties²³. The anatase can be also converted by hydrothermal synthesis into titanium nanotubes²⁴. These nanotubes have an outer diameter of 10 to 20 nm, an inner diameter of 5 to 8 nm and a length of 1 μm . The rutile titanium dioxide form, instead, is commonly used in polymers as a white pigment, as particles from 200 to 300 nm.
- *Alumina particles* are used as fillers in a wide range of size, from 20 nm to micrometric sizes. They are made of spherical crystal particles of Al_2O_3 . Nanoparticles of alumina are frequently used as inert fillers in polymers, but highlight catalytic properties in some conditions^{23,25}.
- *Nanosilica* corresponds to a large family of nanoparticles from various origins²⁶. The most commonly used is a natural one, called diatomite. This filler comes from the skeleton of a unicellular algae (the diatom) forming sedimentary layers. It is constituted from ultrafine particles of 750 nm. Two families of widely used synthetic nanosilicas are pyrogenic silica, forming particles from 5 to 100 nm, and silica fume, forming particles of about 100 nm. Precipitated silica historically used in polymers is not a nanoparticle, as its diameter is between 1 and 10 μm when micronized²³.

1.3.3. Carbon-nanomaterials: graphene and nanotubes

Carbon materials exist in multiple forms such as diamond, graphite, graphene and nanotubes. Graphene consists of a single atomic layer of sp^2 -hybridized carbon atoms arranged in a two-dimensional (2D) honeycomb structure and is a basic building block for graphitic materials of all other dimensionalities as shown in Figure 10. Graphene was successfully isolated by repeated graphite peeling with an adhesive tape in 2004¹⁵. In recent years, various techniques have been established for graphene synthesis: mechanical cleaving (exfoliation), chemical exfoliation, chemical synthesis, and thermal chemical vapour deposition (CVD) synthesis are the most commonly used production methods today²⁷. Graphene is a material with extraordinary properties; for its exceptional values of strength and Young modulus²⁸ (130 GPa and 1 TPa respectively), superior thermal and electric properties^{29,30}, gas impermeability³¹, huge surface area³², is the perfect reinforcing material for polymer-matrix nanocomposite. However, for taking advantage of these tremendous properties in polymer nanocomposites, it is essential to fabricate high-quality graphene (single layer) in large production and obtain an optimal dispersion into the matrix.

Carbon nanotubes (CNTs) can be described as a graphene layer (a single layer of graphite) rolled into a cylindrical shape with axial symmetry (Figure 10). CNTs were first discovered in 1976³³, and then rediscovered and described by Iijima in 1991³⁴. The CNTs present a nanometric diameter and length of some orders of magnitude in comparison with its diameter. In general, three kinds of carbon nanotubes are considered:

- Single-wall carbon nanotubes (SWCNT). They present a diameter between 1 and 2 nm;
- Double-wall carbon nanotubes (DWCNT). Diameter is between 2 and 4 nm.
- Multi-wall carbon nanotubes (MWCNT). They present a diameter between 4 and 150 nm.

Carbon nanotubes are produced by two possible ways: a catalytic chemical vapour decomposition process at medium temperatures (600-1000°C) and an electric discharge (arc) process under helium at high temperature (3000-4000°C). Both processes produce a mix between SWCNT, DWCNT and MWCNT, with surface defects (e.g. some pentagonal cycles in place of aromatic rings), and present important catalytic residues³⁵. Properties of carbon nanotubes are highly dependent on morphology, size and diameter. Carbon

nanotubes can be metallic or semiconducting; it depends on the atomic arrangement of carbon nanotube. CNTs, like graphene, are considered as an excellent filler due to their unique properties such as high aspect ratio, high tensile strength, high conductivity etc³⁵.

Graphene and CNTs based polymer nanocomposite show promising applications in many industries, such as aerospace, electronics, energy, structural and mechanical, environmental, medicine, and food and beverage³⁵⁻³⁷. However, the development and the quality of CNT, graphene or hybrid polymer nanocomposites depends upon a lot of factors such as types and length of CNTs, layers of graphene, purity, aspect ratio, loading and dispersion of CNTs and graphene into matrix, alignment, anti-agglomeration of CNTs and graphene into matrix, interaction between the fillers and matrix etc³⁷. The major obstacle is the achievement of a homogenous dispersion of them into the polymer matrix. Functionalization of fillers is the most effective approach, which is used to improve the dispersion. The CNTs and graphene industry is growing rapidly, and more and more kinds of these nanofillers are now available on the markets; nonetheless, due to their high cost, large scale applications in polymer nanocomposites industry are still inaccessible.

1.3.4. Other nanoparticles

Other nanoparticles are used in polymer nanocomposites. Many of them consist of metallic nanoparticles like nanosilver, nanozinc and nanogold³⁸. These nanoparticles can modify polymer electrical and magnetic properties. In addition, they have a catalytic behaviour, which leads to antibacterial properties at surface.

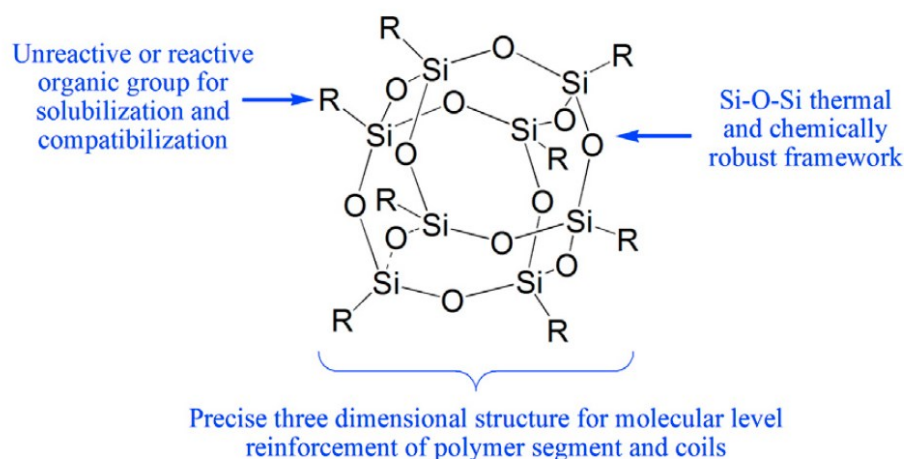


Figure 12. POSS features³⁹.

Polyhedral oligomeric silsesquioxanes (POSSs) are a family of polycyclic compounds of silicon and oxygen with the generic formula $(\text{RSiO}_{3/2})_2n$, where n is an integer and R may be a hydrogen atom or an organic functional group as shown in Figure 12³⁹.

They can be formed as random, ladder, cage, and partial cage structures with a diameter ranging from 1 to 3 nm. Unlike silica, POSS molecule can carry organic substituents on its outer surface that make it compatible with polymers, biological systems, and surfaces of organic nature. The incorporation of POSS in polymers to obtain composites can be responsible for the enhancement of mechanical properties, reduction in flammability and also of heat release on burning⁴⁰. The main challenge restricting the commercial POSS applications is its cost. However, their high efficiency of as fire retardant may make the cost lower than that issued by the use of current fire retardant additives^{39,40}.

1.3.5. Common flame retardant epoxy resin nanocomposites

As discussed in §1.2.1, epoxy resins find a wide range of applications due their versatile and high thermal-mechanical properties. However, their inherent inflammability often limits the applications of epoxies and their composites. In the recent literature, different types of nanofillers have been incorporated in epoxies for the preparation of nanocomposites with improved flame retardant properties. Typically, montmorillonite or bentonite organoclays⁴¹⁻⁴³, graphene^{44,45}, functionalized silica nanoparticles⁴⁶, POSS^{47,48} and carbon nanotubes^{49,50} are used for this purpose in epoxy resins. The fire behaviour of these epoxy nanocomposites has been mostly studied by cone-calorimeter analysis (see §2.1.2): reduction of the rate of heat release (HHR)^{42,44-48}, unique self-extinguishing behaviour⁴¹, and synergistic flame retardant effect^{43,50} were reported by many authors.

In the recent years, epoxy nanocomposites based on organoclays have gained considerable research interest due to the natural abundance, low cost, high efficiency and high aspect ratio of the nanoclays. In addition, the possibility of using liquid epoxy precursors makes the organoclays dispersion into the polymer matrix easy⁴¹⁻⁴³.

Depending on the strength of interfacial interactions between the polymer matrix and nanoclays (modified or not) and the processing conditions three different categories of polymer organoclay structures are achievable (Figure 13)²⁰:

- a) **Phase-separated microcomposite**: there is no intercalation between the silicate sheets and the polymer matrix. The composite material properties stay in the same range as traditional microcomposites.
- b) **Intercalated structure**: polymer chains are intercalated between the silicate layers resulting in a well ordered multilayer morphology built up with alternating polymeric and inorganic layers. The spacing between platelets usually increases.
- c) **Exfoliated nanocomposites**: the individual silicate layers are completely and uniformly separated in a continuous polymer matrix by an average distances that depends on clay loading. Usually, the clay content of an exfoliated nanocomposite is much lower than that of micromposite and intercalated structures.

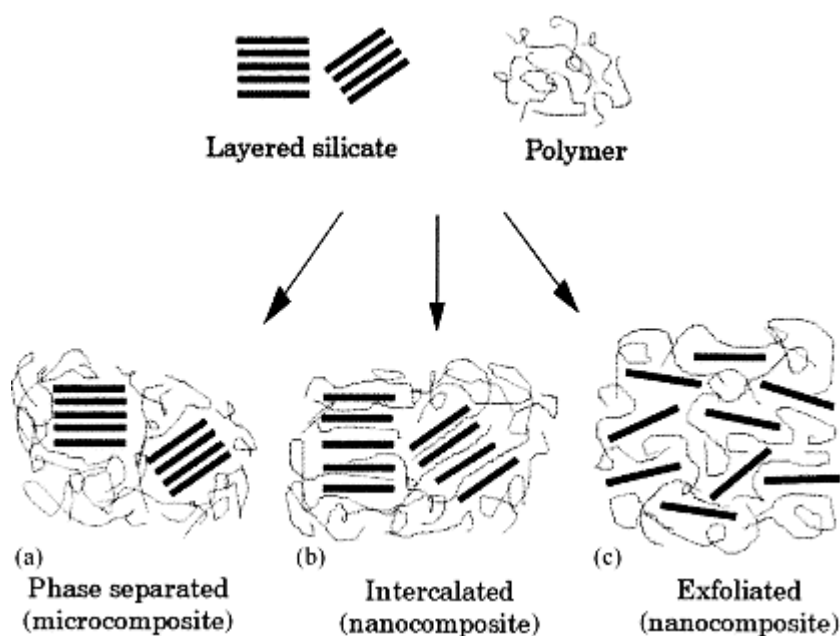


Figure 13. Scheme of different types of composite arising from the interaction of layered silicates and polymers: (a) phase-separated microcomposite; (b) intercalated nanocomposite and (c) exfoliated nanocomposite²⁰.

The flame retardant modes of actions of PLN nanocomposites are schematically represented in Figure 14⁵⁶. When the polymer degradation occurs, the silicates acidic sites may promote the char formation or further crosslinking reactions among the polymer chains. The acid sites can also cause an earlier polymer degradation due to hydrolysis by water either bound to clay, or produced from the dehydroxylation of the aluminosilicate lattice⁵⁶. Hence, the chemical crosslinking improve the polymer thermal-oxidative stability and the formed char acts eventually as a physic barrier for volatiles (combustible gases and oxygen) and heat reducing the heat release rate. Furthermore, the tortuous paths created by the layered silicates limit the mobility of macromolecules and delay the thermal diffusion

in the bulk of the sample (physical crosslinking). Finally, the barrier effect of silicates by themselves may also play a part in PLS nanocomposite flame retardancy in certain conditions^{14,42,56}.

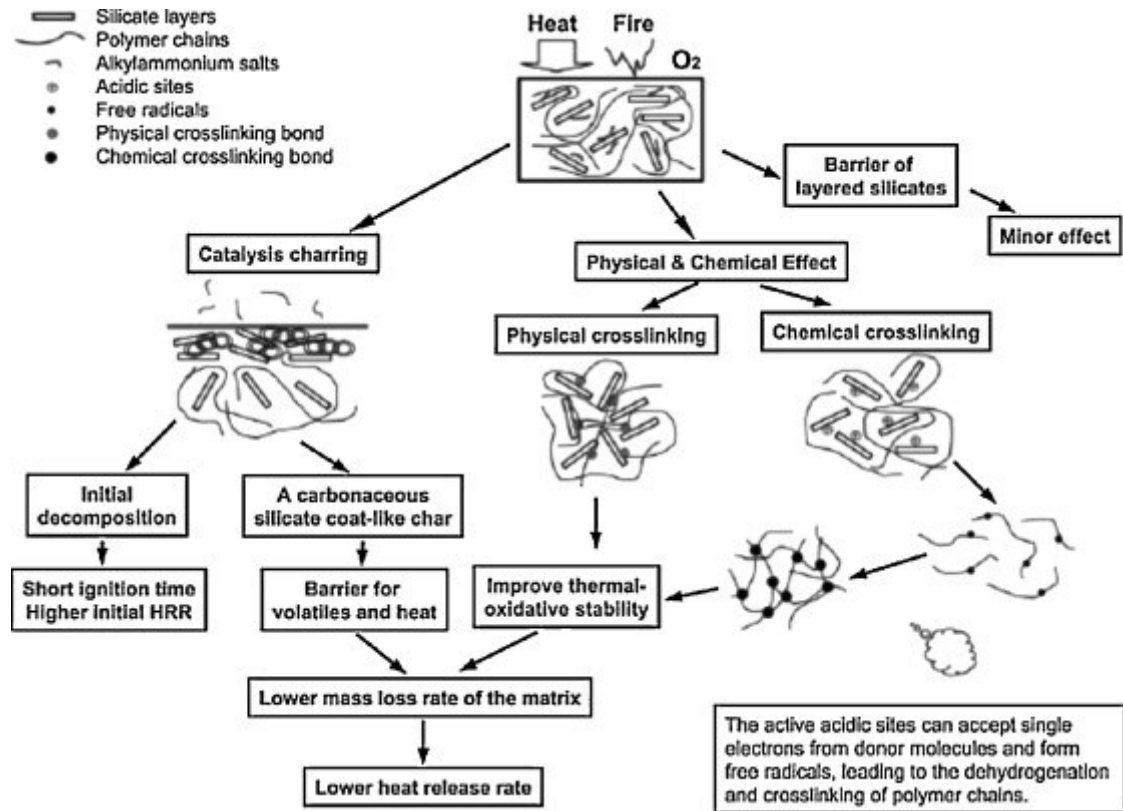


Figure 14. Flame retardant mechanism of PLS nanocomposites⁵⁶.

The clearest evidence for the flame retardancy character of PLS nanocomposites has been achieved through cone calorimetry experiments^{52,56–59}. In the presence of modified or unmodified clays, the HRR levels generally decrease, presenting a peak lower than the HRR curve of the neat polymer matrix^{1,52,54,56,58}. The cone-calorimeter apparatus and its applications on study flame retardancy of polymers will be described in *Chapter 2*, together with the thermo-mechanical properties and the flame behaviour of two bentonite-based epoxy nanocomposites.

1.4. Recycling of CFRPs

The CFRP industry has been experiencing a steady growth that is expanding towards mass-oriented market segments, instead of being limited to niche high value-added market sectors. According to the latest forecasts, the global demand is estimated to reach 194.000 tons per year by 2022⁵. Such a boost in CFRPs is now imposing significant and critical inquiries regarding their end-of-life (EoL) fate; furthermore, this intensification in the use

of CFRPs results in an increase of waste deriving from the production processes (offcuts of prepregs; offcuts and scraps of cured composites) that cannot just be landfilled. These inquiries have led to the development of new procedures and technologies to treat CFRPs in order to have the ability to properly and efficiently recycle and re-use them.

Recycling of CFRPs is one method for reducing environmental impact and resource depletion⁶⁰. Recycling allows to decrease the environmental problems caused by waste accumulation produced from day-to-day applications of polymer composite materials. This helps to conserve natural resources because CFRPs are currently made from non-renewable petroleum derivatives; furthermore, it reduces the quantity of residues in landfills and the quantities of waste requiring a costly disposal. In addition, recycling a CFRP implicates recovering a high cost and energy-intensive materials, the carbon fiber (§1.2.2).

CFRPs, as well as all the others Fiber-reinforced polymers (FRPs), due to their heterogeneous composition, are intrinsically difficult to separate into their base materials: fibres and polymeric matrix. In addition, the cross-linked nature of thermoset resins (which cannot be remoulded), and the combination with other materials (additives, fillers, fixings, honeycombs, metals, hybrid composites, etc.) make even more problematic the FRPs recycling.

For many years, CFRP waste has been disposed of in landfill because it was relatively cheap or not controlled (illegal). Consequently, in order to protect the environment and encourage recycling to take place, legislations, often combined with the use of economic instruments (such as taxes), were introduced⁶¹. The versatile usage and the relatively high cost of the carbon fiber are likely to be the two strongest drivers for recycling of CFRP waste if an economic and environmentally friendly technology can be developed to provide a potential sustainable resource of reusable fibers. However, the uncertainty about how they can be cost-effectively processed is the major barrier of recycling: reclaimed carbon fibres from high-performance applications cannot be reincorporated in the same applications from which they were recovered, so new appropriate applications have to be developed in order to reuse the fibers. The mechanical properties of recycled fibers are also strictly connected to the whole recycling process. Finally, in order to achieve CFRPs closed life cycle, the reclaimed fibres CFRPs have to be transformed into reusable materials; this is possible if reclaimed fibers are re-impregnated with a new polymer matrix

and new recycled carbon fiber polymer (Re-CFRP) are produced. Therefore, the existing manufacturing processes, developed for virgin materials, must be adapted to the unique recycled-fiber form: the recycled carbon fibers in fact are usually fragmented into short lengths, as a result of size-reduction of CFRP waste before reclamation, fiber breakage during reclamation, and chopping of the fibres after reclamation. In addition, all fibre reclamation processes remove the sizing from the fibres, so the recycled is in a filamentised, random, low-density-packing (fluffy) form⁶².

During the last two decades, many different recycling techniques have been proposed and developed for thermoset composite materials: mechanical processes (mainly grinding), pyrolysis and other thermal processes such as oxidation in fluidised bed, microwave, and solvolysis. A general description of the most relevant recycling CFRPs techniques is reported in the next paragraphs.

1.4.1. Mechanical recycling

The mechanical recycling consists of breaking-down CFRP waste more finely by shredding, crushing, milling, or other similar mechanical process. First, the material is reduced to pieces in the order of 50-100 mm in size and then is ground into a finer product ranging from typically 10 mm in size down to particles less than 50 μ m in size. In the mechanical recycling process, all the constituents of the original composite are reduced in size and appear in the resulting recyclates, which are mixtures of polymer, fibre and filler. These powders made of ground composite materials can find application as a filler or reinforcement in new composite manufacturing or in construction industry (e.g. as fillers for artificial woods or asphalt, or as mineral-sources for cement). However, this technology does not recover carbon fibres but products with low-value applications; for this reason, there is no known grinding process exploited industrially to treat CFRPs. The following processes, which allow a separation of the fibres and the matrix, are preferred for CFRPs. Mechanical recycling is mostly used for glass fibre reinforced polymers (GFRPs) or thermoplastic CFRPs.

1.4.2. Pyrolysis

Pyrolysis process involves the thermal decomposition of organic molecules in an inert atmosphere (e.g. N₂ or Ar) and in absence of oxygen. When it is applied to a CFRPs, pyrolysis allows to volatilise into lower-weight molecules the polymeric matrix, while the carbon fibers remain inert and can be eventually recovered. The thermal decomposition of

the polymer chains occurs generally, when the material is heated up to 450°C to 700 °C and it leads to the formation of an oil, gases and solid products (carbon fibers, fillers and char). After pyrolysis treatment, the char contaminates the reclaimed carbon fibers, so a post-treatment in an oxidative atmosphere at 450-600°C is needed to burn it before reusing them. The best advantages of pyrolysis processes are the high retention of carbon fiber mechanical properties and the possibility to recover chemical feedstock from the polymer matrix as well as energy for an almost sustainable process. Among the CFRP recycling processes, pyrolysis have even reached an industrial scale and some CFRP pyrolysis industrial plant are already running⁶¹⁻⁶³. The experimental data of a reliable way to recover and reuse carbon fibers by pyrolysis are presented in *Chapter 4*.

1.4.3. Fluidised bed

Fluidised-bed process has been applied to the recycling of CFRPs⁶¹. This process consists in combusting the polymeric matrix in a hot and oxygen-rich flow using a fluidised bed plant. CFRPs are initially reduced in size and fed into the plan that is filled with a silica sand with a particle size of about 0.85 mm. When the sand is fluidised with a stream of hot air at temperatures in the range of 450–550°C, the resin decomposes; both the oxidised molecules and the carbon fiber filaments are carried up within the air stream, while heavier metallic components sink in the bed. The fibers are then separated from the gas stream in a cyclone, and the resin is fully oxidised into a high temperature secondary combustion chamber. The fluidised bed process does not allow recovery of chemicals from the polymer matrix but energy may subsequently be recovered from these hot combustion products. This technology reclaims clean carbon fibers having a lower strength typically 20% with retention of the original stiffness when processed at 550°C⁶¹. Conversely, mixed and contaminated materials, with painted surfaces or foam cores in composites of sandwich construction or metal insert can be treated thought this technology; for this reason fluidised bed-process is particularly suitable for end-of life waste, however it has not largely been applied to reclaim carbon fibers.

1.4.4. Solvolysis

Solvolysis consists of a chemical treatment using a solvent to degrade the resin; when the fluid is in vapour phase or has a gas-like density in the supercritical fluid state, the process is more a thermal process than a solvolysis⁶⁴. This process offers a large number of possibilities thanks to a wide range of solvents, temperature, pressure and catalysts. This

chemical method for CFRP recycling is based on a reactive medium such as a catalytic solutions, benzyl alcohol, supercritical water, under low temperature (typically $<350^{\circ}\text{C}$)^{61,64}. These reactive solvents, sometimes in mixture with a co-solvent or with a co-reactive solvent, diffuses into the composite and breaks specific bonds. It is therefore possible to recover monomers from the resin and to avoid the formation of char residues. Polyester resins are generally easier to solvolyse than epoxy resins and so require lower temperatures to be degraded. During the last decade this method has been more intensively used to recycle composites, in particular CFRP^{65,66}, as the recovery of carbon fibres has become a commercial interest. Among all the tested solvents, water appears as the most used, sometimes neat, and sometimes with a co-solvent (alcoholic, phenolic, amine)^{61,64}. Often it is used with alkaline catalysts like sodium hydroxide (NaOH) or potassium hydroxide (KOH), but less often with acidic catalysts. A few other solvents have also been used, mainly alcohols like methanol, ethanol, propanol, and acetone or even glycols, with or without additives/catalysts. Numerous lab-scale experiments have been carried out, but only a few studies have reached industrial or semi-industrial scale; in addition, some environmental issues might arise when aggressive and sometimes-toxic solvents are used^{61,64}.

Chapter 2

*New nitrogen-rich heterocycles for organo-modified bentonites as flame retardant fillers in epoxy resin nanocomposites**

***Adapted from:**

T. Benelli, E. D'Angelo, L. Mazzocchetti, F. Saraga, L. Sambri, M. Comes Franchini, L. Giorgini. *Organo-modified bentonites as new flame retardant fillers in epoxy resin nanocomposites*, *AIP Conference Proceedings* **1736** (2016) 020142.

DOI: 10.1063/1.4949717

T. Benelli, L. Mazzocchetti, E. D'Angelo, M. Lanzi, F. Saraga, L. Sambri, M. Comes Franchini, L. Giorgini. *New nitrogen-rich heterocycles for organo-modified bentonites as flame retardant fillers in epoxy resin nanocomposites*, *Polymer Engineering & Science* **57** (2017) 621-630.

DOI:10.1002/pen.24565

2.1. Introduction

In the last century, polymeric materials have greatly changed the world we live in, joining or replacing traditional metallic and natural materials. Composite materials, in particular, took steel and aluminium alloys' place in a wide range of applications, such as construction, transportation, aerospace, and electronics, thanks to their ability to produce high-quality and durable products with good physical, thermal, chemical and mechanical properties⁴. However, due to the organic nature of the polymer matrix and fibers, both natural or synthetic as nylons, polyesters and carbon fibers, composite materials suffer from poor fire resistance⁶⁷. When exposed to moderately high temperatures (300–400°C), indeed, the organic matrix decomposes producing heat, smoke, soot and toxic volatiles⁶⁷.

Fires provoke annual costs ranging around tens of billions of dollar globally, which can be estimated as approximately 1% of global annual Gross Domestic Product (GDP)^{68,69}, and fire related deaths, in the sole Europe, are reported in thousand with many more casualties suffering injuries which may be sometimes life-long. When a fire develops, most of the deaths are caused by inhalation of smoke and toxic combustion gases, carbon monoxide being the most common cause, whilst the injuries result from exposure to the heat evolved from fires. Thus, there are great economic, sociological and legislative pressures on the polymer industries to produce materials with greatly reduced fire risk.

It is worth noting that the major concern for producers of polymeric materials is not so much aimed at obtaining products that do not burn, but at the possibility to make them less ignitable and, when the case occurs that a fire is triggered, they can be flame retarded, or burn less promptly. In this context, fire retardancy, as an outstanding element of safety, is one of the key challenges. Flame retardant systems are intended to inhibit or to stop the polymeric thermal decomposition and combustion process. As a function of their nature, they can either act physically or chemically and they can interfere with the various processes involved in polymer combustion (heating, pyrolysis, ignition and propagation of thermal degradation). While the development of inherently flame retarded polymer systems appears as the most efficient way to overcome the flammability problems, this approach is not always feasible and thus, flame retardants are often a requirement in a commercial polymer formulation. The mode of action of such additives can rely on a number of different approaches, such as the reduction of the flammable gas released through a deposition of a char layer acting as physical barrier or the separation of the comburent from the combustible. Moreover, additives can also limit the heat released during the burning process in order to minimize fire propagation.

In the choice of the flame retardant its chemical nature has also to be taken in consideration because it has a non-negligible impact on the toxicity of the fumes released during material combustion⁷⁰. They, indeed, can increase the yield of released toxic gases (such as carbon monoxide), or even decompose themselves to toxic gases at high temperature⁷¹. Halogenated flame retardants, for example, although they have been among the most widely applied ones, in particular for thermoplastic and thermosetting polymers used in composite organic matrices or in electronic equipment, suffered limitations as possible sources of halogenated dioxins and dibenzofurans, which are extremely toxic compounds⁷², and they are being phased out for their adverse effects on the environment⁷³

to comply with the new environmental legislations. Recently European Community (EC) expressed concern about the use of flame retardants. Restriction of the use of certain Hazardous Substances (RoHS), for example, limits the use of different brominated compounds. According to Registration, Evaluation and Authorization of Chemicals (REACH) registry, instead, only registered flame retardant chemicals with hazard data that underwent various tests concerning emissions and possible end-of-life issues can be used⁷⁴. The World Health Organization (WHO) and the US Environmental Protection Agency (EPA) also recommend exposure limits and risk assessments of polychlorodioxins and similar compounds^{75,76}. Thus, in the last years, there is an increasing interest on the introduction of alternative flame retardants able to meet these new regulations and free from health and environmental concerns. It is worth noting, however, that these additives might affect mechanical properties of the final formulation, since it is known that they might act as plasticizers or reinforces; thus the possibility of creating an effective nanocomposite, with additional mechanical reinforcement, looks as an attractive option. In this context, a lot of efforts have been recently put forward for the preparation and the characterization of polymer matrix nanocomposites in which the dispersion of fillers within nanometric dimensions could improve dramatically the mechanical performances⁷⁷⁻⁸⁰. On the other side, the action that a flame retardant has on the resin thermal stability might also modify the behaviour upon attempt of recovering the end-of-life composite: thermal approach to this problem results indeed, one of the most successful pathway to comply with EU regulation on the recycling, and the presence of such additives might affect the process^{62,81,82}.

In this context, the introduction of boron-, phosphorus-, nitrogen-, and silicon-containing compounds into epoxy resins (e.g. for electrical insulation or as composite matrix) has been shown to be an effective way of improving their flame retardancy⁸³. Among the others, organoclays intercalated with suitable functional cations seem to be very promising for the production of nanocomposites with flame retardant properties^{19,21,42,51-56}. In addition to their low cost, by ion-exchanging the hydrated cations with organic ones, such as bulky alkylammonium salts, it is possible to obtain a more lipophilic organoclay with increased interlayer spacing. This modification helps promoting the intercalation of the polymer chains between 2D-lamellae at nanometric scale, thus increasing the specific surface of the additive and nano-scale interactions between clay and polymer matrix. Hence, even at very low filler concentration (up to 5%), the obtained polymer-layered

silicate nanocomposites (PLSNs), in addition to good flame retardant properties, might also reveal remarkable improvement of thermo-mechanical properties if compared to virgin polymer and conventional microcomposites^{19,42,56,67,84–86}. PLSNs were first reported in the literature as early as 1961, when Blumstein demonstrated polymerization of vinyl monomers intercalated into montmorillonite (MMT) clay^{87,88}, but the first mention of their potential flame retardant properties appeared in 1976 in a Unitika's Patent on Nylon-6 layered-silicate⁸⁹. Nowadays, many researchers report^{19,42,43,56,84,90–93} improvements in term of lowering peak Heat Release Rate (pHRR) for both thermoplastic and thermosetting PLSNs. The pHRR recorded by cone calorimeter, is the most important parameter that allows determining the flame rate propagation in a hypothetical fire scenario⁵⁹.

Since it is well known that nitrogen containing heterocycles show improved thermal stability and inherent fire retardancy, in particular melamine and its nitrogen-rich derivatives^{21,72,94–96}, they can be used to intercalate/exfoliate layered clays, thus imparting fire retardant characteristics to the final material. Thus, stemming from previous encouraging results⁵⁴, in the present work new organoclay-based flame retardants were developed using the same driving idea that a nitrogen rich molecule can provide intrinsic flame retardancy to the additive. Hence nitrogen-rich compounds to be used as organomodifiers, namely 6-(4-butylphenyl)-1,3,5-triazine-2,4-diamine (BFTDA) and 11-amino-N-(pyridine-2-yl)undecanamide (APUA) (Figure 15), were produced starting from a triazinic core or an aminopyridinic one, respectively, through functionalization with a medium/long alkyl chain to promote bentonite exfoliation, and subsequent acidification with HCl, trying to apply low cost reactants and mild reaction conditions. The effect on the curing, the mechanical properties and the fire behaviour of thermosetting epoxy resins were then investigated and compared both to the plain resin and the resin containing the pristine bentonite, in order to better understand the contribution of each component to the overall performance.

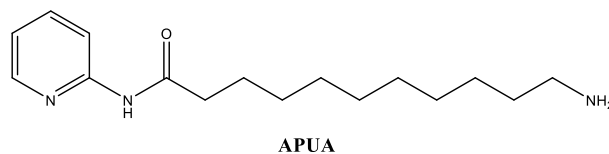
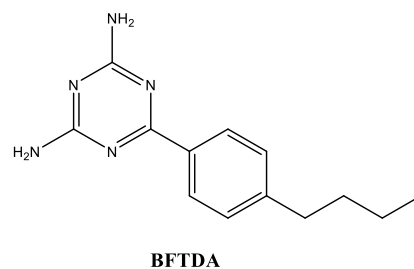


Figure 15. The synthesized and investigated N-rich heterocycles BFTDA and APUA.

2.1.1. Polymer combustion and flame retardancy

The combustion of a polymer is a very complex process that involves physical and chemical phenomena and depends on many factors such as the chemical composition, morphological structure, the shape and the size of the product, the presence of oxygen or other reactive substances, the heat and mass transfer etc⁹⁷. However, the various observed phenomena that occur, often simultaneously, during polymers combustion can be described in a qualitative and simplified way^{67,94,97}.

The combustion starts when a source of energy (radiative, convective or conductive heat) raises the temperature sufficiently to initiate the thermal degradation (pyrolysis) of the polymer chains⁹⁷; a range of volatile intermediate products and radical species are generated near the polymer surface from the scissions of molecules or atoms that are in an end-, side-, or random-chains. During the initial exposure to heat, thermoplastic polymers can soften or melt and take on new shapes by the application of heat and pressure; on contrary, the same phenomena cannot occur in thermosetting polymers.

In presence of air, when the gaseous mixture resulting from the mixing of degradation flammable volatiles with air is within the flammability limits, and the temperature is above the auto-ignition temperature, the combustion begins producing the flame. Alternatively, the ignition can also occur at a lower temperature (called the flash point) triggered by the presence of an external source of intense energy such as a flame or a spark¹⁹. If the oxygen concentration is absent or not enough, no combustion takes place but only the degradation of the polymer chains that, in many cases, leads to the formation of a solid carbonaceous residue (char).

During the combustion, the temperature of the burning polymer can be increased by the initial heat source, if it is still present, or by the heat generated from the exothermal oxidation reactions (thermal feedback). The thermal feedback in fact, provides the fuel necessary to feed the flame by increasing the volatiles rate formation; the heat released from the combustion processes can initiate further thermal degradation reactions promulgating the fuel source to sustain combustion, thus leading to flame spread^{73,94}. During the combustion, not only pyrolysis reactions but also oxidative degradations might significantly affect the volatiles rate production⁹⁷. A schematic and summarizing representation of the discussed polymer combustion processes is shown in Figure 16.

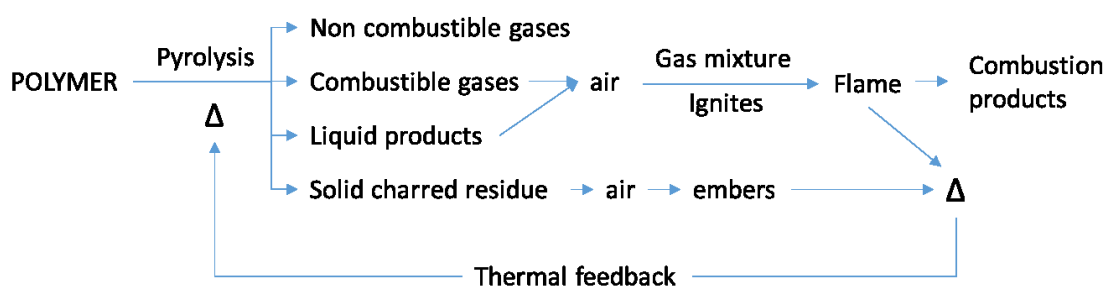


Figure 16. Schematic representation of polymer combustion processes.

A major concern for producers of polymeric materials is not so much aimed at the fact of obtaining products that do not burn, but at the possible ways to make them less ignitable and in case they are triggered, they can be flame retarded, or burn effectively less.

All flame retardant systems aim to inhibit or to stop the polymer combustion process. In function of their nature, flame retardant systems can either act physically (by cooling, formation of a protective layer or fuel dilution) or chemically (reaction in the condensed or gas phase)¹⁹. They can interfere with the various processes involved in polymer combustion (heating, pyrolysis, ignition, flame spread)^{19,58,98}. The main modes of action of flame retardant systems are:

- Reducing the released heat below that required to support combustion
- Modifying the pyrolysis process in order to reduce the amount of flammable gas and promoting the development of char, less flammable and more stable that also acts as a physical barrier between polymer and flame.
- Keep apart the flame from oxygen/air feed

- Adding halogenated additives capable of releasing atoms of chlorine or bromine when the polymer is close to its ignition temperature.
- Reducing the thermal feedback, in order to preventing or limiting other pyrolysis phenomena, by adding a heat sink in the polymer's formulation (such as $\text{Al}(\text{OH})_3$ that endothermally decomposes) or by making sure that a protective coating covers the polymer's surface with a stable char when the polymer is exposed to fire. Char is often generated by intumescent systems.
- Developing inherently flame retarded polymer systems.

Flame retardants are generally incorporated into the polymeric material during the transformation process as an additive or introduced into the polymer during synthesis (as monomers or precursor polymers) or in post-synthesis reactions (as a functionalization) in order to intrinsically improve the polymer flame behavior¹⁹.

2.1.2. Cone-calorimeter

The cone-calorimeter is one of the main apparatus used to evaluate the flame behaviour of a material^{59,71}. It was developed in the early 1980's by the National Institute of Standards and Technology (NIST) to respond to the need for a most significant bench scale instrument to study the flame behaviour of materials. The construction and use of the instrument are subject to international standards (ISO 5660 ASTM E1354, ASTM E1474, ASTM E1740, ASTM F1550, ASTM D6113, CAN ULC 135 and BS 476 Part 15)⁹⁹. The principle of cone calorimeter tests is based on the oxygen depletion that occurs during a combustion process: the heat released by burning materials is directly proportional to the quantity of oxygen consumed. According to Huggett's observation, the proportionality factor is constant from one organic material to another one and is equal to 13.1 kJ/g^{100} .

The instrument can replicate a developing fire scenario forced by external radiation and provides a comprehensive set of fire properties needed to assess material specific flame⁵⁹. In a standard cone-calorimeter test, a sample (100 x 100 x 2-50 mm) is placed on a load cell where from above a cone-shape radiant electrical heater irradiates uniformly the sample with a heat flux (in general from 10 to 100 kW/m^2). Before starting the test, a split shutter mechanism protects the sample from the irradiation and then, when the experiment starts, the shutters are opened and the sample's combustion is triggered by an electric spark. All the gases produced during the test are moved to the exhaust duct by a centrifugal fan

and a hood and a part of them is captured by a gas-sampling unit and sent to the different analysers. The gas flow, oxygen, CO and CO₂ concentrations, smoke density and mass lost are measured^{19,59}. In Figure 17, a FTT- Cone-calorimeter apparatus and a detail of the sample-holder and cone zone are illustrated.



Figure 17. FTT-Cone-calorimeter apparatus and detail of the sample-holder and the cone zone.

The main parameters provided by a cone-calorimeter test are listed below:

- Ignition time or time to ignition (TTI), which is the time elapsed between the exposure of the sample to the irradiation and its ignition triggered by the spark.
- Heat Release Rate (HRR), which represents the thermal power released over time by the sample and its maximum peak (pHRR), expressed in kW/m² and calculated from the oxygen consumption.
- Total Heat Released (THR), which is the integral of the HRR with respect to time expressed in kJ/m².
- Mass loss and mass loss rate.
- Time of flame out (TOF) which is the time elapsed between the ignition time to the flame out.

- Smoke production
- CO and CO₂ production

In conclusion, the cone calorimeter data are very useful to study the fire properties of organic materials. Currently it is largely employed in the development of fire-retarded polymers^{59,71}.

2.2. Experimental

Materials

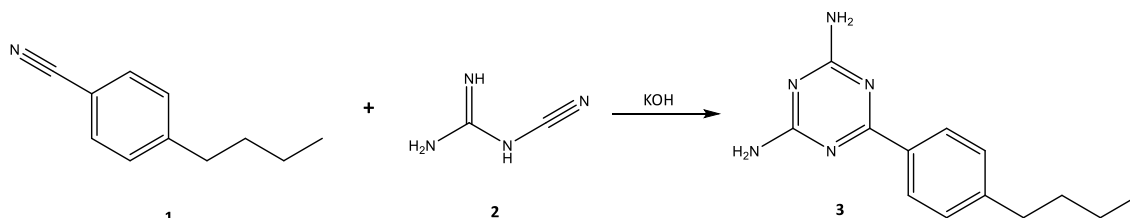
Dicyandiamide (99%, Sigma-Aldrich), 4-butyl-benzonitrile (98%, Sigma-Aldrich), 11-aminoundecanoic acid (97%, Sigma-Aldrich), di-tert-butyl-dicarbonate (BOC₂O) (97%, Alpha Aesar), 1,1'-carbonyldiimidazole (CDI) (97%, Sigma-Aldrich), 2-aminopyridine (98%, Carlo Erba) and all the other commercially available reagents and analytical grade solvents used as received, unless otherwise stated. Chromatographic purifications were performed using 70-230 mesh silica.

Tetrahydrofuran (THF) was purified and dried according to the reported procedures¹⁰¹ and stored under nitrogen.

Bentonite with Cation Exchange Capacity (CEC) of 0.874 meq/g (Sigma-Aldrich), and epoxy resin precursors ElanTech EC157/W61 Polymer/Hardener (named R and H respectively) system (Elantas Europe srl) were used as received without further purification.

Synthesis of 6-(4-butylphenyl)-1,3,5-triazine-2,4-diamine 3 (BFTDA)

The synthesis of BFTDA (**3**) was carried out according to the synthetic route depicted in Scheme 1.



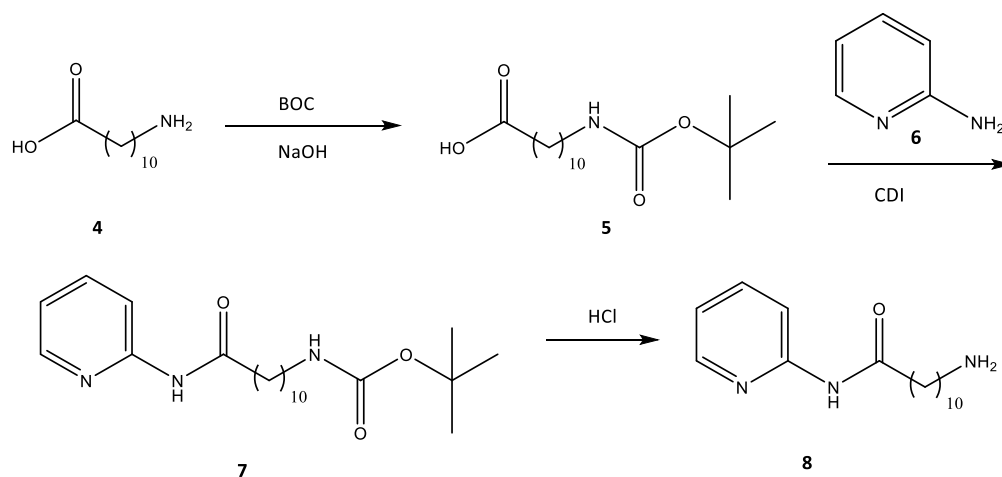
Scheme 1. Synthetic route for BFTDA (3)

4-Butyl-benzonitrile (**1**) (2.5 mL, 14.51 mmol) and dicyandiamide (**2**) (1.525 g, 18.13 mmol) were added to a solution of KOH (163 mg, 2.90 mmol) in 2-methoxyethanol (5mL)

and the resulting slurry was stirred for 5 hours under reflux. The suspension was then cooled down to room temperature and the precipitate was filtered and washed out with hot water, affording **3** as a white solid. Yield 90%. ^1H NMR (DMSO- d_6): δ 8.17 (d, 2H, $J_{\text{HH}} = 8.2$), 7.28 (d, 2H, $J_{\text{HH}} = 8.4$), 6.71 (bs, 4H), 2.63 (t, 2H, $J_{\text{HH}} = 7.6$), 1.64 – 1.51 (m, 2H), 1.39 – 1.24 (m, 2H), 0.90 ppm (t, 3H, $J_{\text{HH}} = 7.3$). ^{13}C NMR (DMSO- d_6): 170.6 (C), 167.6 (C), 146.2 (C), 134.9 (C), 128.5 (CH), 128.2 (CH), 35.2 (CH₂), 33.3 (CH₂), 22.2 (CH₂), 14.2 ppm (CH₃). ESI-MS: 244 m/z (M+1). FT-IR (ATR): 3386-3100 (ν_{CH} arom + aliph), 1699 ($\nu_{\text{C=O}}$ amide), 1674-1494 (δ_{NH} ammonium salt and amide, ν_{CH} arom) cm^{-1} .

Synthesis of 11-amino-N-(pyridine-2-yl)undecanamide 8 (APUA)

The synthesis of APUA (**8**) was performed according to the synthetic route depicted in Schema 2. A detailed description of each reaction step follows.



Scheme 2. Synthetic route for APUA (8).

Synthesis of 11-[(tert-butoxycarbonyl)amino]undecanoic acid 5

Di-tert-butyl-dicarbonate (Boc₂O) (12.36 mL, 53.63 mmol) was added to a suspension of 11-aminoundecanoic acid (**4**) (10.86 g, 49.75 mmol) in dioxane (50 mL) under nitrogen atmosphere and the solution was cooled down up to 0°C in an ice bath. Then a 2M NaOH aqueous solution (25.40 mL) was added dropwise with a syringe and the reaction mixture was stirred for 24h under reflux. After the addition of water (100mL), the resulting solution was extracted twice with ethyl ether (2x60 mL); then the aqueous phase was acidified with a solution of citric acid (25%) up to pH 5 and extracted with ethyl acetate (3x100 mL). The two organic phases were collected, dried and the solvent was removed by rotary evaporator and vacuum pump affording **5** as a white solid. Yield 96%. ^1H NMR (CDCl₃): δ 4.5 (bs,

2H), 3.09 (t, 2H, $J_{HH} = 6.9$), 2.35 (t, 2H, $J_{HH} = 7.4$), 1.69 – 1.56 (m, 2H), 1.51– 1.39 (m, 11H), 1.32 – 1.25 ppm (m, 12H). ^{13}C NMR (CDCl_3): δ 179.0 (C), 156.0 (C), 79.0 (C), 34.0 (CH_2), 30.0 (CH_2), 29.4 (CH_2), 29.25 (CH_2), 29.16 (CH_2), 29.12 (CH_2), 29.0 (CH_2), 28.4 (CH_3), 26.7 (2CH_2), 24.7 ppm (CH_2).

Synthesis of tert-butyl (11-oxo-11-(pyridin-2-ylamino)undecyl)carbamate 7

In a 250 ml dry round flask, a solution of 1,1'-carbonyldiimidazole (CDI) (2.62 g, 27.87 mmol) in anhydrous THF (20 mL) was added under nitrogen atmosphere to a solution of **5** (7.00 g, 23.22 mmol) in anhydrous THF (25 mL) and left to stir at 25°C for 90 minutes until a brick red solution was obtained. Then a solution of 2-aminopyridine (**6**) (4.52 g, 27.87 mmol) in toluene (75 mL) was added and the mixture was left to stir overnight under reflux. Then the solvent was removed by rotary evaporation and the reaction mixture dissolved in EtOAc (100ml). The organic phase was washed with aqueous saturated NaHCO_3 (3x50 mL), and evaporated. The crude product was purified by column chromatography (SiO_2 , hexane/EtOAc 70:30 v/v as eluent) giving **7** as a white solid. Yield 68%. ^1H NMR (CDCl_3): δ 8.84 (bs, 1H), 8.34 – 8.21 (m, 2H), 7.81 – 7.73 (m, 1H), 7.08 (ddd, 1H, $J_{HH} = 0.8$, $J_{HH} = 5.2$, $J_{HH} = 7.3$), 4.54 (bs, 1H), 2.95-3.10 (m, 2H), 2.43 (t, 2H, $J_{HH} = 7.4$), 1.79 – 1.64 (m, 2H), 1.50 – 1.41 (m, 11H), 1.37 – 1.23 ppm (m, 12H). ^{13}C NMR (CDCl_3): δ 172.1 (C), 156.0 (C), 151.5 (C), 146.3 (CH), 139.3 (CH), 119.5 (CH), 114.5 (CH), 79.0 (C), 40.6 (CH_2), 37.0 (CH_2), 34.0 (CH_2), 29.9 (CH_2), 29.26 (CH_2), 29.1 (CH_2), 29.0 (CH_2), 28.97 (CH_2), 28.4 (CH_3), 26.6 (CH_2), 25.2 ppm (CH_2).

Synthesis of 11-amino-N-(pyridin-2-yl)undecanamide 8

Concentrated HCl (37%) (6.25 mL, 13 eq.) was added dropwise to a solution of **7** (2.30 g, 5.90 mmol) in ethyl acetate (25 mL) at room temperature and the mixture was left to stir vigorously for 1h. Solvent was reduced to 2 volumes by rotary evaporation and a 2M aqueous solution of ammonia (30 mL) was added. A white precipitate was formed and then filtered and washed with a water solution of NaHCO_3 (30 mL). The product **8** was obtained as a white solid with a yield of 97%. ^1H NMR (CDCl_3): δ 8.83 (bs, 1H), 8.20 – 8.15 (m, 2H), 7.63 (ddd, 1H, $J_{HH} = 1.9$, $J_{HH} = 7.3$, $J_{HH} = 8.5$), 6.95 (ddd, 1H, $J_{HH} = 1.1$, $J_{HH} = 4.8$, $J_{HH} = 7.3$), 2.63 (t, 2H, $J_{HH} = 7.0$), 2.51 (bs, 2H), 2.32 (t, 2H, $J_{HH} = 7.4$ Hz), 1.70 – 1.56 (m, 2H), 1.45 – 1.33 (m, 2H), 1.32 – 1.11 ppm (m, 12H). ^{13}C NMR (CDCl_3): δ 172.2 (C), 151.9 (C), 147.7 (C), 138.4 (CH), 119.6 (CH), 114.3 (CH), 41.9 (CH_2), 37.8 (CH_2), 33.0 (CH_2), 29.4 (CH_2), 29.33 (CH_2), 29.30 (CH_2), 29.26 (CH_2), 29.14 (CH_2), 26.7 (CH_2), 25.2 ppm

(CH₂). ESI-MS: 278 m/z (M + 1), 300 m/z (M + Na). FT-IT (ATR): 3300-3100 (ν_{NH}, ammonium salt), 3050-2800 (ν_{CH} arom), 2920 and 2851 (ν_{CH} aliph), 1699 (ν_{C=O} amide), 1612-1419 (δ_{NH} ammonium salt and amide, ν_{CH} hetero-arom) cm⁻¹.

Preparation of BENTO-APUA and BENTO-BFTDA organoclays

APUA (**8**) or BFTDA (**3**) (1.5 eq. with respect to bentonite CEC) was dissolved in tetrahydrofuran (the minimum quantity needed) by magnetic stirring and a solution of 6M hydrochloric acid (about 1.5 μL per APUA or BFTDA mmol) was slowly added until the mixture became clear. Then THF was removed by rotary evaporator and the solid salt dissolved in a water/ethanol 1/1 solution (about 6 mL per APUA or BFTDA salt mmol). This mixture was finally added to an homogeneous suspension of Bentonite in a solution of water/ethanol 2/1 (20 mL per gram of bentonite), heated up to 65°C and left overnight under vigorous mechanical stirring. Then the warmed solution was filtered and the solid washed with a hot solution of water and ethanol 1/1. The complete removal of chlorides was checked by titration of the basified water (pH 10) with silver nitrate in presence of K₂CrO₄ (Mohr method). The obtained organoclay was then dried in an oven at 65°C for two days and pulverized in a planetary mill Pulverisette 4 (400 rpm for 3 minutes).

Bento-APUA: FT-IR (ATR): 3627 (ν_{OH}, bentonite structural OH), 3050-2800 (ν_{CH}, arom. and aliph.), 1630 (δ_{OH}, bentonite water), 1652-1419 (δ_{NH}, ammonium salt and amide, ν_{CH} hetero-arom), 1040 (ν_{Si-O}, bentonite), 525 (δ_{Si-O-Al}, bentonite) cm⁻¹.

Bento-BFTDA: FT-IR (ATR): 3626 (ν_{OH}, bentonite structural OH), 2962-2865 (ν_{CH} arom. and aliph.), 1630 (δ_{OH}, bentonite water), 1652-1419 (δ_{NH} ammonium salt and amide, ν_{CH} arom), 1040 (ν_{Si-O}, bentonite), 525 (δ_{Si-O-Al}, bentonite) cm⁻¹.

Preparation of BENTO-APUA and BENTO-BFTDA epoxy nanocomposites

The synthesized organoclay (BENTO-BFTDA or BENTO-APUA) was dispersed via solventless mechanical mixing and further sonication in the epoxy prepolymer ElanTech EC157 (R) (70g) in different amount in order to obtain, upon addition of the amine hardener Elantech W61 (H), final formulations which contain 3 or 5%wt of nanofiller (samples named R-Bento-BFTDA-3 and -5, and R-Bento-APUA-3 and -5). The hardener (H) (R:H = 100:17 by weight) was then added and the mixture was stirred until the system appeared homogenous. The mixture was then poured in the aluminum molds (with six 200x5x2mm parallel cavities or one 100x100x3mm cavity), treated with a commercial

releasing agent and cured according to the optimal curing cycle reported in the datasheet: 24h in isotherm at 40°C, then the temperature was constantly raised up to 120°C in an 8h timespan and finally the mold was kept isothermally at 120°C for further 6h. Once the mold reaches room temperature, the resin stripes and plates were released. The epoxy nanocomposites were named R-*x-y*, where *x* represents the added organoclay (that is bentonite, or APUA/BFTDA functionalized bentonite) and *y* represents the overall amount of nanofiller in the sample (3 or 5%wt). For the sake of comparison, a neat epoxy resin samples R+H, named NEAT, was also produced.

Characterization

¹H and ¹³C NMR spectra were obtained at room temperature, on 5-10% w/v CDCl₃ or DMSO solutions, using a Varian Inova (300 MHz for ¹H) and Varian MercuryPlus VX 400 (¹H, 399.9; ¹³C, 100.6 MHz) spectrometers. Chemical shifts (δ) are reported in ppm relative to residual solvent signals for ¹H and ¹³C NMR (¹H NMR: 7.26 ppm for CDCl₃ and 2.50 ppm for DMSO; ¹³C NMR: 77.0 ppm for CDCl₃ and 39.5 ppm for DMSO). ¹³C NMR spectra were acquired with ¹H broad band decoupled mode. Coupling constants are given in Hz.

FT-IR spectra were recorded on a Bruker Alpha Platinum-ATR spectrophotometer equipped with ATR Diamond window (32 scans, 4 cm⁻¹ resolution, 4000-400 cm⁻¹ spectral window).

ESI-MS analysis were performed by direct injection of acetonitrile solutions of the compounds using a WATERS ZQ 4000 mass spectrometer.

Thermogravimetric (TGA) measurements were carried out using a TA Instruments SDT-Q600 (heating rate 10°C/min) on 10 mg samples under air atmosphere (flow rate 100 ml/min).

Tensile tests were carried out at room temperature with an Instron-type tensile testing machine (REMET TC10), with crosshead speed of 5 mm/min and initial gauge length of 25 mm on samples of size 70×5×2 mm. For each data point, five specimens were tested for each sample to obtain a reliable average and standard deviations for all the mechanical properties.

Dynamic mechanical analysis (DMA) was performed with a NETZSCH 242 E Artemis analyser in three point bending configuration, with 1 Hz oscillation frequency and 20 mm oscillation amplitude set, heating from RT up to 150°C (heating rate 3°C/min).

Wide-angle X-ray diffraction measurements (WAXS) were carried out at room temperature with a PANalytical X'Pert PRO diffractometer equipped with an X'Celerator detector (for ultrafast data collection). A Cu anode was used as X-ray source (K radiation: $\lambda = 0.15418$ nm, 40 kV, 40 mA), and $\frac{1}{4}^\circ$ divergence slit was used to collect the data in 2θ range from 2° to 60° .

Flame behaviour studies were performed using an oxygen consumption calorimeter (Fire Testing Technology Limited FFT Cone Calorimeter model). The tests were performed at an incident Heat flux of 25 kW/m² in horizontal orientation using the cone shaped heater and specimens of 100×100×3 mm (Figure 19). The instrument can work with a heat flow ranging between 5 and 100 kW/m², the higher irradiation levels give better reproducibility, more clearly defined ignition, and shorter measurement times, but correspond to more fully developed fires. Often a smaller irradiation level better fits to the fire protection goals, since it accounts for the material behaviour in a condition close to the starting of a fire, showing its ability to ignite and propagate. Three samples were tested per resin formulation. The Cone Calorimeter provides the following parameters: Heat Release Rate (HRR), calculated from the oxygen consumption, Time To Ignition (TTI), Time of Flame out (TOF), Average Heat Release Rate (HRR as a function of time), peak of Heat Release Rate (pHRR), Total Heat Release (THR) and Time To pHRR (TTP). Experimental data were reproducible to within $\pm 10\%$. The Average Heat Release Rate is correlated to the heat released in a room where the flammable materials are not all ignited at the same time. Two other parameters were calculated separately: the Fire Performance Index (FPI) since it is related to the time available for flashover, and the Fire Growth Rate Index" (FIGRA). These two parameters have been evaluated as they have been accepted as representative of the polymer combustion behavior in a real fire^{21,59}.

2.3. Results and Discussion

Synthesis and characterization of Pristine Bentonite and Organoclays

In order to obtain new flame retardants based on organoclay, bentonite, which is an aluminium phyllosilicate clay consisting mostly of montmorillonite with Calcium and

Sodium ions coordinated inside the interstitial planes, was used as a low cost inorganic starting material. By exchanging the original interlayer cations for organocations indeed, an organophilic surface consisting of covalently linked organic moieties is generated, allowing a better dispersion of this filler in a polymeric matrix. The organic molecules used for ion-exchange need a polar residue, which allows the interaction with the aluminium silicate surface, and an apolar tail, which is responsible of the lipophilic properties. Hence, good clay modifiers which can provide also flame retardant capacity are represented by quaternary ammonium salts bearing long aliphatic chain (more than C10), such as alkyltrimethylammonium chloride^{51,88}. In this context, recently, it was demonstrated that an organoclay modified with a nitrogen rich melaminic derivative functionalized with long aliphatic chains, namely N2,N4-dihexadecyl-1,3,5-triazine-2,4,6-triamine (DEDMEL)⁵⁴, was able to provide an encouraging decrease of 20% in the peak heat released rate (pHRR). The reported synthetic process⁵⁴, besides requiring severe experimental conditions, proved to be difficult to control in terms of number of substitution of the aminic protons.

In order to pursue an efficient and mild synthetic approach, the attention was directed towards the synthesis of a novel similarly N-rich triazine derivative, such as 6-(4-butylphenyl)-1,3,5-triazine-2,4-diamine (BFTDA) (Figure 14). Since previous work highlighted also the positive effect of simple octadecyltrimethylammonium salt (OTAB) on the flame behavior of an intrinsically flammable polymer matrix, a novel compound deriving from a linear aliphatic amine bearing an aminopyridinic N-rich group was also produced, such as 11-amino-N-(pyridine-2yl)undecanamide (APUA) (Figure 14). BFTDA was obtained via a low-cost one-pot 2+3 cycloaddition of dicyandiamide on nitrile groups (Scheme 1) with simple purification steps and high yield (90%). APUA, instead, was synthesized via nucleophilic addition of 2-aminopyridine to 11-aminoundecanoid acid upon protection of amino group with di-tert butyl-dicarbonate (Schema 2).

¹H- and ¹³C-NMR analysis of the synthesized compounds and intermediates are in agreement with the expected structures (See Experimental section).

Once the organic modifiers were successfully obtained, two organophilic clays, based on acidified BFTDA and APUA and labelled Bento-BTFDA and Bento-APUA respectively, were synthesized with an ion exchange process starting from pristine bentonite. X-Ray Diffraction (XRD) analysis of the pristine and modified bentonites (Figure 18) shows an increase in the interlayer basal spacing upon modification (Table 3), accounting for the

occurrence of the ion-exchange, and thus the insertion of the organic modifiers, although the presence of the XRD reflection signifies that the clay is not fully exfoliated.

Table 3. Samples identification and composition

Sample	Composition
NEAT	Pure epoxy resin
R-Bento-3	Epoxy resin + pristine bentonite 3%wt
R-Bento-BFTDA-3	Epoxy resin + Bento-BFTDA 3%wt
R-Bento-APUA-3	Epoxy resin + Bento-APUA 3%wt
R-Bento-5	Epoxy resin + pristine bentonite 5%wt
R-Bento-BFTDA-5	Epoxy resin + Bento-BFTDA 5%wt
R-Bento-APUA-5	Epoxy resin + Bento-APUA 5%wt

Moreover, the extent of such modification of the basal spacing depends strongly on the organomodifier used for the exfoliation process, and in particular, APUA derivative displays a better interaction between the bentonite's lamellae and the organic molecules, possibly owing to the presence of the longer flexible aliphatic chain and to a low steric hindrance.

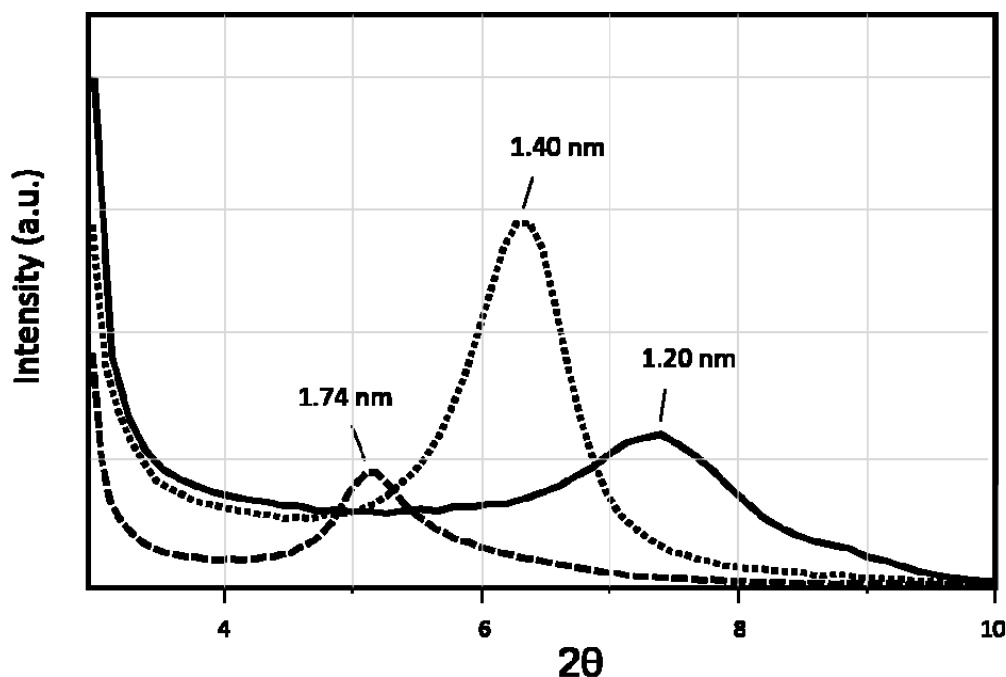


Figure 18. XRD diffractograms of the pristine Bentonite (-----) and of the organo-modified Bento-APUA (.....) and Bento-BFTDA (- - -)¹.

In order to assess the real content of organic substitution within the inorganic layers, both the obtained organoclays and pristine bentonite were characterized by TGA (Figure 19).

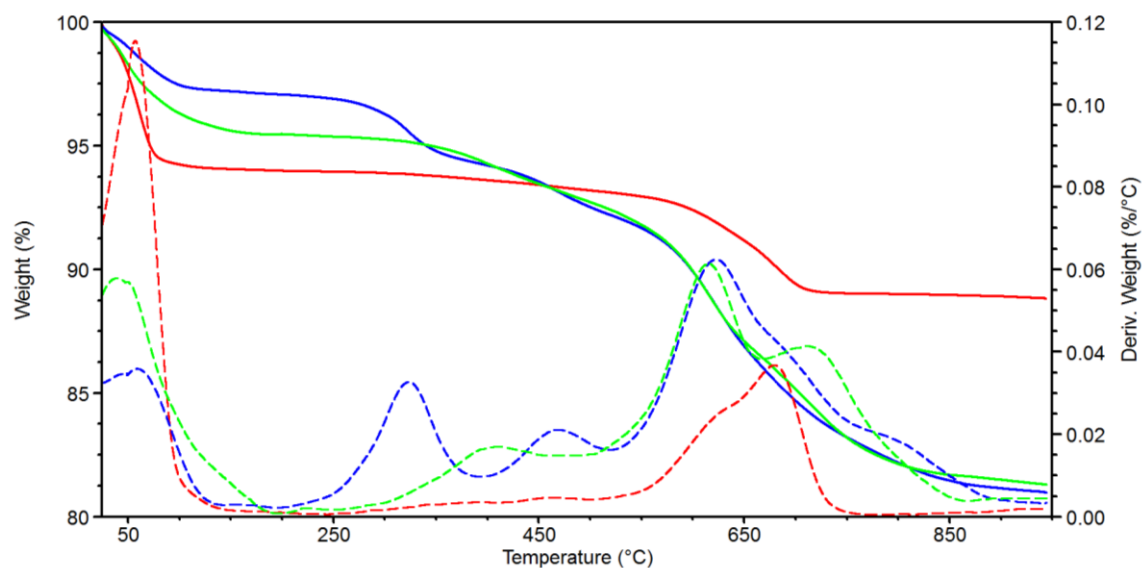


Figure 19. TGA (solid lines) and DTG (broken lines) thermograms of: (a) pristine bentonite (—), (b) Bento-APUA (—), and (c) Bento-BFTDA (—)¹.

As reported in literature¹⁰², the unmodified bentonite shows two main weight losses (Figure 18 and Table 4). The first one (5.9%) occurs below 200°C and is ascribed to the desorption of free absorbed water residing between montmorillonite crystallites (dehydration); the second one is due to the loss of water due to dihydroxylation of the aluminosilicate lattice (5.2%) that occurs around 650°C.

Table 4. Characterization data of bentonite, bento-APUA and bento-BFTDA.

Sample	XRD d_{001} ^a (nm)	Weight loss from 25 to 200°C (%wt) ^b	Weight loss from 200 to 950°C (%wt) ^c	Organic modifier (%wt) ^d	Organic modifier (mmol/g) ^e
Bentonite	1.20	5.9	5.2	-	-
Bento-APUA	1.74	4.2	16.1	10.9	0.394
Bento-BFTDA	1.40	2.8	14.2	9.0	0.370

^a Interlayer basal spacing determined by XRD.

^b Weight loss determined by TGA in air (heating rate 10°C/min) from RT to 200°C.

^c Weight loss determined by TGA in air (heating rate 10°C/min) from 200 to 950°C.

^d Weight loss determined by TGA subtracting the bentonite weight change in the range 200-950°C (5.2 %wt) from the organoclays weight changes in the range 200-950°C.

^e Molar content of organic modifier (mmol of APUA or BFTDA) for 1 gram of organoclay.

Both these weight loss events are evident also in the modified bentonites thermograms, where they might also account for some residual absorbed volatile solvent, in addition to the ones characteristic of the degradation of the organic compounds used for the clay modification. Thus, TGA analysis allowed the evaluation of the organic fraction present in the organoclay, upon assumption that the weight loss below 200°C is not structure

related and can be thus be disregarded from the calculation. Then, it was taken into account the typical weight loss due to dihydroxylation, estimated in 5.2% for the pristine bentonite, and considered to occur even in the organomodified clays, and it was thus evaluated that the organic content is 9.0% wt in Bento-BFTDA and 10.9% wt in Bento-APUA, corresponding to 0.370 mmol of BFTDA and 0.394 mmol of APUA for 1 g of organoclay (mmol/g), respectively (Table 4).

This similar degree of substitution achieved for the organomodified bentonites allows for a significant comparison of the performances of the two organoclays that were thus used to prepare epoxy resin thermoset nanocomposites, starting from commercial components. Epoxy resins are widely used as polymer matrix in composites production^{3,4,6,103} and in electrical/electronic manufacturing and improving their poor fire resistance is thus of paramount importance¹⁰⁴. The application of a fire retardant, however, should not detrimentally affect both the curing process and the overall mechanical performance.

The obtained organoclays were directly dispersed (3 and 5%wt) in the epoxy oligomeric prepolymer component (Elantech EC157, so-called R) via solventless mechanical mixing followed by sonication to produce the relative epoxy prepolymer mixtures; the hardener (Elantech W61, called H) was added to the mixture at a later time (R:H5100:17 by weight). The mixtures were cured according to the suggestions from technical datasheet to produce the four desired organoclay nanocomposites (Table 3). A plain resin sample, obtained from the mixture of R and H (sample named NEAT), and two nanocomposites containing the 3%wt or 5%wt of pristine non-modified bentonite (samples named R-Bento-3 and -5) were also produced for the sake of comparison (Table 3). All the nanocomposites preserve a good transparency even with the higher (5wt%) loading of organoclay (Figure 20), meaning that a good dispersion occurred.



Figure 20. A cone-calorimeter sample of R-BentoAPUA-5.

All the obtained nanocomposites were characterized by infrared spectroscopy in order to assess the presence of the organ modifiers. No significant trend could be observed in the spectra (not shown), which is however not that surprising since, even in the most loaded nanocomposites (5%wt) only about 10%wt of the added nanofiller is the organic fraction providing significant infrared absorptions.

All the obtained nanocomposites were analyzed by DSC in order to assess the efficacy of the curing process¹⁰⁵: the absence of any exotherm transition in the whole range of temperature investigated confirmed that the curing process can be considered almost complete, however no stepwise transition, typical of a glass transition, could be easily detected in the thermograms. Hence, in order to measure the glass transition temperature (T_g) of the resins, DMA analysis was also carried out, showing just a slight increase in the glass transition (T_α) when pristine or organoclay modified bentonite is present in the thermoset in the lower amount, i.e. 3%wt (T_α in Table 5), as a consequence of the hindered chain mobility due to the contact between the crosslinked polymer backbone and the

organomodified clay nanosheets that not only limits molecular mobility, but also broadens the relaxation time spectrum due to stronger interactions.

Table 5. Thermal properties of the obtained nanocomposites.

Sample	T_{α} (°C) ^a	$T_{\max \text{ deg}}$ (°C) ^b	Residue (%wt) ^b
NEAT	126	330	0
R-Bento-3	129	334	2.97
R-Bento-BFTDA-3	128	333	2.74
R-Bento-APUA-3	129	333	2.31
R-Bento-5	127	332	5.04
R-Bento-BFTDA-5	126	335	4.43
R-Bento-APUA-5	126	334	4.43

^a Determined by DMA in three point bending deformation mode at 1Hz frequency oscillation, 20 μ m oscillation amplitude set from RT to 150°C (heating rate 3°C/min).

^b Determined by TGA carried out in air from RT to 600°C (heating rate 10°C/min).

A higher concentration of the nanofillers (5%wt), however, does not affect significantly the position of the DMA α relaxation, and this might account for the presence of not perfectly dispersed organoclay clusters imparting a plasticizing effect to the material which counteracts the previously discussed mobility hindrance action. It can be thus hypothesized that there is a threshold value up to which the nanocomposite might benefit from the nanofillers addition, while above this value some drawbacks set in.

All the nanocomposites were also analysed by TGA in oxidizing atmosphere (Table 5), showing (Figure 21) a slight enhancement of the maximum degradation temperature ($T_{\max \text{ deg}}$) increasing the amount of nanofiller. Furthermore, it is worth noting that all the organoclays containing samples display an inorganic clay solid residue at the end of the TGA run, whose amount well compares with the weight fraction of nanofiller in the feed, taking into account also the degradation of the organic fractions due to APUA and BFTDA. As expected, no residue was detected for the plain resin NEAT (Table 5 and Figure 21).

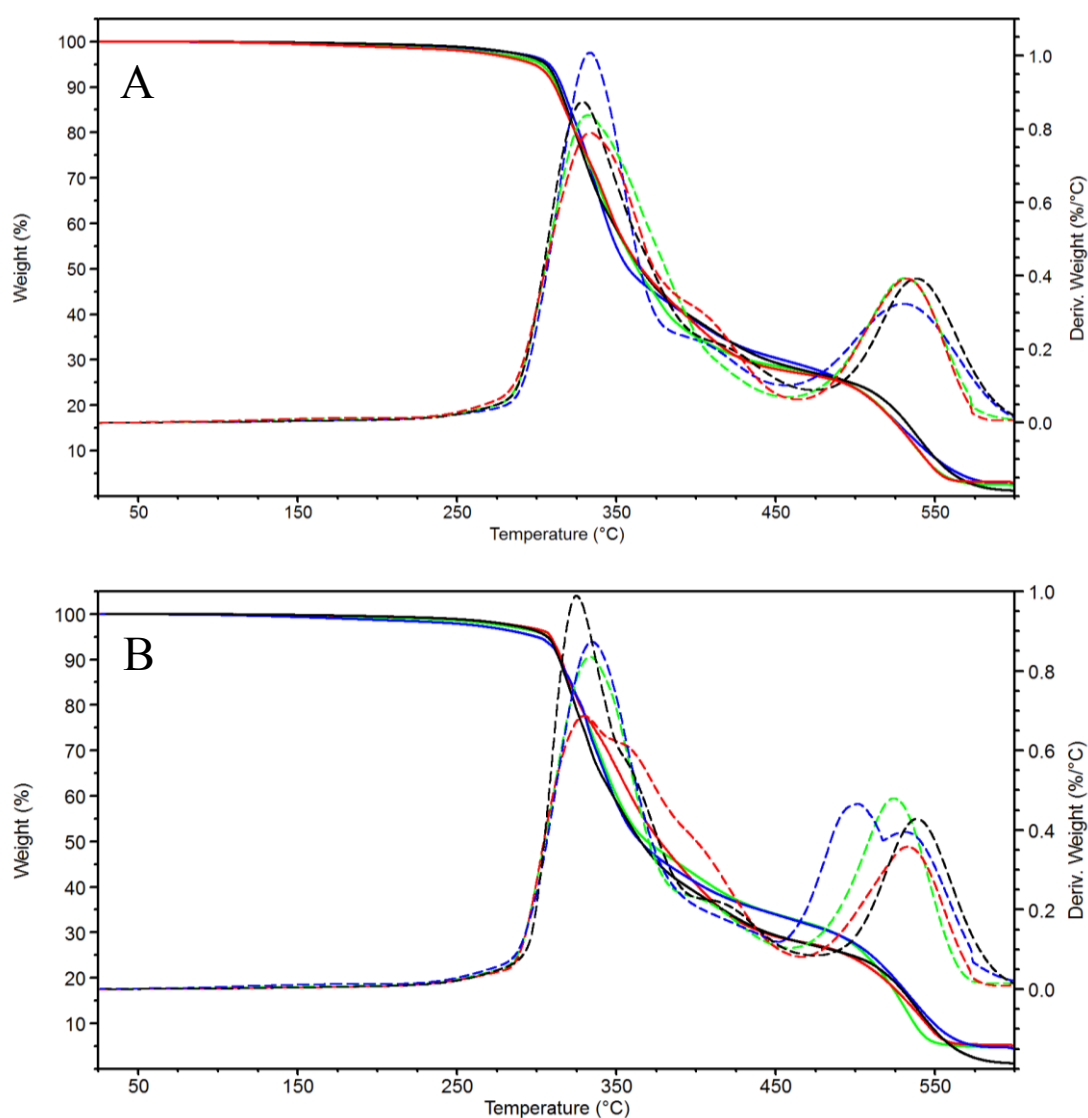


Figure 21. TGA (solid lines) and DTG (broken lines) thermograms of: reference plain epoxy resin NEAT (—), R-Bento (—), R-Bento-BFTDA (—), and Bento-APUA (—) at 3 wt% (A) and 5 wt% (B) load in the nanocomposites¹.

Mechanical tests were carried out in tensile mode in order to provide comparative properties of the plain and modified resins, in terms of Young's Modulus (E), ultimate tensile strength (σ_b) and ultimate tensile strain (ϵ_b). The obtained data (Table 6) show a slight increase of Young's Modulus with the addition of 3%wt of both the plain bentonite and organoclays, while it stays constant in the sample containing 5%wt of nanofillers. This trend is mimicking the one previously discussed for glass transition (see T_g in Table 5) and similarly can be ascribed to the molecular mobility hindrance due to the interaction of the epoxy structure with the reinforcements which helps stiffen the material, i.e. raising E ; however, once reached a given threshold value, the nanofillers are no more homogeneously

dispersed, and their aggregation plasticizes the nanocomposites. This further observation thus strengthens the hypothesis that there is a maximum filler load up to which thermomechanical properties might increase: once this limit is reached, then the performance of the nanocomposite starts to drop down.

Table 6. Mechanical properties of the obtained nanocomposites.

Sample	Young's modulus (GPa)	σ_b (MPa)	ϵ_b (%)
NEAT	1.7 ± 0.1	67 ± 11	6 ± 1
R-Bento-3	1.8 ± 0.1	64 ± 6	4.5 ± 0.6
R-Bento-BFTDA-3	1.81 ± 0.05	63 ± 4	4.3 ± 0.4
R-Bento-APUA-3	1.8 ± 0.1	61 ± 5	4.3 ± 0.3
R-Bento-5	1.7 ± 0.1	40 ± 6	2.9 ± 0.5
R-Bento-BFTDA-5	1.7 ± 0.1	46 ± 9	3.3 ± 0.7
R-Bento-APUA-5	1.7 ± 0.1	47 ± 3	3.2 ± 0.2

No improvement in tensile strength is observed by incorporation of 3%wt organoclays while, for the nanocomposites loaded with 5%wt of organoclays, the ultimate strength drops. The ultimate strain at failure usually decreases when a stiffer filler is added. Thus, as expected, the elongation at break of the investigated nanocomposites with different fillers (Bento, Bento-APUA and Bento-BFTDA) significantly decreases by increasing weight percentage of clay and organoclays. The reduction in both failure strength and strain of polymer/clay nanocomposites is usually attributed to the poor dispersion of the filler in polymer matrix (i.e. agglomeration of the clay in polymer matrix) and lack of strong interfacial interaction^{18,106}. Overall, the addition of these flame retardants seems to slightly improve the composites thermomechanical performances with a 3%wt nanofillers fraction, while a higher extent of modification, i.e. 5%wt of organoclay, leads to a drop in the properties. Finally the flame behaviour of all the produced samples was assessed by cone calorimeter (Table 7), which is one of the most effective bench-scale methods for studying the flammability properties of materials⁵⁹. Tests were carried out with a heat flow of 25KW/m² (about 600°C) which can be roughly compared to a small-scale fire; the results presented here are averages of three runs for each sample. Analyzing the fire behavior of the tested materials, the ignition time (TTI) is almost constant, with no significant variation in the average performance. However results (Table 7 and Figure 21 and Figure 22) show also that the addition of the plain bentonite to the epoxy resin formulation leads to a worse flame behavior than the pristine resin: both R-Bento-3 and -5 show, indeed, a higher peak

Heat Release Rate (pHRR) and an increment of Heat Release Rate (HRR), Fire Propagating Index (FPI) and Fire Growth Rate Index (FIGRA).

Table 7. Data recorded in cone-calorimeter experiments at a heat flux of 25 kW/m².

Sample	TTI (s)	TOF (s)	THR (MJ/m ²)	Mass Loss (g/m ²)	HRR (kW/m ²)	pHRR (kW/m ²)	TTP (s)	FPI ^a (kW/m ² s)	FIGRA ^b (kW/m ² s)
NEAT	141	488	74.3	3070	128	932	199	6.6	4.7
R-Bento-3	150	482	74.0	3040	134	1094	204	7.3	5.4
R-Bento-BFTDA-3	140	520	74.1	3080	136	966	192	6.9	5.0
R-Bento-APUA-3	138	523	74.7	3130	149	772	188	5.6	4.1
R-Bento-5	158	578	88.1	3640	164	1192	210	7.5	5.7
R-Bento-BFTDA-5	145	621	82.2	3410	136	998	188	6.9	5.3
R-Bento-APUA-5	139	476	74.2	3100	163	814	188	5.8	4.3

^a Calculated as pHRR/TTI.

^b Calculated as pHRR/TTP.

Such a behaviour can be tentatively ascribed to some catalytic effect deriving from the presence of metals and acid sites in the pristine bentonite, able to promote thermal degradation of the organic thermoset fraction in the applied conditions. The addition of Bento-BFTDA nanofillers, both at 3 and 5%wt, leads to a significantly improvement of the flame retardant properties (pHRR, FPI and FIGRA) of the nanocomposites if compared with plain R-Bento, but they are still worse than plain resin (NEAT): the N-rich BFTDA is not enough to compensate the negative influence that the clay imparts in terms of flame behaviour. The best results were obtained instead by Bento-APUA containing nanocomposites (Table 7 and Figure 22 and Figure 23): an encouraging decrease of 17% and 29% in pHRR with respect to the plain resin (NEAT) and to the plain R-BENTO-3, respectively, indeed, was obtained already at 3 %wt loading level of organoclay. Increasing the content of BENTO-APUA to 5%wt the measured pHRR decreases of 13% and 32% with respect to the plain resin (NEAT) and to the plain R-BENTO-5, respectively.

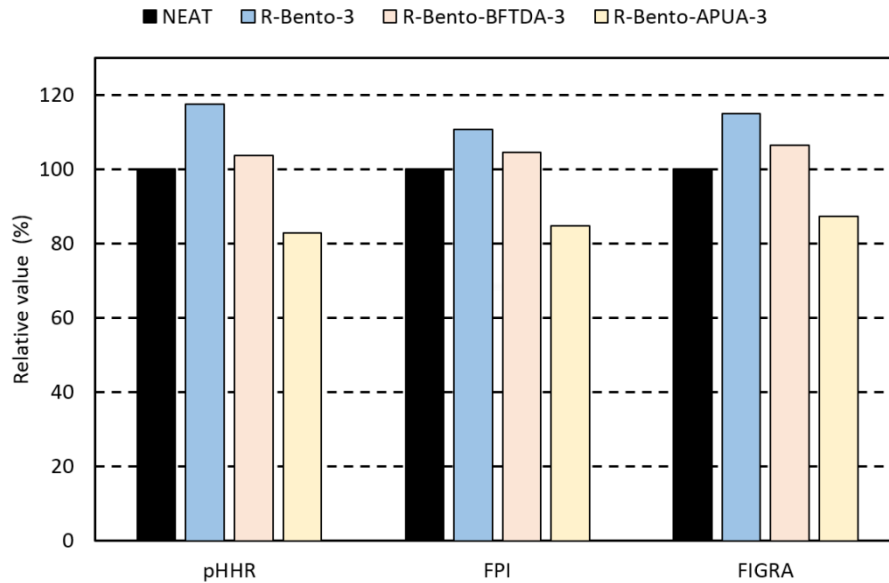


Figure 22. Flame behaviour of the composites obtained with the addition of 3%wt of plain bentonite, Bento-BFTDA and Bento-APUA, expressed as % variation with respect to the pristine resin (NEAT), taken as 100% reference¹.

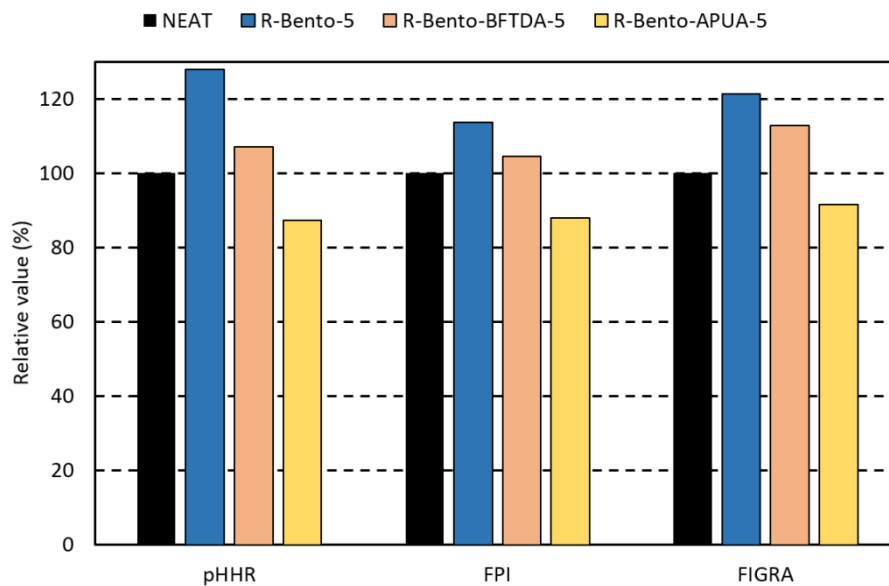


Figure 23. Flame behaviour of the composites obtained with the addition of 5%wt of plain bentonite, Bento-BFTDA and Bento-APUA, expressed as % variation with respect to the pristine resin (NEAT), taken as 100% reference¹.

Such a behaviour suggests that the material will contribute less to the development and propagation of a fire: though releasing the same amount of heat, the process takes place more gradually and with lower peak intensity. For these materials, it will be more difficult to propagate the ignition of new fires and thus helping the containment of the existing one.

The presence of Bento-APUA leads also to a decrease of both FPI and FIGRA indexes (Figure 22 and Figure 23), an overall sign that the material tends to be less prone to fire

propagation. In particular FIGRA is helpful in ranking the materials in terms of potential fire safety because it combines the most intense heat release (pHRR) and time to achieve it (Time To Peak, TTP)⁹².

However, only the whole HRR curve (Figure 24) can adequately represent the specific fire behavior of each polymeric materials (char yield, effective heat of combustion, etc.), the influences from the specimen (thickness, deformation, etc.) and the physical and chemical mechanisms active during the burning (increasing and cracking char layer, endothermic reactions, release of different pyrolysis products, afterglow, etc.).

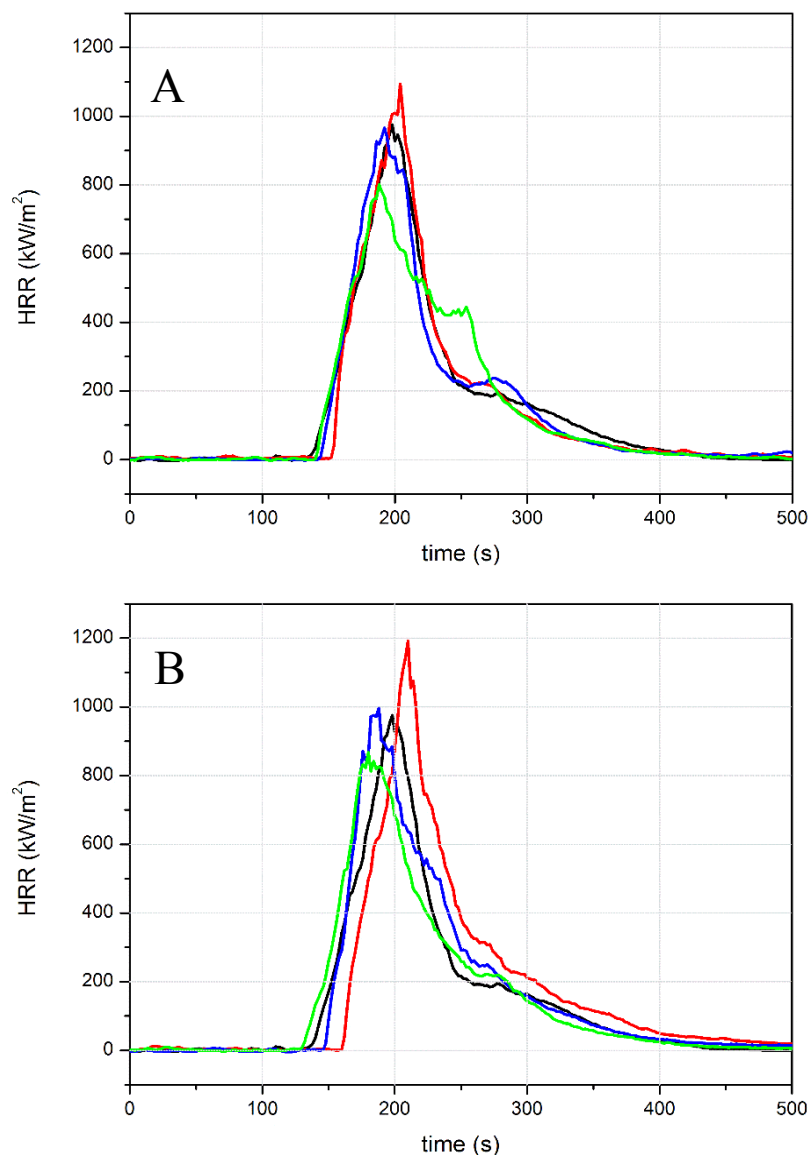


Figure 24. Heat Release Rate (HRR) profiles measured by cone-calorimeter of the investigated nanocomposites: R-Bento (—), R-Bento-APUA (—) and R-Bento-BFTDA (—) at 3%wt (A) and 5%wt (B) of fillers compared to reference plain epoxy resin (—).

In Figure 24, the HRR curves of all the analyzed samples are compared on the basis of the amount of nanofillers (3%wt in Figure 24A; 5%wt in Figure 24B). All the samples show the presence of an initial peak typical of polymeric materials that forms char upon burning: the char formation thickens with time and slows down the ability to release further heat since it inhibits the gaseous fuel transport from the polymer to the flame front thereby reducing the HRR of the burning surface.

While the organoclay nanofillers do not modify the way the sample is burning, they (in particular Bento-APUA) help reducing the effect of such fire. In fact, during decomposition the investigated N-rich heterocycles release nitrogen which inhibits the spread of flames and the generation of toxic smoke: it is accepted that the formation of inert gases dilutes the fuel ones and improves flame retardant behaviour of the organoclay epoxy resin nanocomposites.

Worth noting is that the nanofillers concentration which helps the most in improving the nanocomposite's fire behaviour is the same that also provides the best thermo-mechanical performances.

2.4. Conclusions

Two new organoclays were prepared from the modification of bentonite with nitrogen-based organic compounds BFTDA and APUA and used for the preparation of epoxy resin nanocomposites. The obtained nanocomposites do not display any detrimental effect on the curing process of the thermosets, on the thermal properties and, in the lower amount (3%wt), helps to improve the thermo-mechanical properties of the polymeric matrix. The flame behavior of the obtained nanocomposites was assessed by cone-calorimeter measurements showing that the addition of pristine bentonite leads to an increased flammability of the composite with respect to the plain resin. The bento-BFTDA organoclay leads to a decreased flammability of the composite with respect to the pristine bentonite containing epoxy resin, but its flame behavior is quite similar to the plain resin. The APUA-containing nanocomposites show instead an encouraging decrease of 17% and 29%, in the Peak Heat Release Rate (pHRR) with respect to the plain resin (NEAT) and to the plain R-BENTO-3, respectively, with just a 3 %wt loading level; moreover a reduction of both FPI and FIGRA indexes, an overall sign that the material tends to be less prone to propagating the fire is observed. In this case, it is worth noting that the same amount of nanofillers which helps improving thermomechanical performances is the same that

provides the best fire behavior. These preliminary results are very promising, showing a potential for the application of the selected APUA-modified organoclays as flame retardants, though the actual dispersion of the nanofillers is still to be optimized, in order to attain better mechanical properties together with an improved flame retardant behavior.

Chapter 3

Synthesis and characterization of highly bio-based epoxy resins derived from aromatic lignin derived diols for polymer composites

3.1. Introduction

The uncertainty of data about the available petroleum reserves and other fossil resources (natural gas and coal) as well as the environmental issues related to their continuous consumption have increased the interest of industry and academia to look for alternative, renewable (non-fossil) resources. In addition, the intensive use of these nonrenewable resources has led to a significant release of carbon dioxide, which has a negative contribution to climate changes on the planet due to the greenhouse effect¹⁰⁷.

Nowadays, epoxy-based resins are almost totally petroleum based and make up about 70 % of the thermosetting polymer market: approximately, 90 % of epoxies are synthesized via reaction of bis(4-hydroxyphenylene)-2,2-propane (known as bisphenol A, BPA) and 1-chloroprene 2-oxide (known as epichlorohydrin) in presence of NaOH^{6,108}. The aromatic rings of BPA confer high glass transition temperatures (T_g s) and high glassy moduli (E') at 25°C as well as excellent resistance to chemicals and solvents, when polymerized with an appropriate curing agent^{6,109}. Other cured-epoxy resins advantages such as high corrosion resistance, low shrinkage, and excellent adhesion properties to a wide variety of substrate materials (fillers, reinforcing fibers, metals) and the absence of volatile components during and after cure, play a decisive role in electronics, adhesives, flooring and composites industries^{4,110}. In particular, the global demand on epoxy resin was estimated at roughly \$21.5 billion (USD) in 2016 and, according the latest forecast, the market value will reach \$27.5 billion (USD) by 2020 and increase to \$37.3 billion (USD)

by 2025¹¹¹. Strongest demand is expected from epoxy composite market and epoxy adhesive market¹¹¹.

However, BPA was first studied as synthetic estrogenic agents for clinical use in the 1930s^{112,113}; in recent year, new researches on very-low-dose exposure to BPA demonstrated that BPA may act as an endocrine disruptor interfering with the body's endocrine system and producing adverse developmental, reproductive, neurological, and immune effects in both humans and wildlife^{114,115}. BPA is currently banned for use in baby bottles and cups in Canada, in the European Union, and in more than ten states in the United States of America^{116,117}. However, it is still widely used for all other applications. By contrast, in order to avoid the human exposure to significant levels of BPA, derived by leaching from resins and food and beverage can coatings, research is now focused on finding alternative BPA-free materials, possibly from renewable resources. The use of renewable resources for epoxy-based resins has the potential to decrease their toxicity attributes and environmental impacts.

In order to replace BPA- and petroleum-based epoxies in composite materials, bio-based epoxy resins must have high T_g s (usually greater than 90 °C), relatively short curing times, and adequate mechanical and chemical resistant characteristics. T_g is a fundamental parameter in composite materials as it establishes the maximum use temperatures of the final product^{4,7}. In the last two decades, many renewable resources have been investigated to obtain either partially or fully bio-based epoxy resins. Nature offers numerous opportunities for recovering platform molecules and monomers and assembling structural and functional epoxies. Currently, the most used resources for this purpose are organic agricultural products, by-products, and waste, including bio-transformed products such as fermentation derivatives or products of the microbial activity. Several researches have been reported on the synthesis of bio-based epoxy resins from various renewable resources such as vegetable oils, polyphenols, tannins, cardanol, lignin, starch, sugar, terpenes, terpenoids, and resin acids: the most relevant researches have been collected in recent paper reviews^{108,118,119} and their better properties and potential applications were summarized¹²⁰. All these molecule-precursors need to be epoxidized: the epoxidation reaction involves the use of epichlorohydrin that, despite being traditionally synthesized via a multistep pathway starting with propylene⁶, can, nowadays, be 100 % bio-based¹²¹. In literature, some examples of epoxy resins produced from bio-based epichlorohydrin, which is synthesized from glycerol, a by-product of the biodiesel industry^{122,123}, have been

already reported. However, many of the reported research demonstrate cured, bio-based epoxy resins with low T_g temperatures^{124,125}, high melting point temperatures (T_m s) or very long curing times; all this makes their application in composites manufacturing processes incompatible and problematic.

Among all the potential bio-based epoxy resins resources, lignocellulosics, containing cellulose, hemicellulose, and lignin, are very interesting as they are one of the most abundant renewable resources present on the earth¹²². In particular, lignin is one of the most abundant constituents in lignocellulosics¹²⁶: only the pulp and paper industry produces annually over 50 million tons of lignin as processing waste¹²⁷. Lignin allows for recovering renewable single aromatic chemicals that are well suited for the development of high-performance bio-based- epoxy^{128,129}. However, due to the strong combination of lignin with cellulose and hemicellulose, research on the strategic depolymerisation of lignin and the isolation of high-value specialty platform chemicals has recently become the centre of interest for scientists and industries worldwide: many methods for efficiently isolating suitable lignin-derivatives have already developed^{130,131}.

The Prof. Stanzione's research group has been actively working on the utilization of woody biomass as an alternative chemicals feedstock, the development of next-generation lignocellulosic biorefineries, and bio-based polymers and composites. In a recent work¹³², they reported different lignin derived aromatic diols used for the production of renewable epoxy thermosets. In particular, a bio-based bisphenolic BPA analogue, diglycidyl ether of the bisguaiacol (DGEBG), and three single aromatic diglycidyl ethers from vanillyl alcohol (DGEVA), gastrodigenin (DGEGD), and hydroquinone (DGEHQ) have been synthesized. All these diglycidyl ethers, cured with stoichiometric amounts of an aliphatic diamine, 4,4'-methylenebis(cyclohexyl)amine, have been characterized and their properties compared with two petroleum-based commercial resins, EPON 828 and EPON 862. The simplified structures of these molecules are reported in Figure 25.

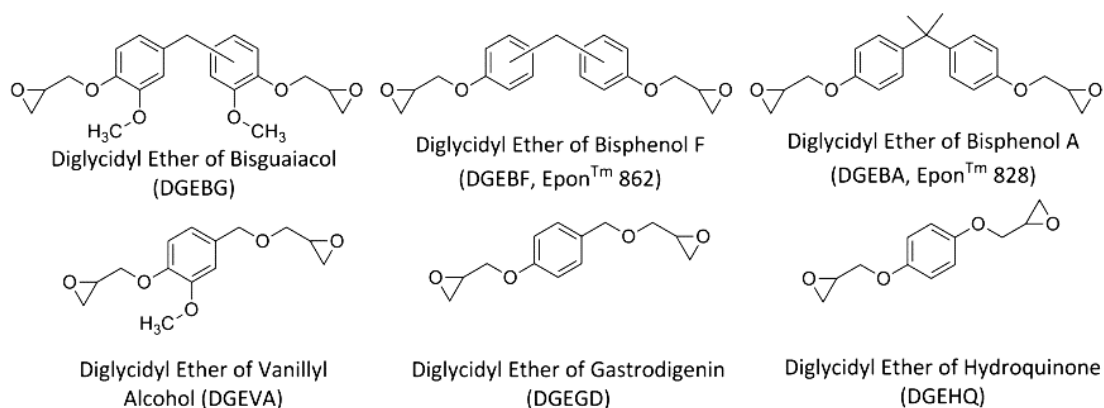


Figure 25. Simplified structures of molecules used in a previous study. (All epoxy resins are shown where $n = 0$)¹³².

Cured epoxy resins displayed high T_g 's and storage moduli at 25 °C even with an aliphatic diamine and a relative short cure cycle (8 hours) have been used. Among these discussed bio-based diglycidyl ethers, the DGEVA and the DGEGD seem suitable for future application in composites manufacturing: the first is a white solid having a low T_m (53 °C) and the second is a clear liquid at room temperature. In addition, vanillyl alcohol (VA) and gastrodigenin (GD) are potential bio-based platform chemicals for the production of epoxy resins. VA is an aromatic diol that can be produced with relatively high yields by reducing the vanillin (4-Hydroxy-3-methoxybenzaldehyde); vanillin is a well-known, pleasant smelling aromatic compound that occurs naturally in the pods of the vanilla plant (*Vanilla planifolia*) and currently, is widely synthesized from the lignin-by-products of the pulp and paper industry^{133,134}. Interestingly, gastrodigenin and its oxidized form, 4-hydroxybenzaldehyde, can be found in an orchid known as *Gastrodia elata*¹³⁵, making these molecules other potential bio-based platform chemicals for the production of epoxy resins.

Recently, the possibility to produce epoxy resins from single aromatic diglycidyl ethers such as vanillyl alcohol, vanillic acid, and methoxyhydroquinone was also reported by Fache et al.¹³⁶; in this work, the authors obtained vanillin-based resins with promising thermomechanical properties and T_g 's in the range of 80 to 110 °C; however they cured these resins with isophoronediamine, another cycloaliphatic diamine.

In this context, with the aim to improve the thermomechanical properties of bio-based resins, it was of interest to cure DGEVA and DGEGD in presence of an aromatic diamine, the diethylmethylbenzenediamine, EPIKURE W. With the future prospective to use these bio-based resins in composites manufacturing in replacement of conventional commercial

epoxy-matrices, all the obtained cured resins data have been compared to the EPIKURE W cured-EPON 828 resin and to the PACM-cured ones¹³². This research was carried out in collaboration with Professor Stanzione during a period of research spent at Rowan University as a visiting PhD student.

3.2. Experimental

Materials

Vanillyl alcohol (VA, 4-hydroxy-3-methoxybenzyl alcohol, 99 %), gastrodigenin (GD; 4-hydroxybenzyl alcohol, 99 %), tetraethylammonium bromide (TEAB, 99+ %), tetrabutylammonium bromide (TBAB, 99+ %), epichlorohydrin (≥ 99 %) and chloroform-d (CDCl₃, 99.8 atom % d) were purchased from Sigma-Aldrich. Methylene chloride (DCM, 99.9%) and a 50% w/w NaOH(aq) solution were purchased from Fischer Scientific. EPIKURE W curing agent (diethylmethylbenzenediamine, DEMBDA) and EPON 828 Resin (Diglycidyl Ether of Bisphenol A – EPON828), EEW=190 g/eq, was obtained from Momentive Specialty Chemicals, Inc. Compressed argon (Ar, 99.999%) and compressed nitrogen (N₂, 99.998%) were purchased from Praxair. All chemicals were used as received.

Synthesis of Diglycidyl Ether of Vanillyl alcohol (DGEVA) and Gastrodigenin (DGEGD).

DGEVA and DGEGD were synthesized as previously reported by Hernandez et al¹³². A three-neck round bottom flask equipped with a reflux condenser, constant pressure dropping funnel, inlet for dry argon gas, an overhead mechanical mixer, and thermometer was charged with vanillyl alcohol (VA, 30.8 g, 0.20 mol) or gastrodigenin (GD, 30.0 g, 0.24 mol), epichlorohydrin (for VA, 149 g, 8.0 mol; for GD, 179 g, 8 mol), and tetrabutylammonium bromide (for VA, 6.48 g, 0.020 mol; for GD, 7.79 g, 0.024 mol) before heating to 60 °C for 6 h with constant stirring. The flask was cooled using an ice bath to ~ 0 °C before adding dropwise a 33 wt % NaOH (aqueous; 65 ml for VA, 79 ml for GD) solution and allowed to slowly warm to room temperature over the course of 12–24 h; the synthetic route is depicted in Scheme 3. Using appropriate amounts of chemicals, the reaction mixture was dissolved in DCM, partitioned thrice with water, dried over sodium sulfate, and concentrated under reduced pressure. The crude products were purified by flash chromatography (SiO₂, hexane/EtOAc from 70:30 to 50:50 v/v as eluent). The purification allows to collect DGEVA (yield=70-75%), DGEGD (yield=70-72%) and

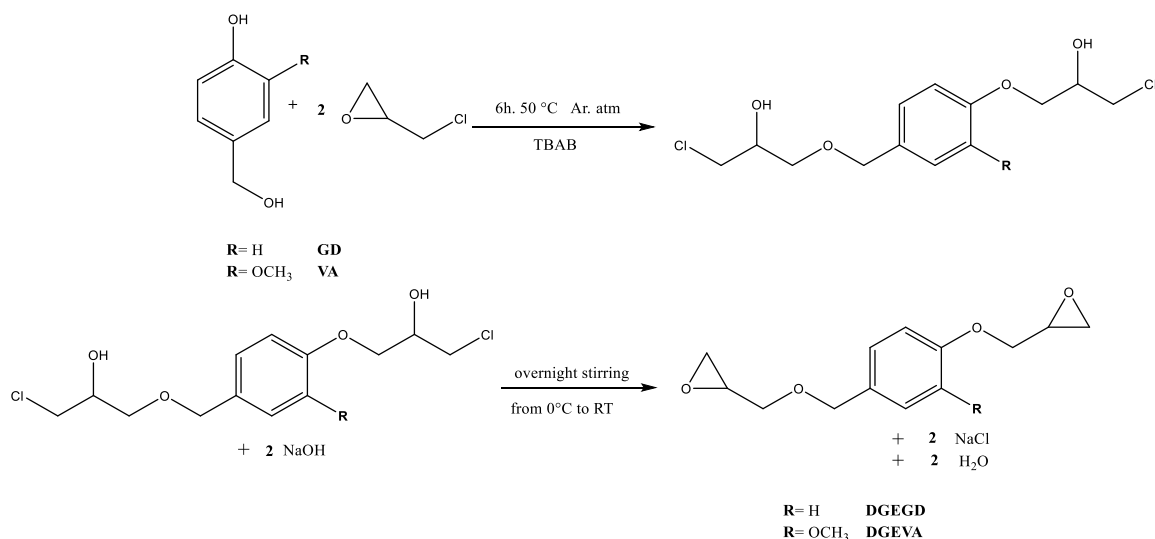
their related monoglycidyl derivatives 3-methoxy-4-(oxiran-2-ylmethoxy)phenyl)methanol (yield=25-30%), here called monoglycidyl ether of vanillyl alcohol (MGEVA) and (4-(oxiran-2-ylmethoxy)phenyl)methanol (yield=15-20), here called monoglycidyl ether of gastrodigenin (MGEGD) (Figure 26).

Diglycidyl Ether of Vanillyl Alcohol (DGEVA) (C₁₄H₁₈O₅). White solid, mp. 53–55 °C. ¹H NMR (CDCl₃): δ 2.61 (1 H, dd), 2.74 (1 H, dd), 2.80 (1 H, dd), 2.89 (1 H, dd), 3.15–3.21 (1 H, m), 3.36–3.40 (1 H, m), 3.40 (1 H, dd), 3.76 (1 H, dd), 3.88 (3 H, s), 4.03 (1 H, dd), 4.23 (1 H dd), 4.52 (2 H, q), 6.82–6.87 (1 H, m), 6.88–6.91 (1 H, m), 6.92 (1 H, d). ¹³C NMR (CDCl₃): δ 44.43 (-CH₂), 45.09 (-CH₂), 50.34 (-CH-), 51.02 (-CH-), 56.07 (-CH₃), 70.47 (-CH₂), 70.85 (-CH₂), 73.29 (-CH₂), 111.78 (ArCH-), 114.05 (ArCH-), 120.47 (ArCH-), 131.74 (ArC-C-), 147.78 (ArC-O-CH₂), 149.83 (ArC-O-CH₃). HRMS (m/z, TOF FD+) calculated: 266.115. Found: 266.114.

Diglycidyl Ether of Gastrodigenin (DGEGD) (C₁₃H₁₆O₄). Colorless liquid. ¹H NMR (CDCl₃): δ 2.60 (1 H, dd), 2.75 (1 H, dd), 2.79 (1 H, dd), 2.90 (1 H, dd), 3.15–3.19 (1 H, m), 3.32–3.37 (1 H, m), 3.40 (1 H, dd), 3.73 (1 H, dd), 3.95 (1 H, dd), 4.21 (1 H, dd), 4.51 (2 H, q), 6.87–6.93 (2 H, m), 7.24–7.30 (2 H, m) ppm. ¹³C NMR (CDCl₃): δ 44.48 (-CH₂), 44.88 (-CH₂), 50.28(-CH-), 51.04(-CH-), 68.94 (-CH₂), 70.75 (-CH₂), 73.07 (-CH₂), 114.71(2xAr=CH-), 129.58 (2x Ar=CH-), 130.74 (Ar=C-CH₂-), 158.34 (Ar=C-O-) ppm. HRMS (m/z, TOF FD+) calculated: 236.105. Found: 236.106.

Monoglycidyl Ether of Vanillyl Alcohol (MGEVA) (C₁₁H₁₄O₄). White solid, mp. 53–55 °C. ¹H NMR (CDCl₃): δ 2.74 (1 H, dd), 2.88 (1 H, dd), 3.32–3.41 (1 H, m), 3.88 (3 H, s), 4.05 (1 H, dd), 4.22 (1 H dd), 4.61 (2 H, s), 6.82–6.87 (1 H, m), 6.80–6.95 (3 H, m). ¹³C NMR (CDCl₃): δ 44.12(-CH₂), 50.02 (-CH-), 55.87 (-CH₃), 70.45 (-CH₂), 72.89 (-CH₂), 113.18 (ArCH-), 114.65 (ArCH-), 120.71 (ArCH-), 131.47 (ArC-C-), 147.98 (ArC-O-CH₂), 149.93 (ArC-O-CH₃) ppm.

Monoglycidyl Ether of Gastrodigenin (MGEGD) (C₁₀H₁₁O₃). White solid. ¹H NMR (CDCl₃): 2.77 (1 H, dd), 2.91 (1 H, dd), 3.32–3.37 (1 H, m), 3.96 (1 H, dd), 4.21 (1 H, dd), 4.61 (2 H, s), 6.87–6.93 (2 H, m), 7.24–7.30 (2 H, m). ¹³C NMR (CDCl₃): δ 44.08 (-CH₂), 50.18 (-CH-), 68.71 (-CH₂), 71.70 (-CH₂), 114.51(2xAr=CH-), 129.78 (2x Ar=CH-), 130.24 (Ar=C-CH₂-), 158.01 (Ar=C-O-) ppm.



Scheme 3. Synthesis route for DGEVA and DGEDG.

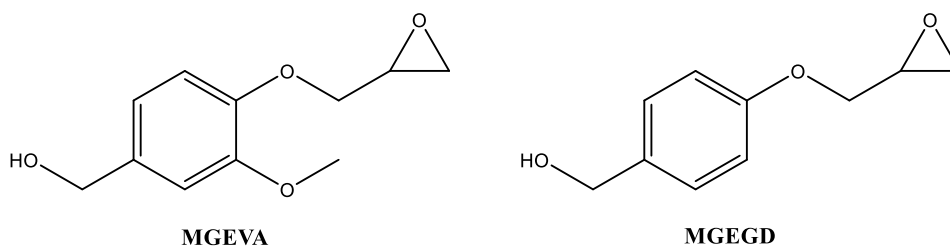


Figure 26. Monoglycidyl Ether of Vanillyl Alcohol (MGEVA) and Gastrodigenin (MGEGD)

Preparation of cured-epoxy resins samples

The synthesized epoxy resins, DGEDG and DGEVA, and a commercial epoxy resin, Epon828, were cured by adding a stoichiometric amount of EPIKURE W, a commercial curing agent, as reported below:

- Epon828/EPIKURE W 100:23 wt/wt%
- DGEDG/EPIKURE W 100:38 wt/wt%
- DGEVA/EPIKURE W 100:33 wt/wt%

Once the curing agent was added, the resins were mixed carefully and heated at 50-55°C to decrease the viscosity. The resins were then poured into an aluminum mold having four cavities with uniform dimensions (75 × 13 × 3.5 mm³) and cured in oven for 3h at 100°C and 2h at 180°C. The cured samples were removed from the oven and allowed to cool to room temperature and then cut and shaped to uniform dimensions for the different

characterizations. Following this curing process, all samples were transparent, indicating the lack of macroscopic phase separation (Figure 28).

Characterization

The synthesized diglycidyl ethers were characterized by ^1H NMR (400.15 MHz, 32 scans at 298 K) and ^{13}C NMR (111 MHz, 512 scans at 298 K) using a Varian 400 MHz FT-NMR Spectrometer.

High resolution mass spectrometry (TOF HRMS) was used to determine the exact mass of the molecules, and spectra were recorded on a Waters GCT Premier High Resolution Time of Flight Mass Spectrometer using liquid injection field desorption ionization (LIFDI) with a voltage field ramped to 1.2 kV and the filament current increased to 50 mA.

The viscoelastic properties of the cured epoxy-diamine thermosets were measured using a TA Instruments Q800 DMA. Each sample was prepared with uniform dimensions of $35 \times 11 \times 2 \text{ mm}^3$ and tested using single cantilever geometry. The tests were performed at a frequency of 1.0 Hz, a deflection amplitude of oscillation of $7.5 \mu\text{m}$, and a Poisson's ratio of 0.35. The heating ramp rate for each test was $2 \text{ }^\circ\text{C}/\text{min}$ from 20 up to $240 \text{ }^\circ\text{C}$. Each batch of samples was analysed in double to ensure consistency with the measured data. The E' onset, E'' peak and $\tan \delta$ peak values were determined for each resin. The T_g was measured as the peak of the loss modulus curve (E''). This value is considered a conservative assignment of T_g as opposed to the peak of the $\tan \delta$ curve. Additionally, the peak of E'' coincides more closely with the inflection of the storage modulus curve (E'). The standard errors for modulus and T_g are $\pm 0.2 \text{ GPa}$ and $\pm 3 \text{ }^\circ\text{C}$, respectively.

The thermogravimetric properties of the cured resins were measured using a TA Instruments Discovery Thermogravimetric Analyzer (TGA-550). Approximately 5-10 mg of sample was placed in a platinum pan and heated to $700 \text{ }^\circ\text{C}$ at a rate of $10 \text{ }^\circ\text{C}/\text{min}$ in N_2 or air atmosphere (45 ml/min balance gas flow rate and 25 ml/min sample gas flow rate). Thermogravimetric properties including the initial decomposition temperature (IDT), temperature at 50% weight loss ($T_{50\%}$), and temperature at maximum decomposition rate (T_{max}), are reported both in nitrogen and air atmosphere. Char content is reported as residue at $700 \text{ }^\circ\text{C}$ under nitrogen atmosphere.

DSC experiments were performed by using a differential scanning calorimeter TA Instrument Discovery DSC 2500. The calorimeter was calibrated using indium as standard.

Each sample (4–6 mg) was heated two times according to a temperature program of 10 °C/min in the range comprised between 25 and 250 °C. A cooling ramp of 20 °C/min was used between the two heating ramps. The reported data are taken from the second scan.

Cured resins densities at room temperature were measured using Archimedes' principle. The standard error for density is $\pm 0.01 \text{ g/cm}^3$.

3.3. Results and Discussion

In order to obtain suitable bio-based epoxy resins for composites applications, two high performance bio-based epoxy precursors, as already reported in literature¹³², were synthesized and cured with a different curing agent having a single aromatic ring, the diethylmethylenediamine (EPIKURE W). The previous aliphatic used curing agent molecular structures, the PACM, and the new aromatic one, EPIKURE W, are shown in Figure 27.

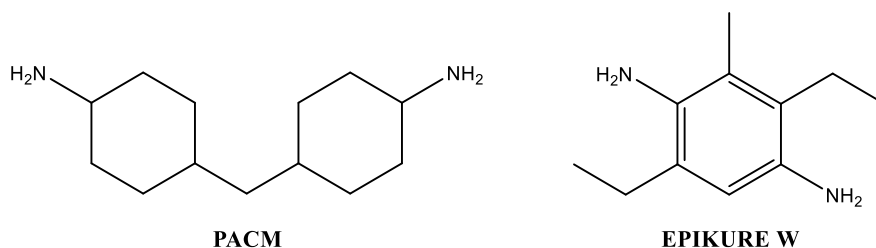


Figure 27. The commercial curing agent molecular structures: PACM and EPIKURE W.

Synthesis and characterization of epoxy resins

A well-known industrial method for preparing glycidyl derivatives involves the use of epichlorohydrin; compounds having hydroxyl groups or aromatic amine groups react with epichlorohydrin in the presence of an alkali metal hydroxide allowing to recover glycidyl derivatives with high yield. An excess of epichlorohydrin minimizes the formation of higher molecular weight epoxy oligomers and acts as a reactive solvent eliminating the need for additional solvents in the synthesis; finally, the unreacted epichlorohydrin can be recovered via distillation, and the epoxy brine washed with water to remove salts formed.

In this work, the DGEVA and the DGEGD were produced following the synthesis route reported in a previous work¹³², as shown in the Scheme 3. This process produces predominantly diglycidyl ethers with a negligible concentration of high molecular weight oligomers which can be easily eliminated by flash chromatography. Thus it was possible to obtain the diepoxidized products DGEVA and DGEGD with high yield (70–85%) and

the related monoglycidyl derivatives MGEVA and MGEGD (yield 15–30%) (Figure 26). The formation of these last ones is due to the higher acidity of the aromatic hydroxyl group that results more reactive with epichlorohydrin with respect to the aliphatic one¹³². The chemical structures of DGEVA, DGEGD, MGEVA and MGEGD were confirmed by ¹H- and ¹³C-NMR analysis (see Experimental section).

Preparation and characterization of cured-epoxy resins

As reported in the Experimental section, the synthesized bio-based epoxy resin precursors, DGEGD and DGEVA, were cured by adding a stoichiometric amount of the single aromatic ring commercial curing agent EPIKURE W. A commercial BPA-based epoxy resin, EPON828 were cured in the same way in order to compare its thermo-mechanical properties respect with the two bio-based resins. Additionally, it was demonstrated^{109,137} that the epoxy-amine stoichiometric affects the final material properties and better properties can be obtained when a stoichiometric composition is used to cure similar resin system^{109,137}.

The stoichiometric curing agent amount was calculated based on the Epoxy Equivalent Weights (EEWs) of neat resins and the Amine Hydrogen Equivalent Weight (AHEW) of EPIKURE W. The EEWs of the DGEVA, DGEGD and EPON828, as previous determined¹³² according to the ASTM D1652, are 133 g/eq., 119 g/eq. and 190 g/eq. respectively. For the DGEVA and the DGEGD, the EEWs are equal to the theoretical value, because any oligomer fraction was removed by chromatography purification and the diepoxy purities was also confirmed by ¹H and ¹³C NMR analysis. The theoretical EPIKURE W AHEW ($AHEW_{EPIKURE\ W}$) is 44.6 g/eq, based on its high purity, molecular weight and considering four amine active hydrogens.

All the resins were cured using a two-step curing program: 100 °C for 2h and 180 °C for 2h. This cure cycle is shorter than the one used in the previous work¹³², but it is adopted to assess the attitude of these bio-based epoxy systems to cure in relatively short time, making them better candidates for industrialization scale up. After curing, all the resins became transparent-yellowish, hard cross-liked polymers (Figure 28). In order to clarify the thermo-gravimetric behavior and thermo-mechanical properties of these cured epoxy-resins, DSC, TGA and DMA experiments, respectively, were performed.

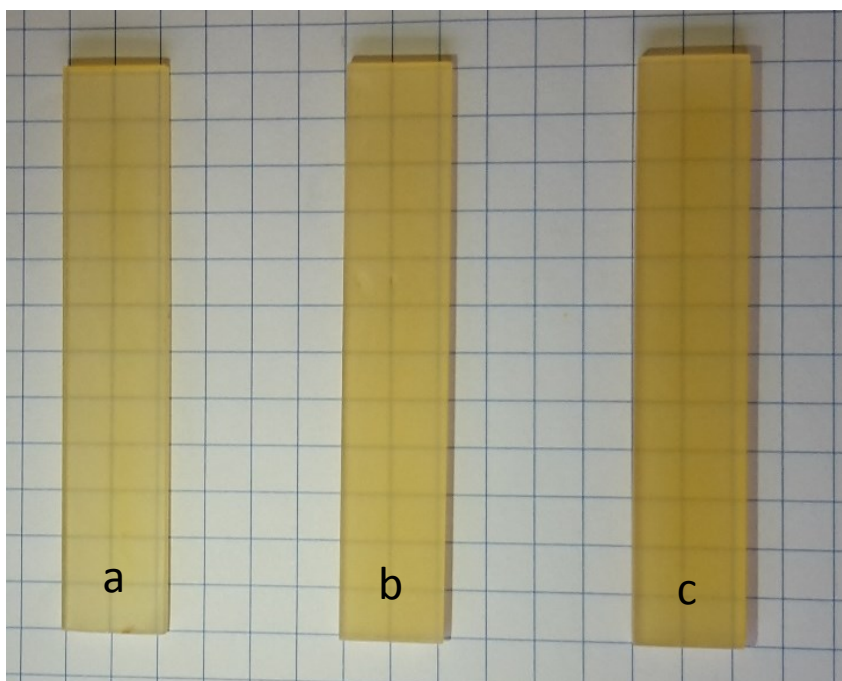


Figure 28. Cured epoxy resins' samples having a 2 mm thickness: a) Epon828 b) DGEGD c) DGEVA.

Figure 29 and Figure 30 show the TGA thermograms and first derivatives (DTG) of the cured resins under air (Figure 29) and nitrogen (Figure 30) atmosphere. Thermal stability factors, including the initial decomposition temperature (IDT), the temperature of 50% weight loss ($T_{50\%}$), and the temperature of maximum decomposition rate (T_{max}) (tallest peak of the thermogram derivative) were determined for both the thermograms under air and nitrogen atmosphere (Table 8); the char content formed in nitrogen atmosphere is also reported. Thermogravimetric curves of all the resin samples, under nitrogen atmosphere, show one main weight loss (Figure 30) that occurs between 300 °C and 450 °C and it can be ascribed to the resin degradation. The thermograms under air (Figure 29) instead show an additional small weight loss starting from approximately 250°C due to the bebbing of the thermal oxidation of the epoxy resins. Complete oxidation-combustion of the char takes place in air with maximum rate at 550 °C (Figure 29).

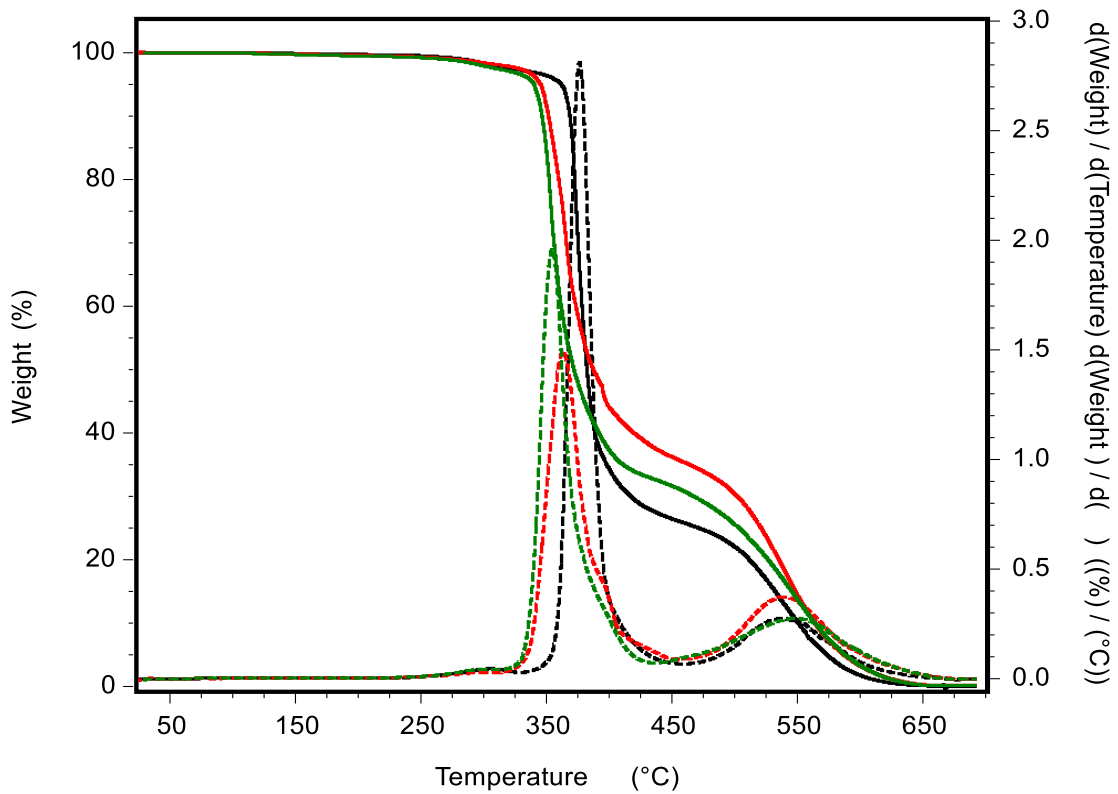


Figure 29. TGA (solid lines) and DTG (broken lines) thermograms under air atmosphere of the epoxy resins cured with EPIKURE W: EPON 828 (—), DGEGD (—) and DGEVA (—).

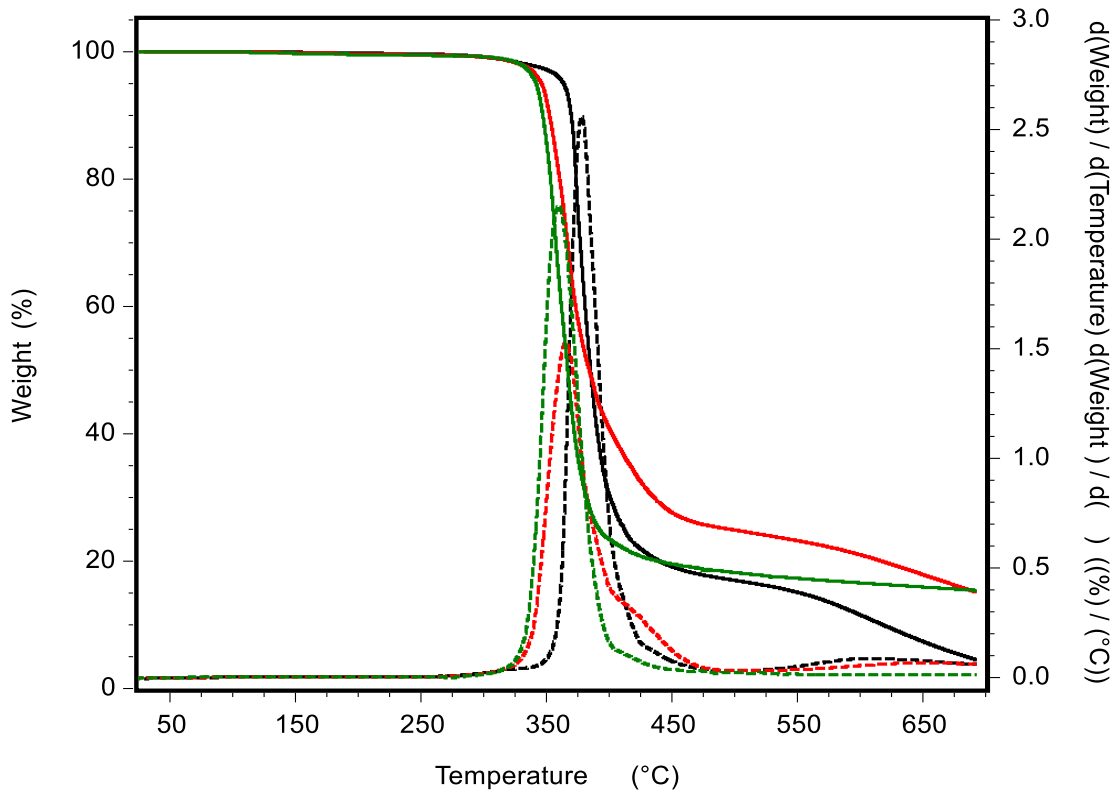


Figure 30. TGA (solid lines) and DTG (broken lines) thermograms under nitrogen atmosphere of the epoxy resin precursors cured with EPIKURE W: EPON 828 (—), DGEGD (—) and DGEVA (—).

Table 8. TGA data of the epoxy resin precursors cured with EPIKURE W.

Epoxy resin precursors	Air			Nitrogen			Char content (wt%) ^d
	IDT (°C) ^a	T_{max} (°C) ^b	$T_{50\%}$ (°C) ^c	IDT (°C) ^a	T_{max} (°C) ^b	$T_{50\%}$ (°C) ^c	
EPON828	364	376	382	361	378	385	4.5
DGEGD	347	363	387	346	366	384	15.1
DGEVA	342	355	372	340	360	367	15.4

^a Determined as the temperature at 5% weight loss (heating rate 10°C/min).

^b Determined as the temperature at the peak maximum of the DTG curve (heating rate 10°C/min)

^c Determined as the temperature at 50% weight loss (heating rate 10°C/min).

^d Determined as the weight residue at 700 °C (heating rate 10°C/min).

Representative DMA curves are plotted as function of temperature in Figure 31 and Figure 32. The cured DGEVA resin show the highest E' at 25 °C (2.92 GPa) while the cured DGEGD and EPON 828 have similar moduli, 2.11GPa and 2.23 GPa, respectively (see Figure 31 and Table 9).

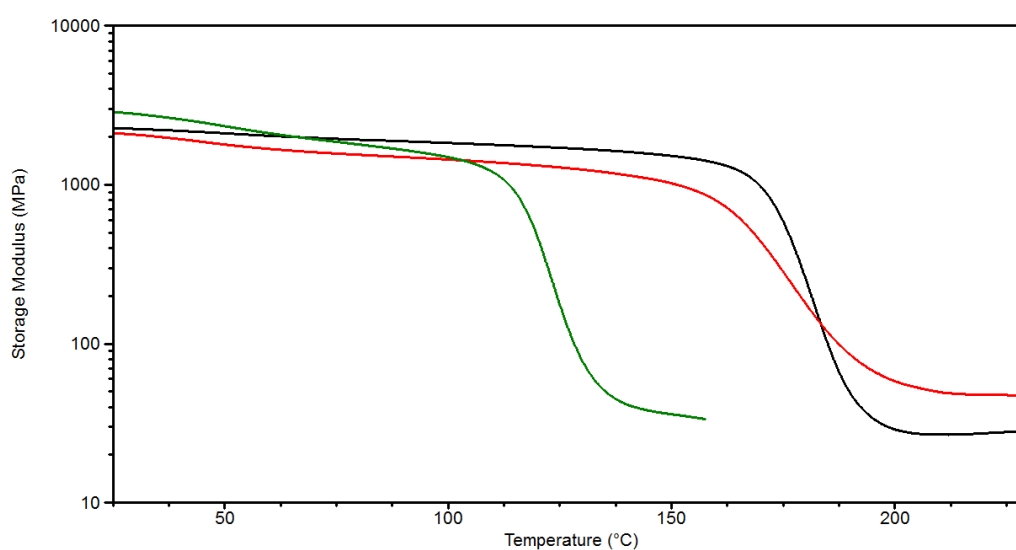


Figure 31. E' curves of the epoxy resin precursors cured with EPIKURE W: EPON 828 (—), DGEGD (—) and DGEVA (—).

Table 9. DMA data of the epoxy resin precursors cured with EPIKURE W.

Epoxy resin precursors	E' (GPa) ^a	E'_{onset} (°C)	T_g (°C) ^b	T_g (°C) ^c
EPON828	2.23	165	176	186
DGEGD	2.11	161	171	186
DGEVA	2.92	115	120	128

^a E' measured at 25 °C

^b T_g measured as the temperature at the peak maximum of the loss modulus (E'') curve.

^c T_g measured as the temperature at the peak maximum of the $\tan \delta$ curve.

These results are in agreement with the E' moduli trend found in a previous work¹³², where the same resin precursors were cured with a stoichiometric amount of an aliphatic amine (PACM). All cured resins display single E'' and $\tan \delta$ peaks (Figure 31 and Figure 32) corresponding to α -relaxations ascribed to the long-range molecular motions and generally used to define the T_g by DMA analysis¹³⁸.

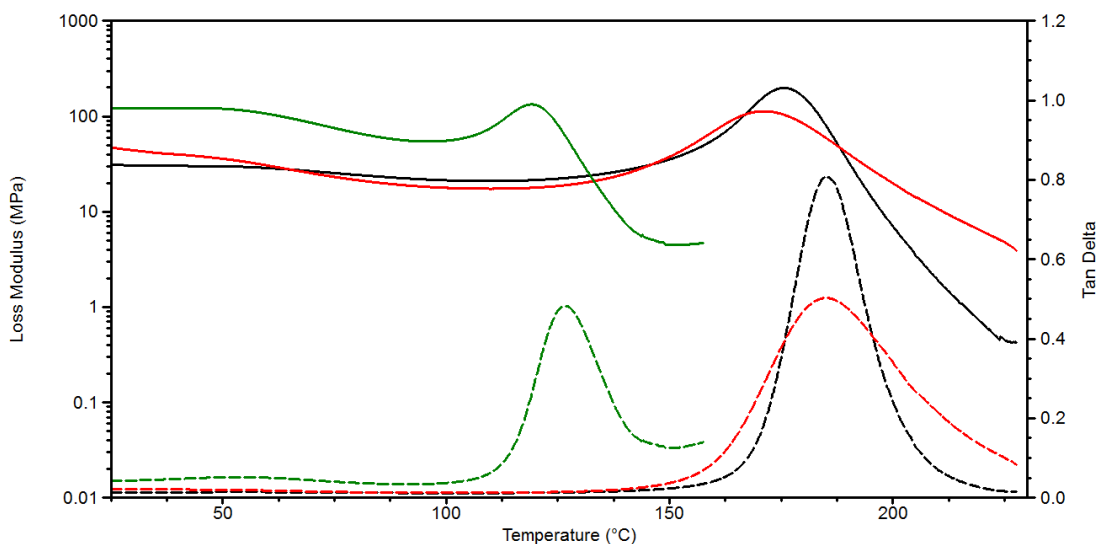


Figure 32. E'' (solid line) and $\tan \delta$ (broken line) curves of the epoxy resin precursors cured with EPIKURE W: EPON 828 (—), DGEGD (—) and DGEVA (—).

In this work, the T_g was measured as the peak of the loss modulus curve (E''): this value is considered a conservative assignment of T_g with respect to the peak of the $\tan \delta$ curve; additionally, the temperature at E' onset was reported as well (Table 9). In DGEVA-EPIKURE W resin, the E'' and $\tan \delta$ curves show also a broad-low peak at 45–55 °C corresponding to a β relaxation, generally due to initial mobility of molecular side chain segment. This β -relaxation has already detected in the DGEVA¹³² base resins and it can be ascribed to the methoxy group in the aromatic ring of the VA. The DGEGD and EPON 828 resins are in fact similar in structure and there are no additional substituents *meta*-attached to their aromatic rings.

The EPON 828-EPIKURE W system has the highest T_g (176 °C); however, the DGEGD based resin presents a comparable T_g (171 °C) and basically, the maximum of the $\tan \delta$ curve occurs at the same temperature (186 °C) of the EPON828 based resin (see Figure 32). As already reported^{132,136}, DGEVA-EPIKURE W resin displays a lower T_g (120 °C) than DGEGD and EPON828-based resins: the presence of the a methoxy in *meta*-position can in fact increase the free volume within the polymer network and effectively lower the

T_g . Finally, the observed E'_{onset} temperatures show the same resins' T_g trends. This last viscoelastic parameter is the most conservative assignment of polymer's T_g because it occurs at the lowest temperature and relates to mechanical failure¹³⁸; thus it should be taken in account when high-performance resins are required, for instance, in composites industry.

DSC analysis is used to study the glass transition temperature (T_g) and the extent of cure in cured epoxy resins¹⁰⁵. The first scan DSC curves of all the resins' samples (see Figure 33) display a stepwise transition ascribed to the glass transition of the resins (I scan T_g); these signals are overlapped with enthalpic relaxations that make difficult an accurate evaluation of T_g values in the first heating scan.

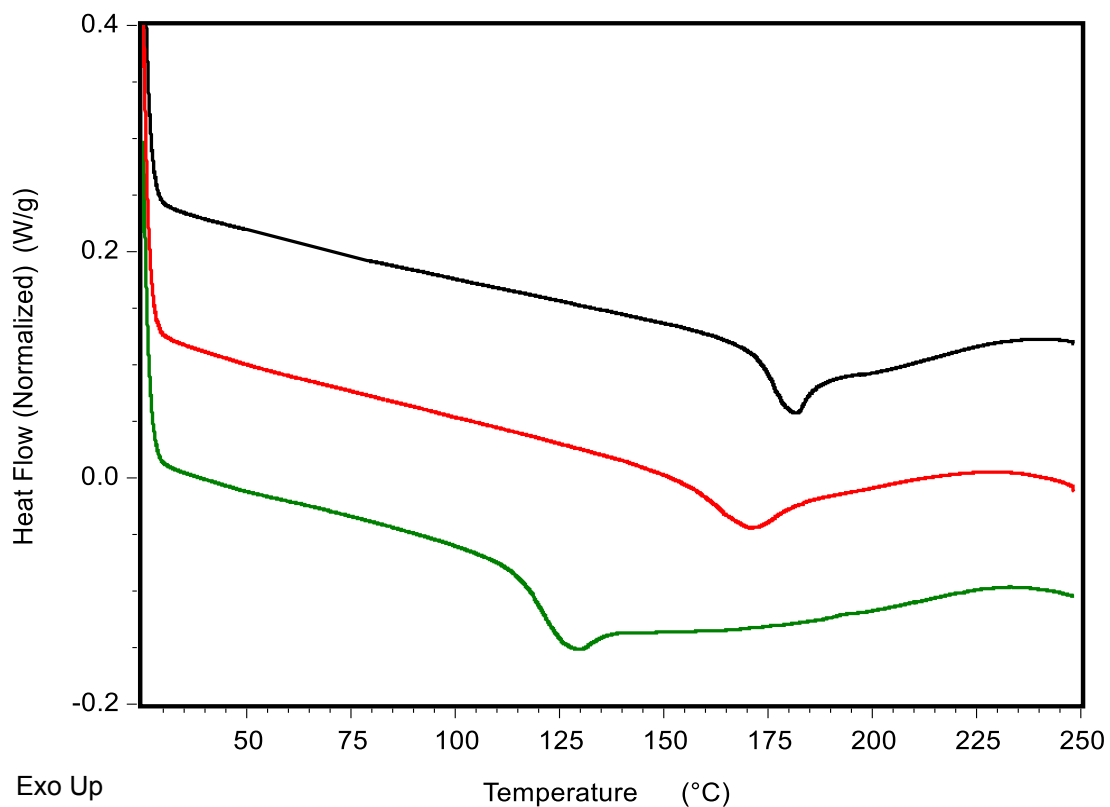


Figure 33. First DSC scans of the epoxy resin precursors cured with EPIKURE W: EPON 828 (—), DGEVD (—) and DGEVA (—).

In addition, a slight exothermic signal can be detected in the samples when heating above 200 C°. This behaviour accounts for a curing process that, notwithstanding the shortened curing cycle, leads to a material with properties stable enough within 200°C, and above their exercise temperature range, taken on the basis of the T_g evaluation. Owing to the presence of the enthalpic relaxation, the T_g values for all specimens were determined from

the midpoints of the corresponding glass transition regions in the second scan curves (Figure 34) and all the results are collected in Table 10. All the resins, as determined by DMA, possess the same T_g trends as those cured with PACM¹³². An increase in all resins' T_g is due to the first scan end temperature 250 °C, which unlocks some residual reactive groups cross linking, since no post-cure treatments were carried out on all the cured resins.

Table 10. DSC and densities of the epoxy resin precursors cured with EPIKURE W.

Epoxy precursor	I scan T_g (°C)	II scan T_g (°C)	ρ (g/cm ³) ^c
DGEVA	115	120	1.19
DGEGD	166	171	1.19
EPON828	172	176	1.16

^c ρ measured according to Archimedes' principle at 25 °C.

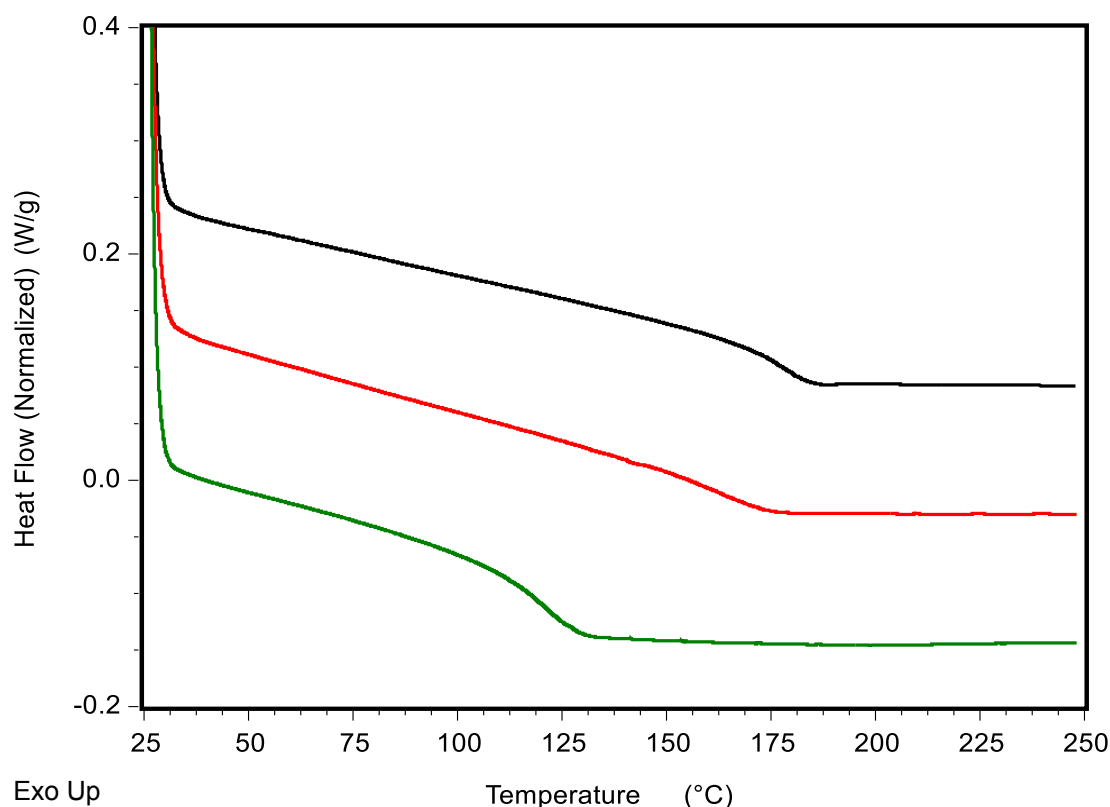


Figure 34. Second DSC scans of the epoxy resin precursors cured with EPIKURE W: EPON 828 (—), DGEGD (—) and DGEVA (—).

The density of the epoxy resins cured with EPIKURE W were measured according the Archimedes' principle: the data, reported in Table 10, show that the two mono-aromatic bio-based resins, DGEVA and DGEGD, have a density slightly higher than the BPA-based one (1.19 g/cm³ and 1.16 g/cm³, respectively). The EPON828-based lower density may be attributed to the isopropyl linkage in bisphenol A linkers that decrease packing and which are not present in DGEVA and DGEGD polymers¹³².

Table 11. Comparative data of EPIKURE W and PACM¹³² cured epoxy resins.

Curing agent	Epoxy-precursor	Density (g/cm ³) ^a	T_g (°C) ^b	Char content (%) ^c	E' (GPa) ^d	T_g (°C) ^e
EPIKURE W	EPON 828	1,16	176	7,3	2,23	186
	DGEGD	1,20	171	17,8	2,11	186
	DGEVA	1,19	120	15,9	2,92	128
PACM	EPON 828	1,16	149	2,3	2,37	158
	DGEGD	1,18	123	3,6	2,29	132
	DGEVA	1,20	100	6,9	3,02	107

^a ρ measured according to Archimedes' principle at 25 °C.

^b T_g measured as the temperature at the peak maximum of the loss modulus (E'') curve.

^c Determined by TGA residue at 650 °C in a nitrogen atmosphere and heating rate 10°C/min

^d E' measured at 25 °C

^e T_g measured as the temperature at the peak maximum of the tan δ curve.

The main relevant differences between the PACM and EPIKURE W cured resins are detectable in Table 11 and in Figure 35. All the EPIKURE W cured resins show a general improvement of many thermo-mechanical properties, and they never display a worsen behaviour.

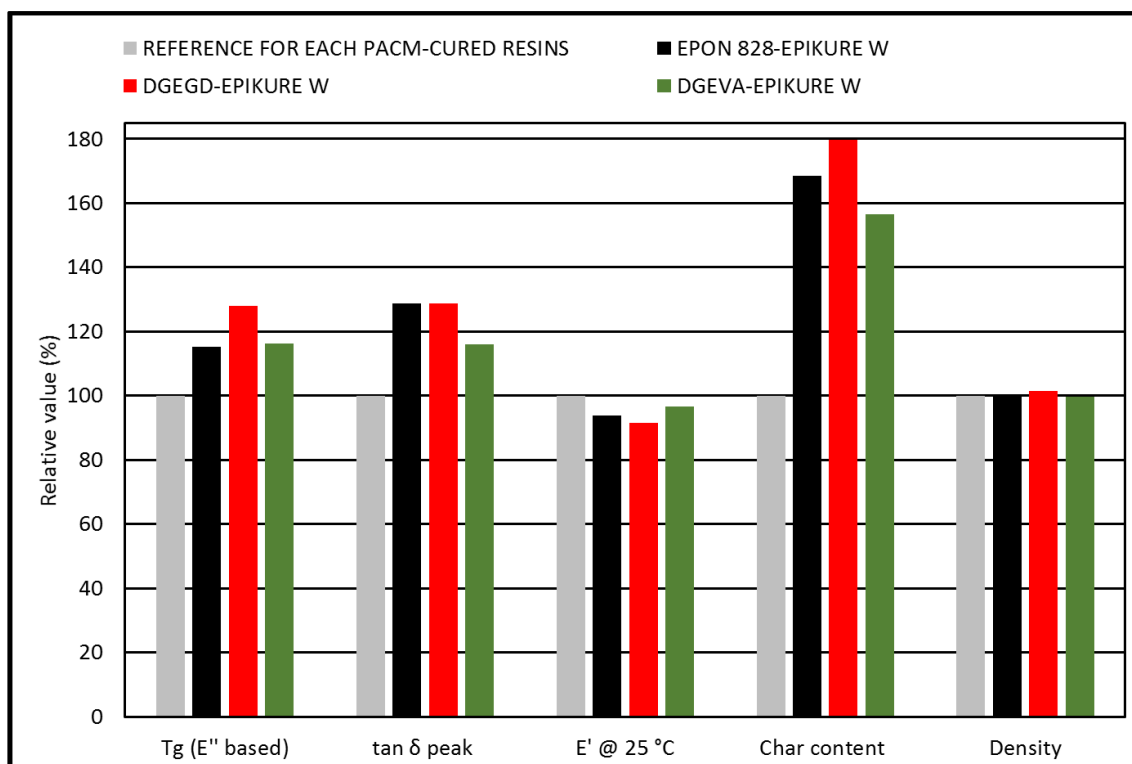


Figure 35. EPIKURE W-cure resins' properties expressed as % variation with respect to the same epoxy precursor cured with PACM, which is taken, in each case (grey bar), as 100% reference.

Noteworthy are the improvements in the resins' T_g which are as high as +20 °C, + 47 °C and + 27 °C for the DGEVA, DGEGD, and EPON 828-based resin, respectively. Such a

significant increase in T_g is a very remarkable results, whose attainment is often pursued in the field of epoxy resins for composite materials production. The T_g attained for DGEGD falls in the range of epoxy precursors for High T composites, whose request is growing in importance owing to a wider application of CFRP materials in temperature sensitive environments. Another interesting result is the char yield displayed by all of the EPIKURE W-cured resins that is at least the 50% higher (Figure 35) than in PACM-cured resins. Such an observation rises the interest in further evaluation of this particular formulation in the field of flame retardancy^{19,83,98}. Finally, the DGEVA and DGEGD cured with EPIKURE W display comparable E' moduli at 25°C and almost the same density. The obtained data stress the possibility of replacing the present fossil BPA based epoxy resin widely used in the market, with some bio-based sustainable products without compromising the thermoset behaviour, and indeed, increasing some of their properties.

3.4. Conclusions

Two bio-based resins, the DGEVA and the DGEGD, were synthesized and characterized. Both the resins and a commercial BPA-based epoxy resin (EPON 828) were cured with the aromatic commercial curing agent EPIKURE W and their properties were compared with those already obtained in a previous work¹²³, using another curing agent, PACM. It has been observed that:

- The thermo-mechanical properties for both the bio-based and the commercial are generally improved or never display a worsen behaviour when the resins are cured using a short time cure program.
- The resins' T_g s are as high as +20 °C, + 47 °C and + 27 °C for the DGEVA, DGEGD, and EPON 828-based resin respectively
- The char yields are high as +50%, +80% and 70% for the DGEVA, DGEGD, and EPON 828-based resin respectively
- The bio-based DGEGD resin archives thermo-mechanical properties which are completely comparable to those of the EPON828-EPIKURE W commercial epoxy resin system

In a prospective to replace BPA- and petroleum-based epoxies in composite materials, these results suggest that the thermo-mechanical properties of bio-based epoxy resins can be improved by simply changing the curing agents. This approach may encourage the commercialization of bio-based epoxies and their use in composites application. Finally,

the interesting properties achieved for the DGEVA and DGEGD cured with EPIKURE W make them suitable candidates in the replacing of the BPA-petroleum resin in composites applications.

Chapter 4

Validation of carbon fibers recycling by pyro-gasification: the influence of gasification conditions to obtain clean fibers and promote fiber/matrix adhesion in epoxy composites*

***Adapted from:**

L. Mazzocchetti, T. Benelli, E. D'Angelo, C. Leonardi, G. Zattini, L. Giorgini. **Validation of carbon fibers recycling by pyro-gasification: the influence of gasification conditions to obtain clean fibers and promote fiber/matrix adhesion in epoxy composites**, *Polymer Composites Part A* submitted

4.1. Introduction

In recent decades, carbon fibres (CFs) have found widespread application in a growing number of fields, such as automotive, aerospace and defence, wind turbines, sport, and leisure¹³⁹. Though their discovery dates back to T.A. Edison in 1879¹⁴⁰, their application as high-performance light-weight reinforcement has just recently had a boost mainly in luxury-related high added value fields, such as aerospace, defence, wind turbines, sport and leisure. Consequently, the carbon fibre industry has been experiencing a steady growth which is lately expanding towards more mass-oriented market segments such as the mainstream automotive and motorcycles, where they are applied in the form of CF Reinforced Polymers (CFRPs) to replace metal parts in vehicles in order to provide them with lighter weight. Accordingly, the demand for carbon fibers, that grew from 27000 tons in 2009 to 53000 tons in 2014, is foreseen to more than double by 2021 with an expected request of 116000 tons¹⁴¹. Such a boost in the CFRP exploitation is now raising the

awareness about their fate: a strong increase in CF waste is indeed expected, coming both from the production processes (prepreg offcuts; offcuts and scraps of cured composites) and the End of Life products (EoL). The current EU legislation does not provide specific regulation for composites' waste. Their disposal is indirectly involved in the 2000/53/EC EU Directive, which requires a 95% recovery and 85% recycling extent of total End-of-Life Vehicle weight by 2015 and limits the use of non-metal components if not complying with the Directive requirements. However, while attempts are made at obtaining green composites¹⁴² and green nanocomposites⁷⁹, thermoset CFRPs still dominate the market, and presently they cannot be easily recycled or recovered, neither by disassembling of their components nor by re-melting and re-moulding. Hence research efforts are focusing on adequate recovery techniques for these components to match the EU Directives. Though several disposal techniques are presently available for treating CFRPs⁶⁴, they are still far from optimized and they are characterized by some serious drawbacks. For example, mechanical treatment leads to powdery materials with low added value, which can be mainly applied as fillers⁶¹. When, however, valuable material recovery is pursued, either thermally or chemically, it necessarily involves some preliminary shredding and crushing treatment of the waste, with a significant energy consumption. Moreover, thermal treatments have to be carefully controlled in order to avoid loss of valuable products or undesired modifications in the chemistry of the recovered products^{62,143,144}, while solvolysis brings in additional chemicals which then require their own disposal¹⁴⁵. On the other hand, energy recovery, which mainly consists of incineration treatments of mixed waste streams, leads to the loss of valuable materials and the production of polluting emissions, imposing the use of expensive gas cleaning devices. Moreover, the latter approach does not take into account the notion of secondary raw material, first introduced by the EU Directive 2008/98/EC, which has the purpose of moving the EU closer to a 'recycling society', seeking to avoid waste generation and using it instead as a resource.

Considering the still relatively high cost of the virgin fibers, both in terms of economic (approx. 30 €/kg¹⁴⁶) and energetic cost (183-286 MJ/kg¹⁴⁷), a process able to give back CFs with a lower energy consumption than the production of virgin fibers appears environmentally attractive and offers economic benefits to manufacturers. In this frame, the acquisition of technological skills allowing an added value recovery of wastes, instead of their simple disposal, is a key enabling process in the implementation of the EU requirements.

Several companies offer CFRPs recovery services and their recycling into marketable products¹⁴⁸ with the aim of addressing the issue of EoL CFRP parts. The most appealing approach is represented by pyrolysis, a process in which organic materials are thermally decomposed into simpler components when subjected to strong heat under an oxygen deprived atmosphere. When pyrolysis is applied to CFRPs, treated as a single flow of waste, it involves the thermal cracking of the matrix fraction, no matter if thermoplastic or thermosetting, producing a volatile stream made of a condensable component (pyrolysis oil) and a non-condensable fraction (gas). These fractions can both be used as a source of valuable products for further manufacturing¹⁴⁹ or as a fuel. In the latter case, the high carbon and hydrogen contents of both volatile and non-volatile components result in a high calorific value which can be profitably used to practically fully sustain the pyrolysis process⁶³. At the end of the process a solid residue can be recovered, that in the case of CFRPs is mainly composed of carbon fibers. Reports from industry suggest that the production of recovered CFs (Re-CFs) through pyrolysis of CFRPs waste will consume only 5-10% of the energy required for the production of virgin fibers^{62,150}. During the process, a layer of pyrolytic carbon can form onto the fibers^{62,81} hampering a good adhesion when infused with new resin. However, these Re-CFs can be nevertheless considered highly valuable products after a gasification upgrading process^{149,151} which gives back fibers in a suitable condition to be used as feedstocks in a secondary raw material generation approach.

In order to optimize the whole pyrolytic process, Curti S.p.A. has recently proposed an innovative static-bed batch pilot reactor^{152,153} able to combine, in one single process, the main advantages of the different disposal techniques. In fact, pyrolysis can be carried out on the whole parts, up to 2 m in diameter, in order to save the energy costs of shredding the feed wastes, and simultaneously recovering energy and materials. Moreover, though the pyrolysis tests were carried out in a demonstrative pilot plant, which was not optimized in terms of energy balance, the gaseous and liquid by-products display an overall Gross Calorific Value (GCV) able to sustain about 75% of the process energy requirement. It is hence possible to foresee that, upon a convenient optimization of the plant energy issues during scale up, the process might reach a complete energetic self-sustainability⁶³.

The present work aims thus at demonstrating the potential of the recovered carbon fibers as secondary raw materials, validating a process able to recycle the composite's carbon-fibers fraction and close their Life Cycle in a Cradle-to-Cradle approach. Hence, in this

study the solid residue (carbon fibers covered by a carbonaceous layer) obtained upon pyrolysis in Curti's pyrolysis pilot plant was characterized and subjected to a further gasification step in different working conditions to provide clean fibers. For the sake of comparison, the same process was applied to the corresponding virgin fibers, in order to assess the impact of the oxidation step onto their properties, without the bias of the pyrolysis treatment, with the aim of helping to identify the most convenient gasification conditions. The effects of the process on the recovered fibers, as well as on virgin fibers, were evaluated by SEM and Raman. Finally, the reinforcement behaviour of virgin and recovered fibers, with or without the gasification treatment, was tested in the production of Chopped-CFRPs.

4.2. Experimental

*Pyrolysis of CFRPs: the case of a pilot bench-scale plant*⁶³

Recently Curti S.p.A. developed an innovative pyrolysis pilot plant having a batch static kiln reactor, supplied by electric power, that can treat different materials¹⁵². In last few years, this plant has been using to pyrolyze tires¹⁵³, CFRPs⁶³ and Glass Fiber Reinforced Polymers (GFRPs)⁸¹ with the aim of developing environmentally and financially sustainable processes to dispose of end of life materials (EoL) and/or any waste deriving from their manufacturing processes.



Figure 36. Typical uncured prepreg cut-offs with low density polyethylene (LDPE) protective film (a) and cured CFRPs scraps (b)⁶³.

Since the recycled carbon fibers used in this thesis (*Chapters 4 and 5*) come from this plant, a brief description of the whole CFRPs pyrolysis process is reported in order to clarify how

this plan works when CFRPs are fed. All the pyrolyzed materials were supplied by Ri-Ba Composites srl as uncured prepreg cut-offs or cured CFRPs scraps owning epoxy resin based matrixes (Figure 36).

A typical CFRPs pyrolysis run

The batch pilot plant is able to treat up to 70 kilograms of Carbon Fiber Reinforced Polymers (CFRPs), both cured and uncured, per pyrolysis cycle. The pyrolysis experiments can be performed isothermally at different temperatures, specifically temperature between 400 °C and 600 °C are used.

In a typical run, CFRPs waste (Figure 36) were placed into the reactor. After closing the lid, the reaction chamber was flushed with nitrogen in order to remove air, the system was heated at 8 °C/min rate up to the set point, and then maintained at the desired temperature for a total residence time of 150 minutes. Due the organic components within the feeding materials, the polymer matrix and/or the polymeric protective films on the surface of uncured preregs, several gases were generated and, at the same time, moved outside the reactor. The gas stream was conveyed to a water-cooled coil condenser and the condensed phase was collected via a demister. Consequently, the pyrolytic process led to three main products: a gas phase, an oil fraction and a solid residue. The relative yields depend on the pyrolysis conditions applied (temperature and residence time) and on the materials loaded into the reactor (uncured preregs or cured CFRPs). Generally, a solid residue ranging from 57 to 72 wt% remains inside the reactor and is made of carbon fibers covered by a layer of char: the recycled carbon fibers used and discussed in this thesis comes from this solid fraction. A 14-18 wt% of oil and a 15-30 wt% of gases (calculated by the difference between the weight of the material fed into the reactor and the sum of the solid and liquid weights) can be recovered and used for the energy and/or materials recovery. The oil fraction contains a complex mixture of C₆-C₁₂ aliphatic and aromatic organic compounds and, the gases one a mixture of H₂, CH₄, CO, CO₂, ethylene, ethane and C₃, C₄ and other species.

Sustainability of the CFRPs pyrolysis process

A certain amount of electric energy is supplied during the CFRPs pyrolysis process. It was estimated that the present pyrolysis pilot plant requires an average of 324 MJ/batch. Taking in account this value and the potential calorific value of the liquid and solid fractions, a first energy balance can be calculated. For instance, approximately 242 MJ/batch are

potentially recoverable from the pyrolysis of CFRPs cured scraps treated at 500°C. In this way, the combustion of the liquid and gas fractions, might can sustain about 75% of the process energy requirement. In this respect, it is worth recalling that these interesting data were obtained in a demonstrative pilot plant that was not perfectly optimized for treating CFRPs waste only. However, the possibly of recovering high added value carbon fibers by a still optimizable almost self-sustainable process, might lead to a complete energetic self-sustainability process that provides carbon fibers that can be reused, as it will be discussed later, in the composites industry, making the whole process remunerative as well.

Materials

Virgin chopped fibers (20 mm) were obtained cutting down Unidirectional Fabric UC 301 based on Toray T700S 12K dry fabrics. These fibers will be labelled as “VF”. The solid residue derived from pyrolysis of CFRPs was supplied by Curti S.p.A. The epoxy composite cured samples based on the same Toray T700S 12K dry fabrics were supplied by Ri-Ba Composites srl and include cured scraps coming from different stages of the manufacturing process.. These fibers will be identified as “Pys”. The two components epoxy resin used for chopped fiber composites production is the ElanTech EC157/W61 Polymer/Hardener system obtained from Elantas.

Post-Pyrolysis gasification treatments

The gassification treatment was carried out both on the solid residue derived from the pyrolysis at 500°C of CFRPs cured scraps (Pys) and on the virgin fibers (VF). After a preliminary TGA assessment, a small sample (tenths of mg) of the virgin and pyrolyzed carbon fiber fabric was isothermally treated at 500°C or 600°C for 10, 20, 30, 40, 50 and 60 mins in air. Then, according to the obtained results, two specific treatment conditions were selected, namely 500°C for 20 and 60 minutes and at 600°C for 20 minutes, and a higher amount of downsized (20 mm) and disentangled fibers, sufficient for further characterization and composite production, was treated accordingly. All the gassified samples, upon cooling to Room Temperature (RT), were weighed and characterized by Scanning Electron Microscopy (SEM) and Raman spectroscopy. The obtained carbon fibers and their labelling samples are reported in Table 12.

Chopped Carbon Fiber Reinforced Polymers (Re-CCFRPs) Production

Carbon Fibers of the average 2cm length (20g), either pristine (out of the pyrolysis reactor, Comp-VF) and only pyrolyzed (Comp-Py) or after muffle treatments in different thermal condition (Comp-VF and Comp-Py 500 or 600, gassified at 500 or 600°C, respectively) and time (eg. Comp-VF and Comp-Py 500.20 or 500.60, gassified at 500°C for 20 or 60 min, respectively), were mixed with a pre-mixed two-components epoxy resin mixture in a fiber/matrix=60/40 weight ratio for the production of Re-CCFRPs. The resin formulation was prepared according to the supplier Technical Data Sheet (hardener:prepolymer = 17:100 weight ratio). The resin/Re-CF mixture (33.3g) was poured into a 100 x 100 x 5 mm mould and hot-press cured at 50bar pressure according to the following procedure: the mould was inserted in the press with the plates already heated at 70°C, where it was kept in isotherm for 30 minutes, then the temperature was raised at 110°C at which temperature the sample was kept isothermally for further 45 minutes. After cooling down to RT, each composite panel was cut into 100x15 mm stripes in order to perform thermal and mechanical characterization. The prepared composite materials are reported in Table 13.

Methods

Thermogravimetric analysis (TGA) was carried out using a TA Instruments SDT-Q600 apparatus. Preliminary oxidative treatment experiments were carried out on approximately 15-30 mg of material in oxidizing atmosphere (air: flow rate 100ml/min) from RT to either 500°C or 600°C where samples were kept isothermally for 60 minutes. TGA runs intended for fiber fraction determination were carried out on approximately 20-30mg of composite sample heating it from RT to 500°C at 20°C/min heating rate in inert atmosphere (nitrogen: flow rate 100ml/min) leaving it in isotherm for 15 minutes, then cooling the sample down to 300°C before switching to oxidizing atmosphere (air: flow rate 100ml/min) before heating again at 20°C/min heating rate up to 500°C, where the sample is once again kept isothermally for 15 minutes. The obtained residue, before fibers start a continuous constant degradation, is taken as the composite fiber content.

In order to investigate the morphological aspect of the fibers and the fracture surface of the composites, micrographs were taken with a Scanning Electron Microscope (SEM) ZEISS EVO 50 EP in Environmental mode with ≈ 100 Pa pressure in the chamber, equipped with INCAEnergy 350 EDX microanalysis system. The distribution of fiber diameters was

determined with the help of an image analysis software, measuring about 100 fibers in two different images (50 fibers per image) per fiber type.

Raman spectra on fibers were recorded with an Ar⁺ laser light source (514.5 nm). The Raman spectrometer is a Leica DMLM Renishaw 1000 RAMAN Micro-Spectrometer equipped with microscope (objectives 5x, 20x, and 50x), a rejection filter (notch or edge), a monochromator (1200 lines/mm) and a charge-coupled device thermoelectrically cooled (203 K) detector.

Apparent Density (AD) was determined for each coupon produced for mechanical tests (roughly 100x10x2.5mm) as the ratio between measured weight and volume. The Average Apparent Density (AAD) has been determined averaging all the calculated AD for each composite batch.

Dynamic mechanical analysis (DMA) was performed with a NETZSCH 242 E Artemis analyzer in three-point bending configuration with a 40mm span, with 1 Hz oscillation frequency and 20mm oscillation amplitude, heating from RT up to 150°C a 3°C/min heating rate; samples for DMA are about 50x10x2.5mm (the exact dimensions were measured for each coupon).

Tensile tests were carried out at room temperature with an Instron-type tensile testing machine (REMET TC10) equipped with a 10kN load cell, using a crosshead speed of 5 mm/min and initial gauge length of 50 mm. Five specimen were tested for each formulation, chosen among those with the AD values closest to the AAD and the results were averaged.

4.3. Results and discussion

Gassification treatments and characterization of carbon fibers

Since the pyrolysis process is intended to be applied for recycling purposes, no regular shape and thickness of the feed is expected, hence the solid residue output of the process might be variable in size and shape. Depending on the size of the feed objects, it was observed that when thickness exceeds few prepreg layers, i.e. in the case of thick composites^{103,105}, the outer layers display an almost complete lack of residues and low resistance to separation. The inner layers, instead, are characterized by the presence of some resin residue that prevents the fiber layers from an easy separation and makes the

woven carbon fiber mats stiffer and harder to separate⁶³. In all cases, however, a thin layer of pyrolytic carbon was observed to coat CFs recovered after pyrolysis. In order to selectively remove the amorphous pyrolytic carbon, as well as some residual resin, without damaging the fibers, it is possible to perform an oxidative treatment (gasification) that, in order to facilitate the scale up of the whole process, should be preferentially carried out at a temperature compatible with the condition applied for the pyrolytic batch, i.e. 500 and 600°C⁶³. However, it was reported in the literature⁶⁴, that the gasification (oxidation) conditions might play a crucial role on the resulting fibers properties. Hence, with the aim of assessing the intrinsic effects that such treatment might have on carbon fibers, besides what might have happened during pyrolysis, virgin dry fibers (VFs) were subjected to the same oxidative conditions applied to remove char from the pyrolytically recovered ones (Pys).

First, both virgin and pyrolytically treated fibers were analysed by TGA in oxidizing atmosphere applying a fast heating segment to the target temperature, then 60 minutes' isotherm at 500°C and 600°C respectively, in order to provide a preliminary assessment of the treatment impact on the samples' weight loss as depicted in Figure 37.

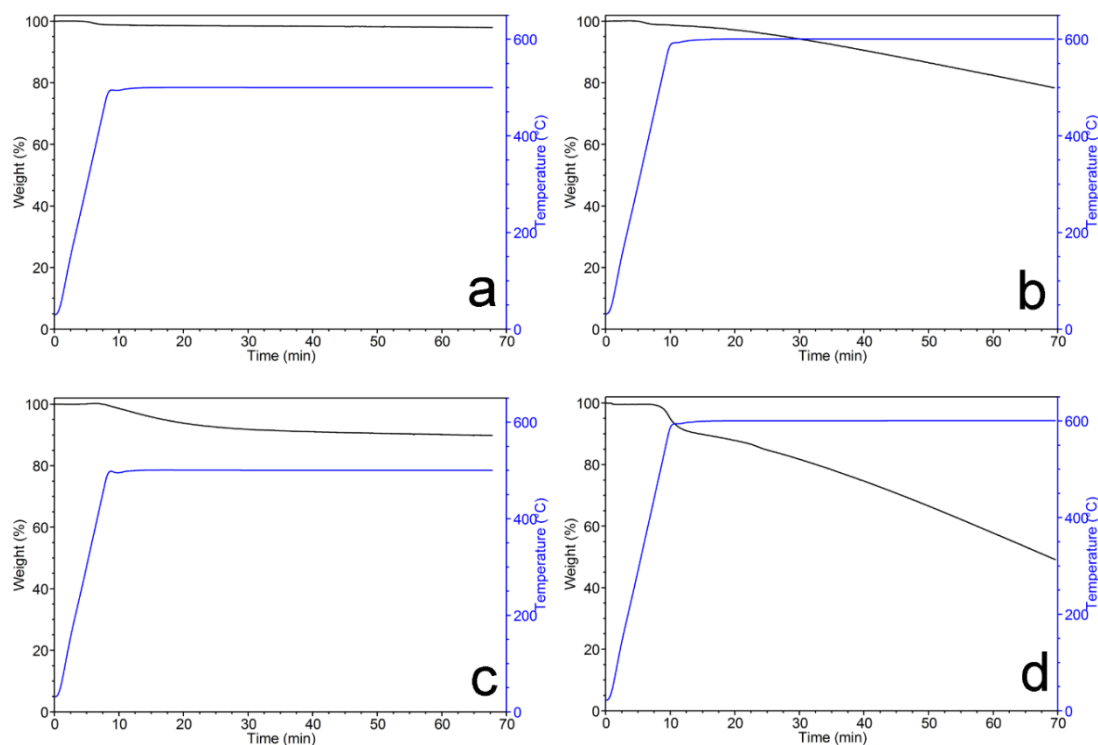


Figure 37. Thermogravimetric analysis (TGA) in oxidizing atmosphere of VFs, a) and b), and Pys, c) and d). Set point temperature at 500°C, a) and c), and 600°C, b) and d).

Both VFs thermograms, Figure 37a and Figure 37b, show a double weight loss event regardless of the temperature at which the isotherm has been carried out, namely 500 or 600°C. The first event, which begins around 310°C (T_{onset}), takes place during the heating of the sample while the second one occurs during the isotherm step, i.e. above 500°C. The first weight loss is comparable for the two samples (1.2% in the two runs). Moreover, while in both cases the first degradation event is characterized by a common weight loss rate around 0.5 %wt/min, the second one, located during the isotherm, is strongly affected by the temperature set point: at 500°C (Figure 37a) the weight loss rate is about fifty times slower than the first event (0.01%wt/min) and stays constant along the whole isotherm step, while treating the sample at 600°C (Figure 37b) the process is generally sped up, and the weight loss rate increases until, after 20' isotherm, it reaches almost the same rate as the first weight loss (0.4%wt/min). Preliminary thermogravimetric analyses were analogously performed on pyrolyzed solid residues (Figure 37c and Figure 37d). In this case, both thermograms show a single weight loss event starting around 400°C, thus lacking the 1.2% low temperature loss. The absence of the latter feature in the pyrolyzed fibers suggests that such event might be due to the thermal decomposition of the fiber sizing, that is expected to be present only in the virgin fibers: according to the literature¹⁵⁴, for the same kind of dry fibers this surface treatment is reported to represent about 1.1-1.3% of the fibers weight, and it is indeed expected to degrade at lower temperatures than the fibers themselves. Pyrolyzed fibers, hence, display just a steady degradation whose rate depends once again on the applied isotherm temperature. In the case of the pyrolyzed fibers the rate is higher: in particular, the loss rate in the isotherm at 500°C gets steady after 20' isotherm and is 5 times higher than the one registered for the virgin fibers (0.05%wt/min for Pys vs 0.01%wt/min for VFs), while for the 600°C isotherm the rate doubles (0.8%wt/min for Pys vs 0.4%wt/min for VFs). The observed trends account for the fact that during the isotherm at 600°C the fibers themselves are degrading, while the increase in the overall weight loss rate for the pyrolyzed specimens can be associated with the burning off of the char residue covering the fibers' surface. With the aim of assessing the possibility to scale up the process, after downsizing and disentangling the fabric, fibers (both VFs and Pys) were thus gassified, in aliquots ranging around the tens of grams, at 500°C and 600°C for 10, 20, 30, 40, 50, and 60 minutes. In Figure 38, small samples of Py fibers after gasification at 500°C and 600°C are reported, together with VFs and Pys for the sake of comparison. In this case, fabrics were purposefully non-disentangled prior to the treatment, with the aim of highlighting the difference in their aspect as a function of

the gasification conditions. As a matter of fact, it can be noticed that the aspect of the fibers changes when treated at 600°C for more than 30 minutes, with the fabric that shrinks, loses its glossy look and each tow that starts coming easily apart. This observation well compares with the TGA trend observed in Figure 37, where smaller sized pyrolyzed fibers begin to display a severe weight loss after about 30 minutes at 600°C. The weight losses registered for each of the above discussed treatment are displayed in Figure 39, showing that the trend is quite similar to the TGA curves, and thus validating the simulated gasification profiles reported in Figure 37.

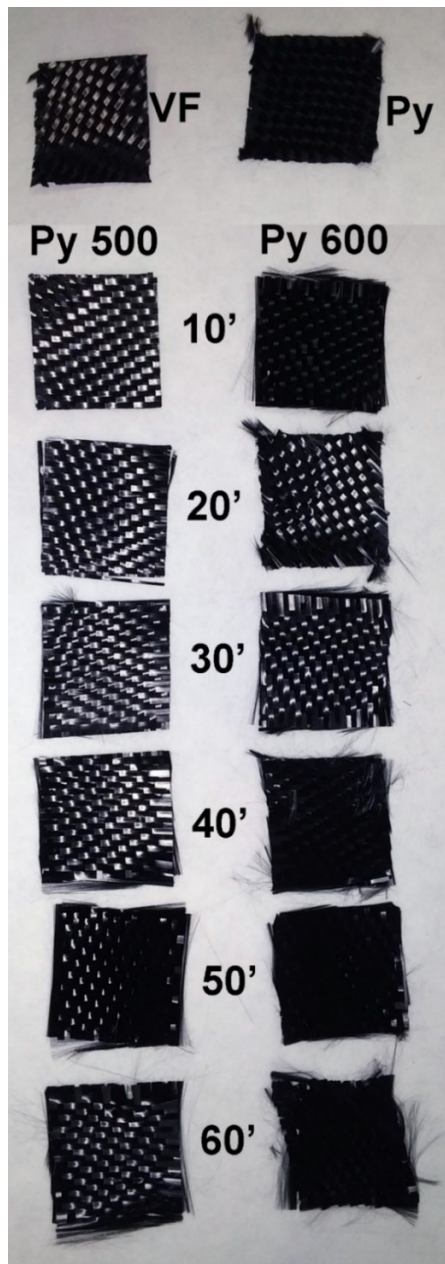


Figure 38. Picture of a sequence of small fabric samples made of VFs and Pys at the top of the picture, and different Py samples, after gasification at 500°C (left column) and 600°C (right column) as a function of time, as specified in the figure.

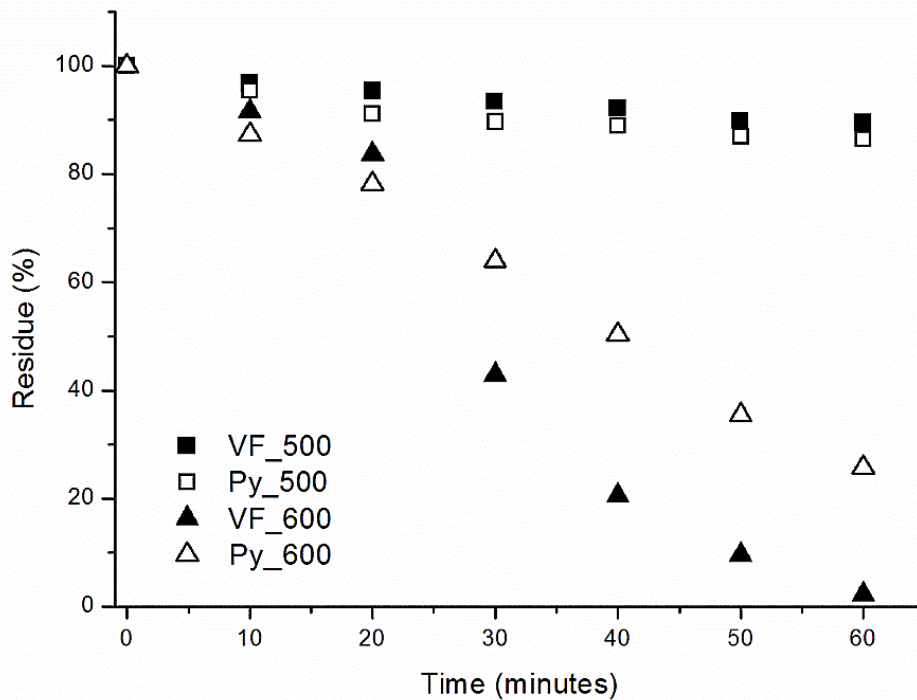


Figure 39. Mass loss of Pys and VFs after gasification at 500°C and 600°C as a function of time.

In particular, Py fibers show that, when treated at 500°C, they first degrade faster, then reach a stable weight loss trend after 20 minutes, both in TGA and in muffle oven; at 600°C too, after 20 minutes the degradation reaches a stable trend. Hence the up-scaling of the oxidative process to hundreds of grams of disentangled shortened fibers (required for further production of the composite panels) is carried out for both virgin and pyrolyzed fibers only for selected conditions, chosen according to such observations, i.e. at 500°C for 20 (samples labelled VF_500.20 and Py_500.20) and 60 minutes (VF_500.60 and Py_500.60) and at 600°C for 20 minutes (VF_600.20 and Py_600.20). Data obtained for these batches are reported in Table 12 and a deeper investigation of such fibers is detailed hereafter. Data reported in Table 12 demonstrates that the up-scaling of the oxidative treatment well compares with the previously reported weight loss data. The average diameter of untreated VFs, as measured from SEM pictures, agrees with literature data for T700 standard fibers¹⁵⁵, and it is slightly affected by the mildest treatment (-2.8% for VF_500.20).

Table 12. Data concerning the oxidative treatments carried out on fiber batches suitable for further composite panel production.

	T _{ox} (°C)	t _{ox} (min)	Weight loss (wt%)	Average diameter (µm)	Variation in diameter ^{a)} (%)	Atom fraction ^{b)}	
						C (%)	O (%)
VF	--	--	--	7,00 ± 0,51	--	97.4±0.5	2.6±0.5
VF_500.20	500	20	4	6,80 ± 0,62	-2.8	95.0±0.5	5.0±0.5
VF_500.60	500	60	9	6,32 ± 0,69	-9.7	93.0±0.6	7.0±0.6
VF_600.20	600	20	17	6,26 ± 0,63	-10.6	93.4±0.9	6.6±0.9
Py	--	--	--	7,67 ± 0,52	+9.5	95.4±0.6	4.6±0.6
Py_500.20	500	20	8	6,99 ± 0,52	0	95.1±0.5	4.9±0.5
Py_500.60	500	60	12	6,75 ± 0,45	-3.5	92.3±0.3	7.7±0.3
Py_600.20	600	20	18	6,76 ± 0,41	-3.5	92.1±1.1	7.9±1.1

^{a)} The diameter variation is referred to the untreated VF.

^{b)} Based on EDX surface analysis.

This observation supports the previous finding that the preliminary weight loss in VFs, already beginning around 300°C, could be correlated to the loss of the sizing. Both the harsher treatments (500°C for 60 minutes and 600°C for 20 minutes) produce a comparable decrease, around 10% of the original value, in the average diameter which is higher than VF_500.20, while the weight loss for VS_600.20 is almost twice than VF_500.60. The Py fibers, as obtained from the pyrolytic treatment, show an average diameter of about 7.67 µm which is about 10% greater than the starting pristine VF, as expected for a fiber covered in a layer of char deriving from resin pyrolysis. The fibers are strongly affected already by the gasification carried out at 500°C for 20 minutes, which is able to reduce the diameter to the original T700 fiber value (VF) prior any oxidative treatment, i.e. fibers still coated in sizing. Increasing the residence time up to 60 minutes leads to a 3.5% decrease in the average diameter with respect to pristine virgin fibers, similarly to the diameter reduction obtained with the oxidizing process carried out at 600°C for 20 minutes. Both processes reached a diameter value comparable to VF 500-20. The performances registered for VF and Py fibers in the different gasification conditions highlight the fact that virgin fibers appear more prone to degrade in oxidizing atmosphere than pyrolyzed ones (about -10% in diameter for VFs vs. -3.5% for Pys): this behaviour might find an explanation in the protective action that the char layer might impart onto the fibers' surface. The overall VFs diameter decrease can be only partly justified with the loss of sizing (just 1.2% weight loss

from TGA results can be attributed to the loss of the surface sizing), which would however apply just to the milder 500.20 gasification condition. The same treatment when applied to Pys, whose outer layer is made of char, appears to be not even sufficient for char removal. Stronger gasification parameters (500.60 or 600.20), when applied to Py fibers, lead indeed to a further decrease in diameter reaching the same value as VF 500-20, which is taken as the size of the carbon fibers, once the sizing has been removed, thus accounting for the complete burning out of the char layer. When the same harsher treatments are applied onto VFs, their degradation is definitely higher, with an average diameter 10% smaller than pristine fibers, confirming the tendency of virgin fibers to undergo a higher degradation. It is well known in the literature¹⁵⁶ that thermo-oxidative degradation of carbon fibers is a complex process where two important factors play an important role: while the tendency of C atoms to reach their oxidized state (CO or CO₂) is the thermodynamic driving force of the chemical process, factors hampering the oxygen diffusion towards the graphitic carbon can act as a limiting factor for the degradation process. While it was already demonstrated that fibers protected by a resin layer, when treated in air, degrade less promptly than naked ones⁶¹, in this context, the amorphous carbon deposit might represent the sacrificial layer subtracting the oxygen from reaching the fibers' graphitic surface. Moreover, though the diameter decrease is similar, the weight loss associated with the 600.20 treatment is definitely higher both for VFs and for Pys, possibly owing to the oxidation of the carbon fibers starting from the unprotected fibers ends, in conditions where the graphitic C oxidation is favoured (graphitic C is reported to be stable below 600°C)¹⁵⁶. It is indeed worth to note the fibers are downsized prior to the thermal treatment, thus emphasizing this issue. The hypothesis of char removal from the pyrolyzed fibers is verified via SEM imaging (Figure 40): the micrograph reported in Figure 40a clearly shows that the pyrolyzed solid residue, analysed as received from the pyrolysis reactor, is made of fibers with a rough surface and spotted resin residues. These residues link together the fibers and make them stiff. Previous work proved that such rigid fibers are not conveniently wetted by resin precursor when used for a new composites production⁶³. Py_500.20 SEM micrograph (Figure 40b) does not display the spotted resin residues anymore, while the rough surface remains, as a symptom of an incomplete coating residue removal; both Py_500.60 and Py_600.20 instead (Figure 40c and Figure 40d respectively), show a smooth surface, as expected upon char removal. Worth noting is that in none of the applied oxidative conditions pitting or local damaging of the fibers surface is observed, suggesting

that the applied conditions from Figure 40c and Figure 40d should be convenient for char removal without affecting the fibers.

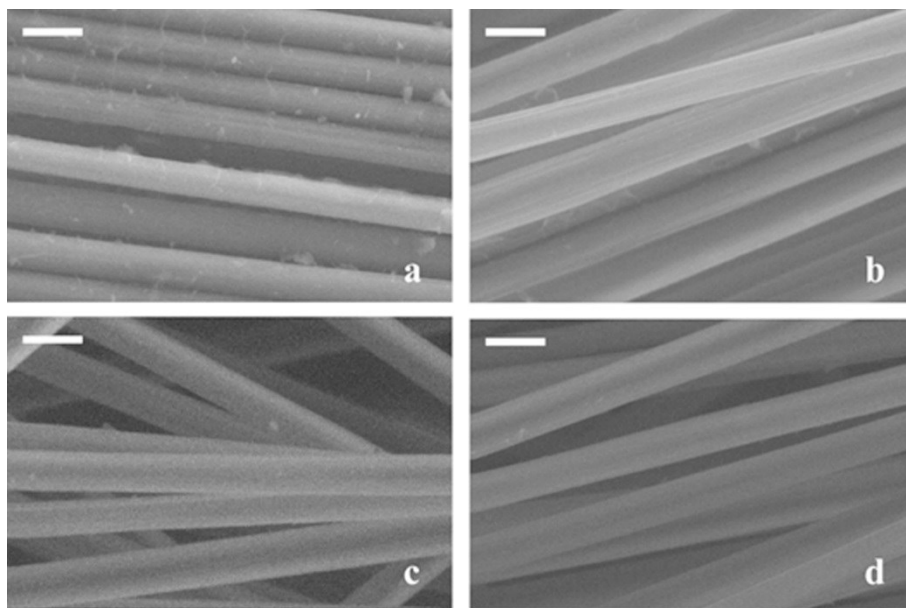


Figure 40. SEM micrographs of (a) Pyrolyzed solid residue, Py; (b) Py_500.20; (c) Py_500.60; (d) Py_600.20. Scale bar: 10 μ m.

Even when the most aggressive oxidation treatment is applied (600°C for 20 minutes), the fibers appear intact and no sign of damaged surface or local degradation are visible, as instead observed by Pimenta¹⁵⁷. The EDX analysis carried out on the differently treated fibers shows that, as expected, an increase in the Oxygen atomic fraction at the fibers surface is observed (Table 12), and the extent of such increase depends on the applied gasification conditions. Worth noting is that while the actual Oxygen content recorded after an analogous oxidation step stays quite similar for both the virgin and pyrolyzed fibers, the overall air treatments seems to affect more significantly the surface of virgin fibers, where the oxygen fraction before treatment is significantly lower than in the pyrolyzed ones (2.6% for VF vs 4.6% for Py, as reported in Table 12).

Further confirmation of the previously discussed effects of the gasification treatments is sought via Raman spectroscopy: this technique, when coupled with a microscope to guide the probe, allows to precisely record spectra in the areas of interest. Raman spectra of both virgin and pyrolyzed fibers, pristine and after different gasification treatments, are thus reported in Figure 41. The Raman spectra of the virgin and pyrolyzed fibers, without any additional treatment (Figure 41A and Figure 41B, curves (a)), focused in the 1100-1800 cm^{-1} spectral range where the most interesting events can be observed (Figure 41), display two significant peaks at 1560 and 1360 cm^{-1} respectively. These signals are well known in

the literature¹⁵⁸ for carbonaceous materials and they belong to absorptions typical of both graphitic and amorphous carbon, the so-called G and D peaks respectively.

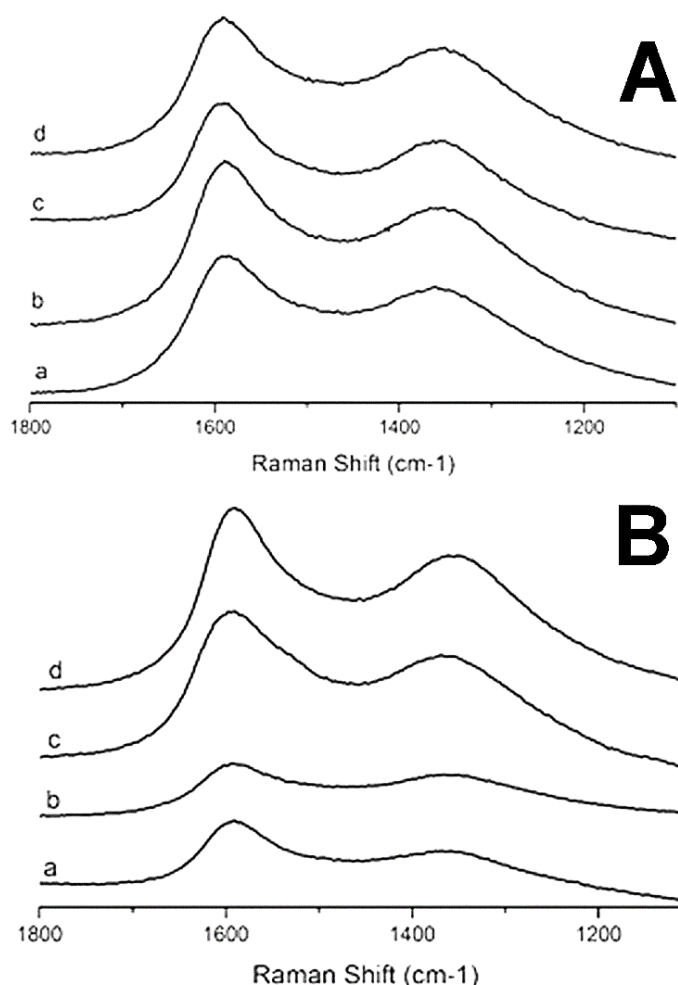


Figure 41. Raman Spectra of (A) VFs and (B) Pys after different oxidation treatments: (a) no treatment; (b) 500°C for 20 minutes; (c) 500°C for 60 minutes; (d) 600°C for 20 minutes.

The G-peak is attributed to the bond stretching of all pairs of sp^2 carbon atoms in both rings and chains, while the D-peak is due to the defect induced on the sp^2 structure¹⁵⁸. Though the two absorptions are both present in pristine VF and Py fibers, the intensity of the signals in the pyrolyzed fibers is definitely lower than in the virgin ones. While evaluation of the relative intensities of these two signals can be directly correlated to the fraction of graphitic and amorphous carbon it is, however, quite difficult to provide significant evidence of D/G peak ratio modification when low graphitization fibers (low modulus) are analysed, as in this case. Nevertheless, the sharpness of the signals in VFs can be related to the lack of organic residues and the broadness and poor definition of peaks in Pys is an evidence of resin and char residue deposited on the fibers surface¹⁵⁹. The

oxidative process has almost no influence on the Raman spectra of virgin fibers (Figure 41A, spectra b to d), as expected owing to the lack of surface char.

Raman spectrum of pyrolyzed/oxidized solid residues instead (Figure 41B, spectra b to d) changes as a function of the applied treatment. Indeed, Py_500.20 shows a similarly poorly defined spectrum (Figure 41B spectrum b) as the one recorded for the plain untreated Py fibers: this observation is thus a further proof that these gasification conditions are not adequate to completely remove the char from fibers' surface. D and G peaks become narrower and sharper when the oxidation process is carried out in more aggressively conditions (Figure 41B, spectra c and d), thus accounting for char-free fibers. Since no significant differences in the D and G peak definition can be observed, we can assume that an oxidizing process at 500 for 60 minutes and at 600°C for, at least, 20 minutes, are both sufficient to clear the fibers surface from char and resin after the pyrolysis of CFRPs, and this is in good agreement with the observation of the weight loss during the oxidative process and with SEM micrographs discussion.

Composites production and characterization

Recycled carbon fibres from high-technology applications cannot presently be reused for the same original applications, not only because of the possible lack in performance outlined in previous studies, but mainly owing to a form factor which cannot be controlled when dealing with a waste stream as a process feeding⁶⁴. Therefore, new appropriate applications have to be developed in order to reuse the fibres, and chopped fibers composites might thus be the most convenient approach. Though in general short-fibers reinforced materials cannot perform as good as the long fiber ones, nevertheless they can be used for a wide number of applications such as internal panels for automotive, lightweight sports equipment and, more generally, where lightness is a premium property, while performance not as much. Thus, the possibility of using some recycled fibers, whose mechanical properties can be around 80/90% of the initial values, depending on the applied recycling process¹⁶⁰⁻¹⁶², might be economically promising. This approach might also help widening the fields of use of such chopped carbon fiber composites, since the secondary raw material approach might provide a wider and possibly cheaper source for the reinforcement, without weighing on the pristine fibers market. A preliminary attempt at re-using the fibers after pyrolysis and gasification carried out on the fiber produced in the Curti pilot plant suggested that the obtained composites could reach good performances⁶³.

However, such a preliminary work was not carried out in optimized conditions, thus no actual reliable conclusion could be drawn. Hence, in the present work, the previously discussed fibers, both virgin and pyrolyzed, which were chopped down to a suitable length (about 20mm), were mixed with a two-components epoxy resin formulation (feed: CCF/resin=60/40 ratio) in order to produce Short Carbon Fibers Reinforced Composites (SCFRC) based on both the pristine and oxidized virgin fibers (Comp-VF) and the pyrolyzed (Comp-Py) ones. In this case, fibers length was shortened with respect to previous work (20 vs 25mm)⁶³ to provide a better mixing with the resin, thus also allowing to increase their content in the final composite from 50 to 60%wt. Moreover, the curing cycle was optimized with respect to the preliminary work, with the addition of a low T isothermal step promoting an efficient resin and fiber mixing to improve the compactness of the obtained panels. While all the previously discussed fibers were used to produce composites, as reported in Table 13, Py fibers without any additional treatment lead to strongly heterogeneous samples, with voids and separation between resin rich regions and dry fibers areas, detectable even by a naked eye.

Table 13. Thermo-mechanical properties of chopped carbon fiber reinforced composites.

	AAD ^a (g/cm ³)	Fiber fraction ^b (%)	T _g ^c (°C)	E (GPa)	σ _b (MPa)	ε _b (%)
Comp-VF	1.38±0.04	62	102	3.9±0.4	140±18	7±1
Comp-VF_500.20	1.37±0.04	61	99	3.9±0.3	102±22	5±2
Comp-VF_500.60	1.37±0.03	65	100	4.3±0.5	106±10	4±1
Comp-VF_600.20	1.37±0.05	60	99	3.8±1.8	97±31	3±1
Comp-Py	0.9±0.21	/	/	n.d.	n.d.	n.d.
Comp-Py_500.20	1.32±0.05	61	103	4.1±0.3	149±27	6±1
Comp-Py_500.60	1.34±0.02	62	99	3.7±0.4	132±17	6±1
Comp-Py_600.20	1.33±0.02	58	100	3.2±0.4	133±22	7±2

^a Average Apparent Density (AAD) determined as the average of the ratio between measured weight and volume of the single bars as cut in the convenient dimension for mechanical tests.

^b Calculated by thermogravimetric analysis as described in the experimental section.

^c Determined by DMA analysis.

Composites were obtained as flat panels that were then cut in coupons suitable for further characterization. Each of the obtained coupons was measured and weighted in order to obtain an index of the compactness of the sample, defined as Apparent Density (AD): the AD of each coupon has then been averaged in order to provide information about the

overall homogeneity of the samples. Comp-Py shows the lowest Average Apparent Density (AAD) out of all the produced panels confirming that no good compaction can be reached when rigid char coated fibers are used, since the amorphous carbon coating layers prevents the fibers bundles from correctly being impregnated by the resin, thus making the composites unsuitable for further characterization, as previously reported⁶³. SEM micrographs (Figure 42) of samples purposefully fractured, clearly highlight the difference between Comp-Py with scarcely impregnated fibers, which keeps also a prevailing unidirectional orientation as in the starting bundle, and a poor resin infiltration among them (Figure 42A and Figure 42C), and Comp-Py_500.60 which shows a homogenous mix of fibers and resin (Figure 42B and Figure 42C). The latter is also representative of all the other Comp-X panels. For all the other samples, the overall AAD was significantly improved with respect to the preliminary work⁶³ upon the application of the modified procedure. It is also worth to point out that none of the fibers has been subjected to a further sizing treatment after the gasification process: hence, besides the untreated VFs, none of the fibers brings a surface coupling agent helping to promote adhesion toward the polymer matrix in the composite production. With the aim of assessing the actual carbon fibers fraction in each composite, all the samples were analyzed by TGA. Measurements were carried out first in an inert atmosphere up to 500°C to pyrolyze the resin component; then, after lowering the temperature down to 300°C, the atmosphere was switched to air to remove the carbonaceous residue derived from the incomplete resin degradation (the same phenomenon that occurs during the pyrolysis process) by oxidation at a temperature which is raised again up to 500°C where the sample is kept isothermally for 30'. The cooling step before switching to the oxidizing atmosphere is applied to slow down the oxidation of the char residue, thus avoiding an uncontrolled heat release that might negatively affect the fiber stability.

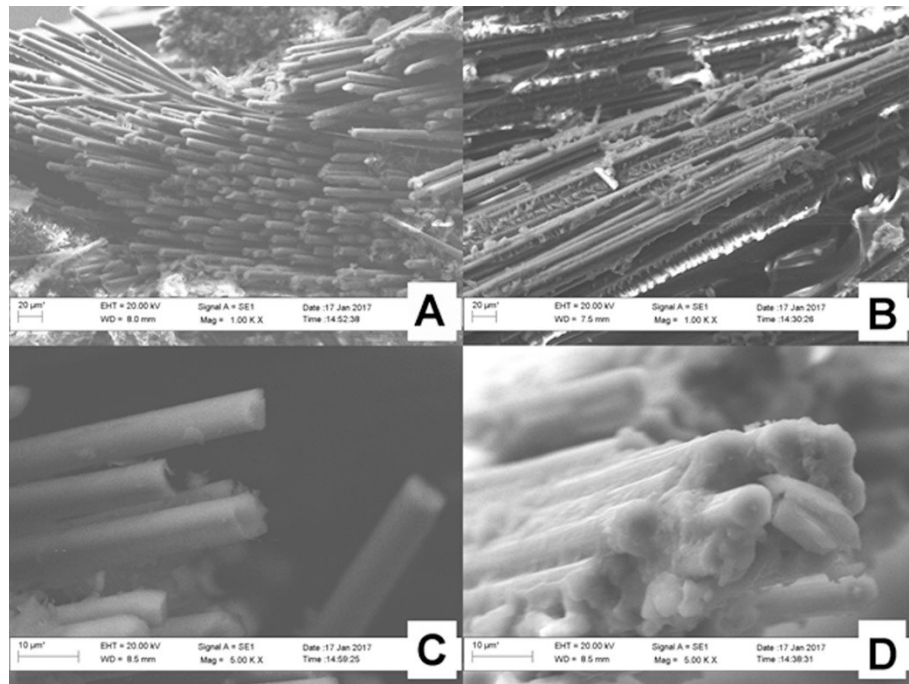


Figure 42. SEM micrographs at different magnification, 1000x (A and B) and 5000x (C and D), of fracture surfaces of Comp-Py (A and C) and of Comp-Py_500.60 (B and D).

It was, indeed, proved earlier in the present paper that, in those circumstances, the resin can be completely removed, as displayed in Figure 42A for the process applied to the pure epoxy resin, while the fibers are safely maintained (Figure 42B), thus providing a quick and reliable method for the determination of the fiber fraction in the composite, as reported in Table 13.

TGA thermograms display indeed a first degradation process attributed to thermal degradation of the resin component¹⁶³ that, irrespective of the fiber used, begins around 300°C, and a second stepwise weight loss attributed to the gasification of the char residue, occurring upon the second heating process in oxidizing atmosphere. As displayed in Figure 43 for Comp-VF 500-60, when the carbon fibers themselves begin to undergo thermal degradation after switching to the oxidizing atmosphere, the 1st derivative of the weight loss curve perfectly highlights the change in the process rate, thus proving the threshold limit taken in order to define the resin content in the samples reported in Table 13. The adopted TGA process displays that the fiber content is well representative of the resin/fiber original feed, with no substantial modification.

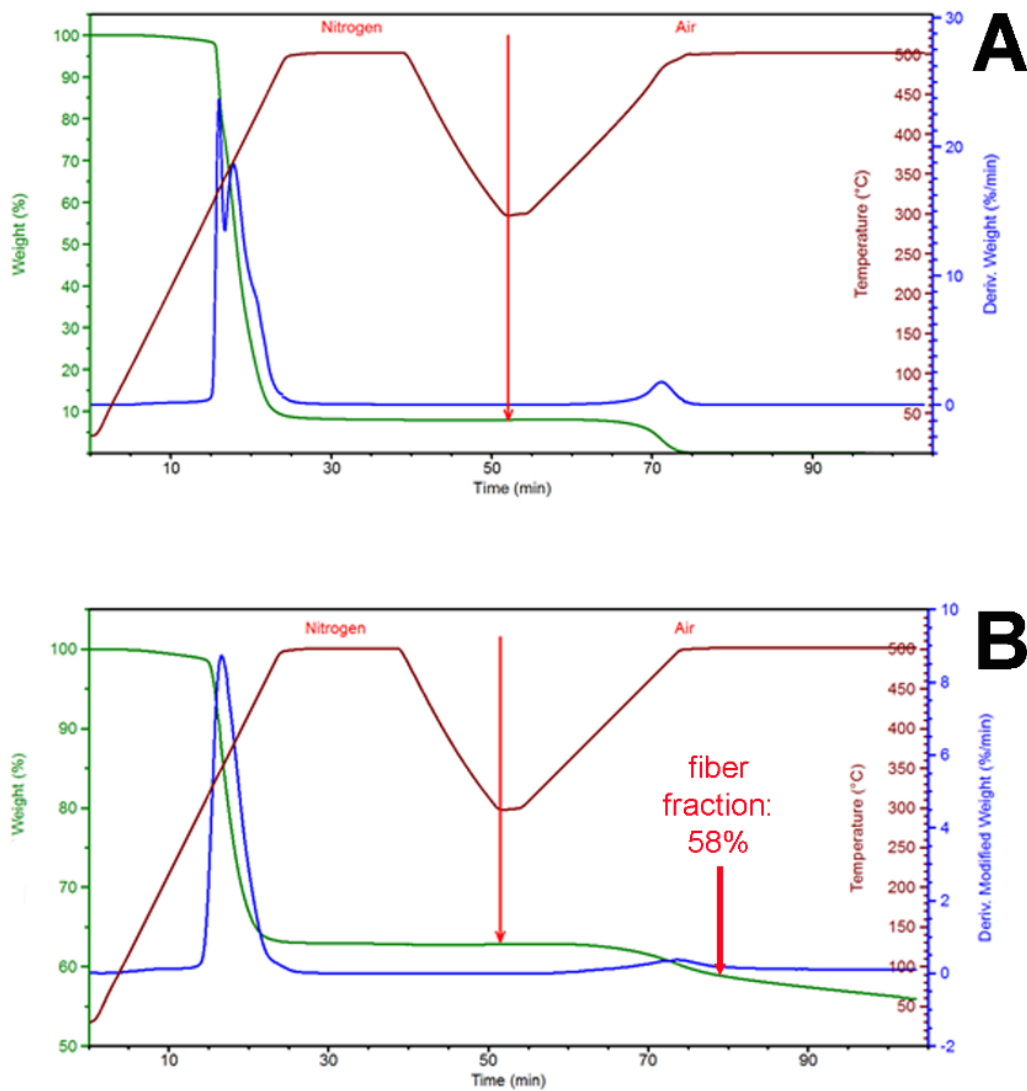


Figure 43. TGA thermograms of pure epoxy resin and of Comp-VF 500-60 showing the approach used to determine the fiber fraction in the composites. First, the weight losses of the pure resin are identified, then in the composite the residual weight is taken where no more degradation ascribed to the resin is present: this value is considered as the fiber fraction.

Mechanical stress/strain measurements in tensile mode were carried out with the aim of providing comparative properties of the composites obtained with recycled fibers with respect to those obtained from virgin pristine fibers as well with those obtained from oxidized virgin fibers. Owing to the previously discussed lack of good compaction, mechanical tests were not carried out on Comp-Py specimen. As a guideline, five samples for each formulation were analyzed, selecting those whose specific AD was the highest, in order to avoid voids and imperfections as much as possible. Test results, recorded in Table 13, show that higher mechanical performances were obtained with respect to the preliminary data⁶³. Besides an expected increase in the mechanical properties due to the augmented fiber fraction in the composites, the obtained data stem also from the better

compaction achieved in the present case (see AAD in Table 13). When comparing the properties of Comp-VF with the ones registered for composites obtained from oxidized virgin fibers, the latter display a significant drop in their ultimate performance at break. On the other hand, the properties of Comp-VF well compare with those observed for the composites produced with all the pyrolyzed/gassified fibers, both in terms of Young modulus and of ultimate strength and elongation, with a slight decrease for the sample treated up to 600°C, Comp-Py_600.20. Such a result represents a significant improvement with respect to the preliminary data⁶³, since it demonstrates that the pyro-gassified fibers can reach properties comparable to the analogue virgin ones. It is worth to point out that Comp-VF performance would benefit, among other parameters, of the surface sizing treatment that might help promote fiber matrix adhesion and which was reasonably removed upon oxidation. The latter statement stems from the observation that all the oxidized VF fibers display a decrease in their diameter, thus supporting the hypothesis of outer layers removal, and with them the sizing too. In this case, the lack of performance might be due to some decrease in the single fiber properties upon gasification treatment, and some lack of adhesion, which is not sufficiently replaced by the oxidized groups that forms on the carbon fibers during gasification. The presence of such oxidized groups which, upon curing of the epoxy matrix, might promote covalent bonds with the resin via the oxygen rich moieties on the fiber surface, thus acting as a multifunctional cross-linker as sketched in Figure 44, could be one of the reasons of their ability to provide a reinforcing action comparable, or even better, than the sizing coated VF.

Such a possibility looks attractive also for the use of the pyro-gassified fibers in the presence of different matrices, such as phenolic resins or polyurethanes, etc. The surface oxygen content measured by EDX (Table 12) indeed, well compares with the Comp-VF fiber series as well as Comp_Py performance, besides the one of Comp-Py_600.20. In the latter case, indeed, the slight decrease of the mechanical performance is associated to the highest surface oxygen fraction. It is worth to note that both Comp-VF_600.20 and Comp-Py_600.20, the composites obtained out of the fibers treated at the highest temperature, do not display the best results in terms of mechanical behavior, suggesting that such a high temperature, besides being able to completely remove char residues, could be detrimental for the fiber properties as previously reported by Meredith¹⁶⁰. Moreover, it should also be kept in mind that the pyrolytic fibers studied in this work are obtained working at 500°C, hence the possibility of oxidizing the fibers at the same temperature used for pyrolysis can

foresee the application of an *in line* thermal treatment carried out directly on the hot solid residue at the end of the pyrolysis process. Finally, the obtained positive result was proof of the reliability of the obtained recovered carbon fibers when used as secondary raw material, thus encouraging a significant investment by Curti S.p.A. to promote the scale up of the overall process to provide an integrated pyro-gassification semi—industrial plant, that is presently being finalized.

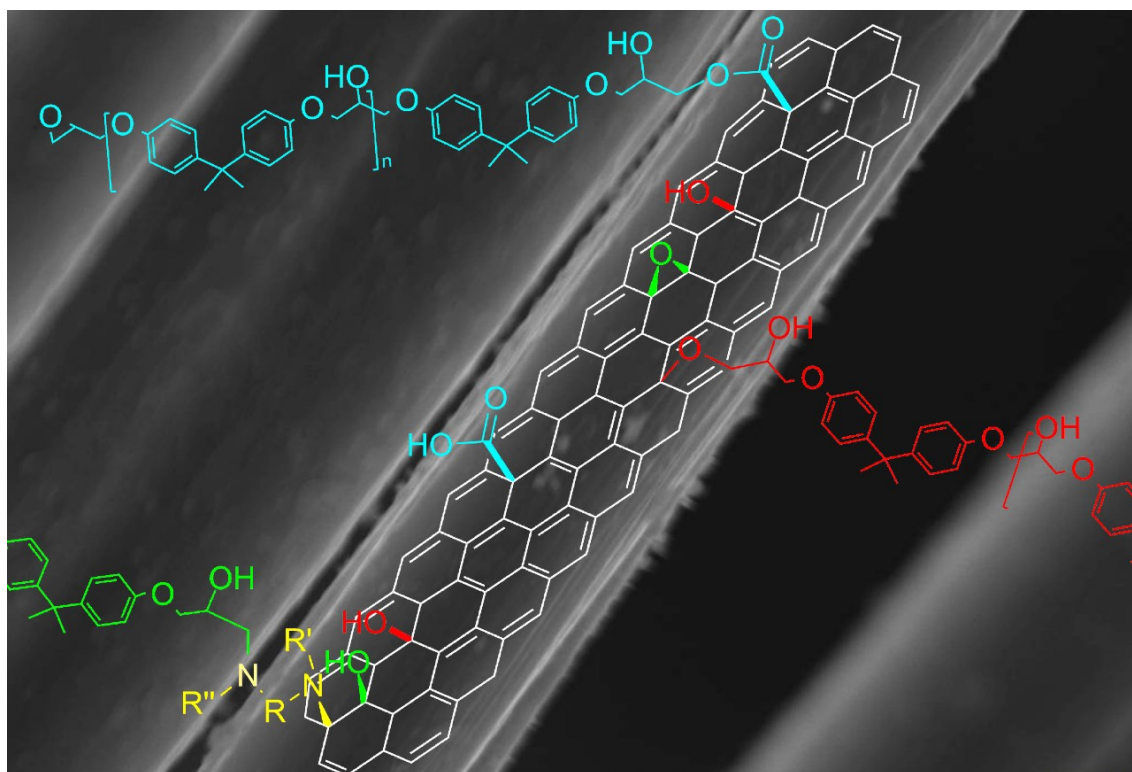


Figure 44. Sketch of the reactivity of oxidized groups on surface of the pyro-gassified fibers in the presence of epoxy resin promoting fiber/matrix interphase adhesion.

4.4. Conclusions

In the present work, the application of an oxidative treatment was assessed both on virgin and on pyrolyzed carbon fibers, showing that no additional damage comes to the fibers that were already subjected to high temperature treatment in the pyrolysis batch. On the contrary, the char layer, whose removal requires the oxidation treatment, acts as a protective coating hampering an excessive damage of the fibers. Moreover, when such oxidized fibers are used to produce short fiber reinforced composites upon reduction of their length to 20 mm, their final performances are comparable to those of a pristine fibers composite, where fibers still bear a sizing treatment. This behavior can be ascribed to the formation of oxidized groups on the fiber surface, which can promote chemical adhesion

between the graphitic layer and the crosslinking matrix. Hence, while for the pyrolytic fibers to be positively re-used an additional oxidation treatment is necessary, here it was demonstrated that such a treatment can be carried out in the same condition as the pyrolysis process and is able to boost the fiber/matrix adhesion, given that gasification conditions are finely controlled and tuned for application. These results provided sufficient validation of the pyro-gasified CF quality, which lead to the scale up of the process to produce an integrated pyro-gasification semi—industrial plant.

Chapter 5

Toward more sustainable high-performance CFRPs by coupling bio-based epoxy resins and recycled carbon fibers.

5.1. Introduction

Nowadays carbon fiber reinforced polymers (CFRPs) are the most important structural composites having extraordinary mechanical and physical properties like lightweight, low coefficient of thermal expansion (CTE), high stiffness and high strength^{4,7}. These multifunctional materials are now used widely, not only in the aerospace or military industries, but also in large and increasing number of commercial mechanical engineering applications, such automotive, sports goods, civil engineering, medical equipment, pressure vessels, wind power, transport⁵. Commonly, these CFRPs are made of epoxy thermoset polymer matrixes and carbon fibers, which are almost all petroleum-derived^{3,4}.

Carbon fibers possess exceptional specific tensile strength and modulus ranging from 20-1000 GPa and 1-7 GPa, respectively, which represent the highest values for any commercial reinforcing fibers^{7,164,165}. Currently, carbon fibers are typically made from PAN-fibers (more than 90%) and a small part from peach precursors, consequently their fabrication and price are strongly influenced by the price and availability of fossil fuels and energy required for their manufacturing (see §1.2.2).

Despite the total dependence on non-renewable sources of their current precursors, the worldwide demand for carbon fibers continue to grow: according to the latest estimates, it will rise to some 117.000 tons by 2022⁵. This growing demand can be directly associated with the unique advantages of CFRPs and their new industrial applications. Cost-effective

and renewable alternative to PAN for carbon fiber precursors are under investigation since the first commercialization of carbon fibers. Cellulosic fibers, like Rayon, have been used commercially and investigated most extensively; although it is possible to get rayon carbon fibers with good properties, their expensive manufacturing process stopped their production and currently there are no commercial carbon fibers made from rayon^{165,166}. Current research studies on carbon fibers from bio-based precursors have received increasing attention; among naturally occurring biomass, lignin and cellulose are considered as potential carbon fiber precursors because of their low cost and carbon-forming chemical structure^{146,164,167}. However, no bio-based carbon fibers with comparable tensile strength and modulus have been obtained so far, and this makes inappropriate their application in CFRPs production. By contrast, in the last decades, a number of recycling technologies have been proposed and developed to reclaim high-quality recycled carbon fibers from scraps or end of life (EoL) CFRPs^{61,64,168,169}. Among these, pyrolysis process allows recovering cost-effective carbon fibers that still preserve high performance in term of elastic modulus and failure straight and it is currently the only process which has now reached early stages of commercialisation^{62,63,81,157,163}. We must consider that recycled carbon fibers have usually a short length^{63,64,145,170}: the recycled carbon fibers in fact, come from CFRPs waste that are shredded, crushed or cut into small pieces before the reclamation treatment and chopped again after it in order to conform the recovered carbon fibers to a homogenous length before reusing them^{61,63,145,157}. Furthermore, recycled carbon fibers cannot be reused in same applications but they can be randomly incorporated into matrix materials, like in short carbon fiber-reinforced polymers (SCFRPs) manufacturing. Despite the lower performance, SCFRPs show some advantages in comparison with the continuous fiber-reinforced composites, like lower cost, isotropic mechanical properties and easier and cheaper manufacturing processing¹⁷¹.

In *Chapter 4*, the potential of the pyro-gasification process to produce carbon fibers as secondary raw materials that can be reused in non-structural application was demonstrated. Boing¹⁷² estimated that recycling carbon fiber can be done at approximately 70% of the cost and using less than 5% of the electricity required to make new carbon fibers. A LCA study¹⁵⁰ highlighted that when carbon fibers are recycled and reused to replace virgin carbon fibers, the impacts to the environment are considerably reduced. Hence, at this time the reuse of recycled carbon fibers, having comparable properties to the virgin's ones,

might be a more environment sustainable choice when a low cost and eco-friendly SCFRPs is required.

If it is still difficult to obtain valid carbon fibers from bio-based precursors or less energy intense processing routes, there are instead many opportunities to develop partially or fully bio-based epoxy resins^{118–120,132}, which are suitable for the CFRP manufacturing. In *Chapter 3*, for instance, two bio based epoxy resins were studied and their properties appeared suitable for CFRP applications; many others high performance bio-based epoxy resins have already obtained and reported in different reviews^{118–120,124,132}.

The primary aim of this work was to couple recycled carbon fibers recovered via pyrolysis with bio-based resins. In *Chapter 4* and in a previous work⁶³, it was demonstrated that an additional oxidation treatment is necessary in order to efficiently re-use the carbon fibers reclaimed from the pyrolysis of cured and uncured CFRPs waste. This post-treatment not only can be carried out at the same temperature as the pyrolysis process, but also improves the fiber/matrix adhesion when the oxidation/gasification conditions are finely controlled (see *Chapter 4*).

To the best of our knowledge, currently there are no examples of CFRPs obtained by coupling bio-based epoxy resins and recycled carbon fibers. By contrast, numerous works on the use of natural fibers with bio-based polymers and thermosetting epoxies are already published^{142,173–177}.

Thus, the recycled carbon fibers obtained by pyrolysis, and post-treated in an oxidative environment at 500 °C for 60 minutes (see *Chapter 4*), were used for the production of composite materials together with the two novel, highly bio-based epoxy resins precursors reported in *Chapter 3*: DGEVA (Diglycidyl Ether of Vanillyl alcohol) and DGEGD (Diglycidyl Ether of Gastrodigenin).

More sustainable composites have been produced and characterized and their thermomechanical properties were compared to those one of composites obtained with virgin fibers (Vi) and/or petroleum epoxy resin (EPON828). This research was also carried out in collaboration with Professor Stanzione, both at Rowan University and at University of Bologna.

5.2. Experimental

Materials

Virgin chopped fibers (30 mm) were obtained cutting down Unidirectional Fabric UC 301 based on Toray T700S 12K dry fabrics. These fibers will be labelled as “Vi”. The recycled carbon fibers (Re) (30 mm) were obtained as reported in *Chapter 4* (see Experimental), from pyrolyzed Toray T700S 12K based carbon fiber post-treated at 500°C for 60 minutes under oxidizing atmosphere. Both virgin and recycled carbon fibers are used without any other treatment.

The two bio-based resins pre-polymers, DGEVA and DGEDG were synthesized following the synthetic routes reported in *Chapter 3* and in the previous work¹³². The commercial BPA- and petroleum-based epoxy resin pre-polymer (EPON 828) and the curing agent/hardener EPIKURE W (Diethylmethylbenzenediamine) were purchased by Air Products and Chemicals, Inc and used as received.

Preparation of Vi-SCFRPs and Re-SCFRPs

The epoxy pre-polymers were cured in the same way as reported in the experimental section reported in *Chapter 3*. The epoxy resin systems (15g) were prepared by adding and stirring a stoichiometric amount of the hardener EPIKURE W to each pre-polymer in the amounts reported below:

- | | | |
|---------------------|--------------|----------------|
| • Epon828/Epikure W | 100:23wt/wt% | 12.15:2.85 g/g |
| • DGEDG/Epikure W | 100:38wt/wt% | 10.89:4.11 g/g |
| • DGEVA/Epikure W | 100:33wt/wt% | 11.24:3.76 g/g |

Then Virgin (Vi) or Recycled (Re) Carbon Fibers (15g) were added and carefully hand-stirred with pre-mixed bio-based or commercial pre-polymers-hardener systems in a fiber/matrix=50/50 weight ratio. Being DGEVA solid at RT ($T_m = 53$ °C), only for the preparation of DGEVA-based composites, the curing agent and the carbon fibers were added at approximately 55°C. The random-oriented resin/Carbon fiber mixture (30 g) was transferred into an aluminium mold with a 85 x 85 x 5 mm cavity which was closed with a counter-mold tailored to allow the excess resin to come out from the edges (see Figure 45). The materials were then hot-press cured according to the following procedure and cure-cycle: the mold was inserted in the press with the plates already heated at 100°C, where it was kept in isotherm for 30 minutes and the pressure was raised gradually up to

100 bars in the first 5 minutes. After that, the temperature was raised at 180°C and the sample was kept isothermally for further 90 minutes. Finally, before opening the hot-press plates, the mold was allowed to cool to 100 °C and then removed from the hot-press.



Figure 45. Pre-impregnated random-oriented carbon fibers transferred into the mold cavity (on the left), the filled mold with the counter-mold inserted before the cure occurs (on the right).

The hot-press cure was performed on a CARVEN Bench Top Laboratory Manual Press with Electrically Heated Platens (Model 4122) with 12 tons capacity. The complete hot-press cure process is schematically illustrated in Figure 46.

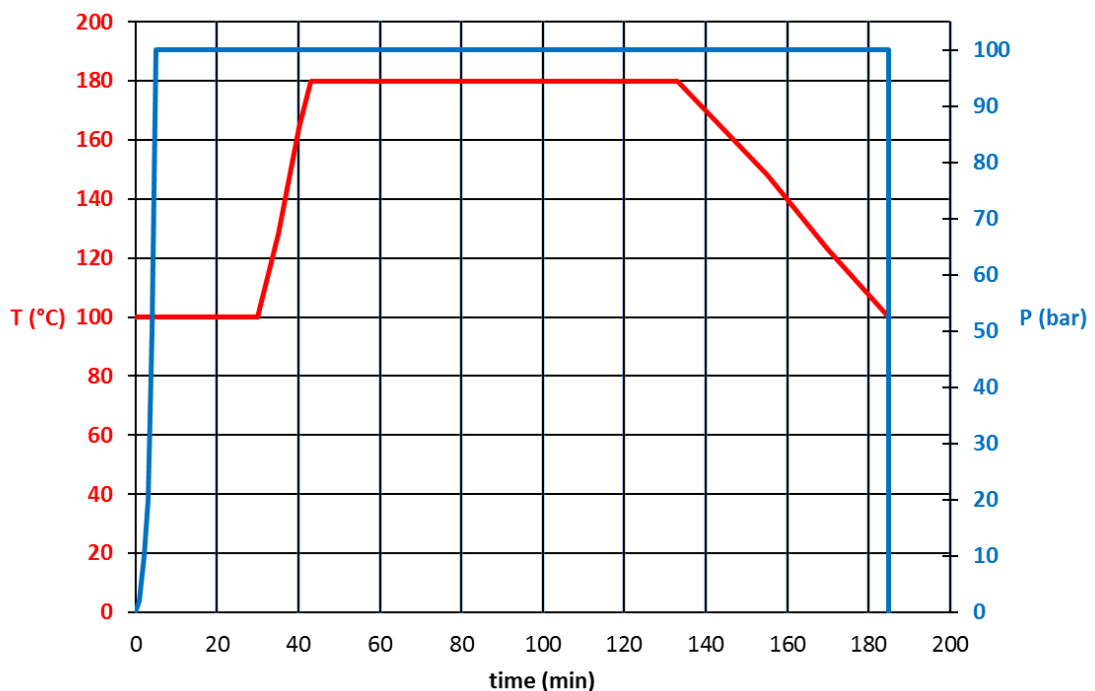


Figure 46. Hot-press used composite cure cycle.

After cooling down to RT, a 85 x 85 x 2 mm composite panel was removed from the mold (see Figure 47). Thus, we obtained composites containing recycled carbon fibers and the

bio-based resin precursors (Re-DGEGD-C and Re-DGEVA-C) or the petroleum one (Re-EPON828-C). For the sake of comparison, the virgin carbon fibers were combined also with EPON828 (Vi-EPON828-C). At least two composite panels were produced for each resin/fiber combination.



Figure 47. Pictures of composite panels after cure: Re-DGEVA-C on the left and Re-DGEVA-C on the right.

Every single composite panel was then cut for the preparation of the different specimens in order to perform thermal and mechanical characterization (Figure 48).

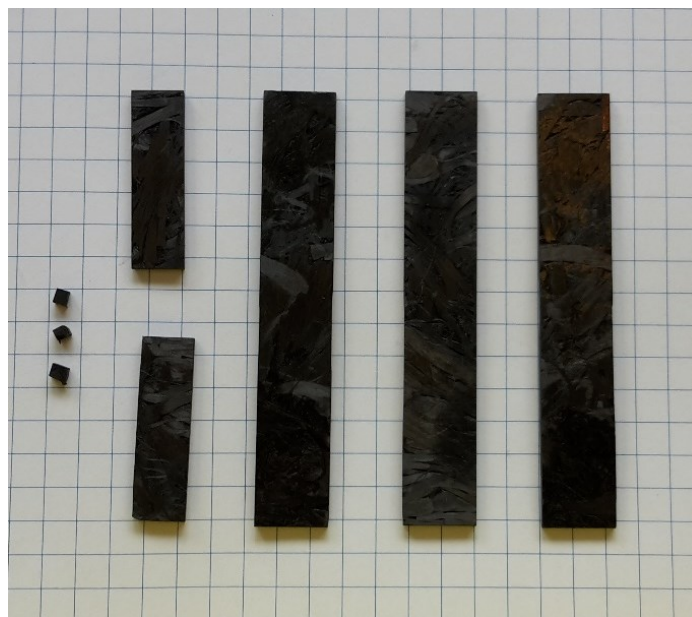


Figure 48. Example of the different specimens used for the characterization of the composites: from the left TGA, DMA and tensile test samples, respectively.

Characterization

The viscoelastic properties of the all cured composites were measured using a TA Instruments Q800 DMA. Each sample was prepared with uniform dimensions of $35 \times 11 \times 2 \text{ mm}^3$ (Figure 48) and tested using single cantilever geometry. The tests were performed at a frequency of 1.0 Hz, a deflection amplitude of oscillation of $7.5 \mu\text{m}$, and a Poisson's ratio of 0.35. The heating ramp rate for each test was $2 \text{ }^\circ\text{C}/\text{min}$ from 20 up to $250 \text{ }^\circ\text{C}$. Each sample was run in triplicate to ensure consistency with the measured data. The E'' peak and $\tan \delta$ peak values were calculated for each resin. Additionally, the temperature at the E' onset point was calculated and reported. The standard error for modulus and T_g are reported in $\pm 2 \text{ GPa}$ and $\pm 3 \text{ }^\circ\text{C}$, respectively. All the DMA data are reported in Table 15.

The thermogravimetric properties were measured using a TA Instruments discovery Thermogravimetric Analyzer (TGA-550). Approximately 15-10 mg of all composite samples (Figure 48), taken from different areas of the composite panels, were placed in a platinum pan and analysed according to the following method developed to estimate the carbon fiber content. First, samples were heated from RT to 500°C at $20^\circ\text{C}/\text{min}$ heating rate in inert atmosphere (nitrogen 45 ml/min balance gas flow rate and 25 ml/min sample gas flow rate), left in isotherm for 30 minutes and cooled to 350°C . Then the atmosphere was switched to air (same balance and sample flow rate) and the samples were left in isothermal for 5 minutes before heating them again at $20^\circ\text{C}/\text{min}$ heating rate up to 550°C ; a final 20-minute isothermal step completed the composite TGA runs. The obtained residue is taken at 70' of the TGA-running time, corresponding to the end of the char combustion, identified as peak in the DTG curve (see Figure 49). Thermogravimetric properties, including the onset temperature (T_{onset}) and the temperature at maximum decomposition rate (T_{max}), are determined from the first heating ramp under nitrogen atmosphere. The standard error for TGA temperatures data and carbon fiber fraction are $\pm 3 \text{ }^\circ\text{C}$ and $\pm 2 \%$, respectively.

Tensile tests were carried out at room temperature with an Instron-type tensile testing machine (REMET TC10) equipped with a 10kN load cell, using a crosshead speed of 1 mm/min and initial gauge length of 30 mm. At least five $85 \times 15 \times 2 \text{ mm}$ specimens (Figure 48) were tested for each different composites. The Young's modulus (E), between the 0.25% and the 0.5% of deformation, the stress (σ_b) and the strain (ϵ_b) at break were calculated. The data standard error are reported in Table 16.

A Scanning Electron Microscope (SEM) ZEISS EVO 50 EP in Environmental mode with ≈ 100 Pa pressure in the chamber was used to examine the fracture surface of the samples' composites after tensile tests.

All composites' densities at room temperature were measured using Archimedes' principle. At least three DMA-samples (Figure 48) for each composite were used. The standard error for density is ± 0.01 g/cm³.

5.3. Results and discussion

Bio-based composites production and characterization

Short carbon fiber are currently produced by cutting virgin continuous carbon fiber tow and are commonly used with thermoplastic matrixes in injection molding technologies^{3,8}. Currently, random-short carbon fibers prepreg, having a thermosetting matrix (typically epoxy or polyester resins) are commercialized and used in automotive and aeronautic industry. SCFRPs offer a significant advantage over long-fiber composites in manufacturing of complex parts and possess isotropic and lightweight properties^{3,8,178,179}. The main handicap of using randomly oriented short-fiber composites is the significant loss in specific mechanical properties^{8,62,171,180}; this loss can be partially compensated from the high performance of carbon fiber (tensile moduli and strength) but it is not enough to produce composites for structural application^{3,8,62,157,181,182}. The SCFRPs properties do not depend only on the types of the matrix and fiber, but also other factors contribute, such as manufacturing processes, fiber concentration, fiber length, fiber orientation and fiber matrix adhesion: all these factors are interconnected^{3,8,63,157,181,183}.

SCFRP composites have already obtained in a lab-scale manufacturing process by using compression-molding techniques; usually short carbon fibers are added and carefully hand-stirred with a liquid thermoset matrix and the mixture are subsequently placed in a particular purpose-made mold and cured in a heated platens hot-press under pressure^{61,63,145}.

In this work, the recycled fibers and bio-based epoxy resins discussed in *Chapter 4* and in *Chapter 3* respectively were combined in order to obtain new more sustainable composites by a hot-press compression molding in an aluminum mold specially manufactured for this study. The mold was designed with a cavity with a tailored counter-mold that can close the mold leaving a very small spacing along its outside-edges (Figure 45). This mold

configuration allows the resins excess to come out and, at the same time, to apply a uniform pressure on the pre-impregnated fibers that should ensure a homogeneous composition and a decrease of void in the final composite panel. Furthermore, this lab-scale manufacturing process allows obtaining a high carbon fiber fraction in the final composites.

The hot-press cure cycle (Figure 46) and manufacturing process conditions were optimized with respect to the two previous works^{63,132} and the results were presented in *Chapters 3* and *4*.

The produced composites and their compositions are shown in the list below:

- Vi-EPON828-C, which is made of short virgin carbon fibers and EPON828/EPIKURE W epoxy resin system
- Re-EPON828-C, which is made of short recycled carbon fibers and EPON828/EPIKURE W epoxy resin system
- Re-DGEVA-C, which is made of short recycled carbon fibers and DGEVA/EPIKURE W epoxy bio-based resin system
- Re-DGED-C, which is made of short recycled carbon fibers and DGED/EPIKURE W epoxy bio-based resin system

All the composites were obtained as flat panels (Figure 47) that were cut and shaped to uniform dimensions for their characterization (Figure 48). Each composite panel was first weighted in order to get its final weight after the demolding: in fact, as said before, only the resin can come out during the cure so, subtracting the final composite weight to the known the amount of feeding carbon fibers (15g), we can have a preliminary estimation of the residue resin content within the composite. For all the composite panels the average resin content was estimated to be around the 28 ± 1 wt%, corresponding to a fiber content of about the 72 ± 1 %.

Since TGA requires just a few mg sample size, the output of such an analysis would provide data, which might be strongly affect by local fluctuation in the specific composition. Hence, at least triple replica for each sample is required to provide statistically significant results. The previously introduced TGA carbon fiber content estimation approach (*Chapter 4*) has been applied; however, owing to the high charring ability and to the higher thermal resistance of the presently used resins, in the present case some modifications have to be applied to obtain reliable results. As shown in Figure 49,

first of all an inert atmosphere up to 550°C is used to break-down the resin component; then the temperature is lowered, the atmosphere is switched to air and the temperature raised again to fully burn the char residue derived from the resin degradation. The resin's char combustion can be clearly identify as a peak in the 1st derivative TGA curves (DTG) under air atmosphere (Figure 49). When the peak intensity decreases and the DTG curve reaches a plateau-zone, the char degradation is completed and the further weight loss can be attributed to the carbon fiber degradation, that usually occurs under oxidation condition at temperatures above 500 °C⁹; thus, at this transition point the weight residue mostly correspond to the fiber content. The whole method is based on the assumptions that the carbon fibers losses weight that occur at these temperatures are insignificant and the char residue derived from the resin degradation burns completely during the analysis. As reported in Figure 49, in this work the fiber content is taken as the residue at the 70th minute. The TGA estimated fiber content is 72±2 wt% for all composites except for Re-DGEVA-C where it is 70±2 wt%.

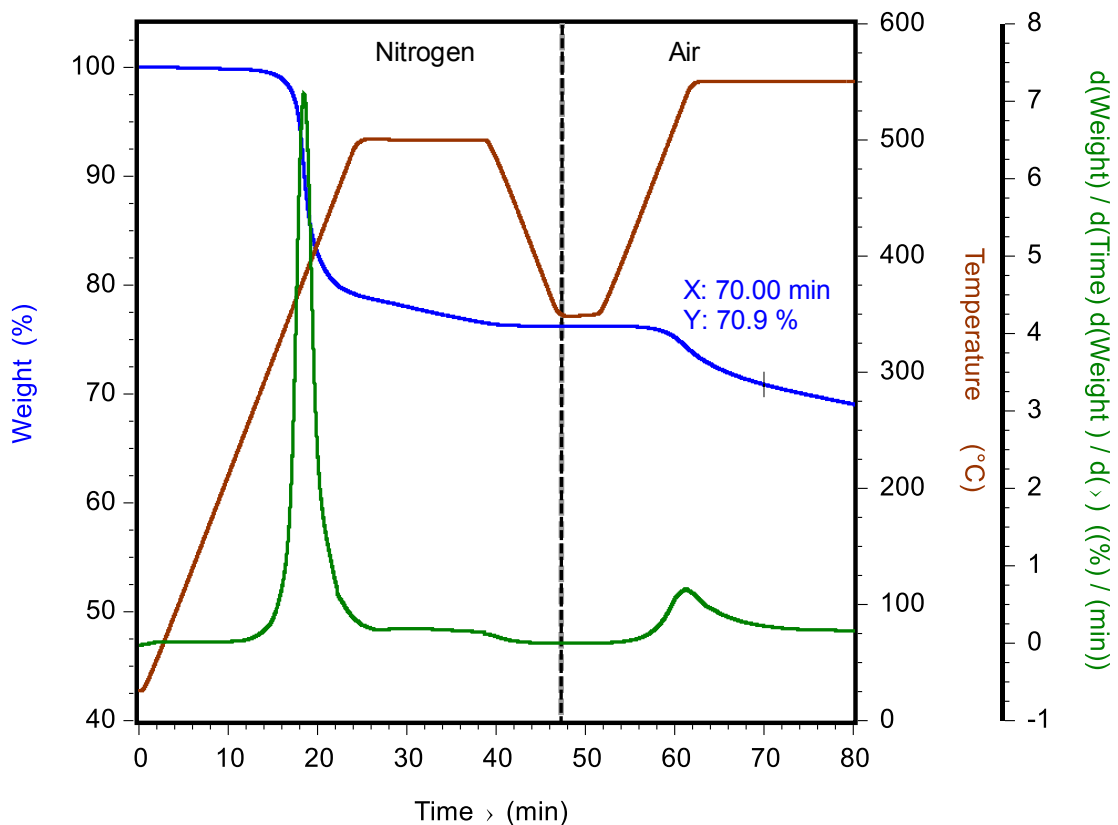


Figure 49. TGA (—) and DTG (—) curves of Re-DGEGD-C and their temperature profile (—).

Moreover, from the TGA and DTG curves (Figure 49), the T_{onset} and the T_{max} of the first degradation process, attributed to thermal degradation of the resin component¹⁶³, were determined (Table 14). Despite the TGA data have been collected with a different heating rate, these display a similar behavior of the plain resins TGA data discussed in *Chapter 3*. All the composites are thermally stable up to 350 °C, a temperature that is consistent with the data reported in the literature^{63,169} and much higher than the CFRP service temperature^{3,8}.

Table 14. TGA data and densities of all produced SCFRPs composites.

Sample	Density (g/cm ³) ^a	T_{onset} (°C) ^b	T_{max} (°C) ^c	Fiber fraction (wt%) ^d
Vi-EPON828-C	1.51	377	396	72
Re-EPON82-C	1.47	374	394	72
Re-DGEVA-C	1.45	358	375	70
Re-DGEGD-C	1.47	361	382	72

^a Measured according to Archimedes' principle at 25°C.

^b Determined at the TGA-curve onset point in nitrogen (heating rate 20°C/min)

^c Determined as the temperature at the peak maximum of the DTG curve in nitrogen (heating rate 20°C/min).

^d Determined at the 550°C-isothermal step in air at the 70th minute.

In order to clarify the quality of the SCFRCs samples, the density for each different composite were obtained according to Archimedes' principle (Table 14). All the produced composites possess close average densities ranging from 1.45 to 1.51 g/cm³. The higher density (1.51 g/cm³) was measured in Vi-EPON828-C while the relatively lower values in all recycled carbon fibers based composites. Nevertheless, the densities are in agreement with the expected density for a quasi-isotropic epoxy CFRP (1.55 g/cm³)⁸. In addition, the density data suggest that even with a manual lab scale process, a high carbon fiber dosage (about 70%), and the lack of sizing on recycled carbon fibers, a good compaction has been reached in all the fabricated composites.

Thermo-mechanical properties of the all produced SCFRPs were measured using DMA. All the composites show an E' modulus at 25°C which is an order of magnitude higher than their own plain resin (Figure 50), confirming the good reinforcing properties of both virgin and recycled carbon fibers. Considering a standard error of ± 2 GPa, the absolute values of the E' modulus (Table 15) are quite similar to each other. The data variability is expected, and indeed observed, probably owing to the random carbon fibers orientation^{8,161,178,180}. Moreover, the high quantity of carbon fibers in the feed, 50 wt%,

makes difficult to manually obtain an efficient and perfectly homogeneous impregnation during their manufacture.

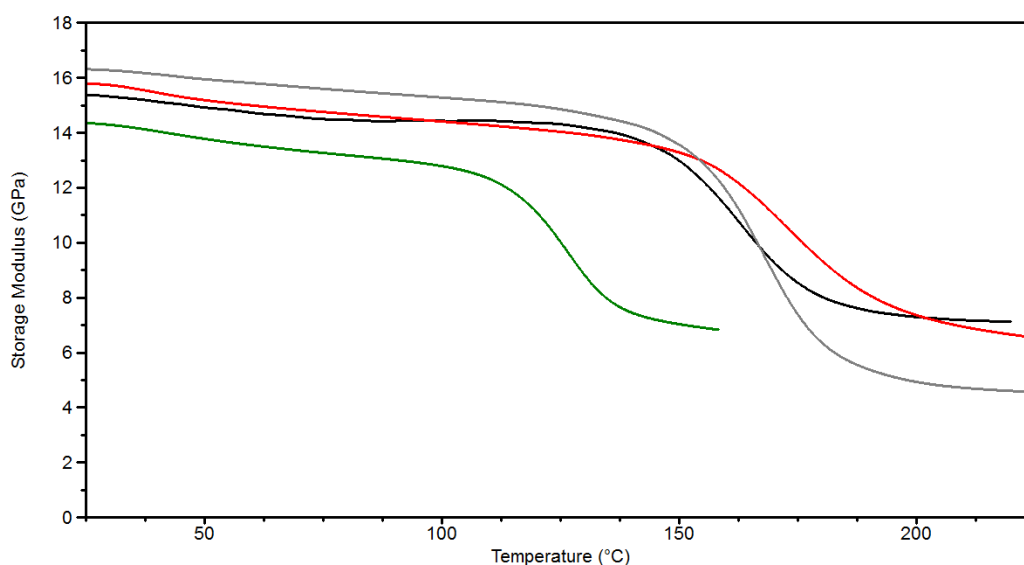


Figure 50. DMA E' curves of Vi-EPON828-C (—), Re-EPON828-C (—), Re-DGEVD-C (—) and Re-DGEVA-C (—).

Nonetheless, the variability of the DMA measured E' modulus is still within acceptability. In the DMA analysis in fact, a deformation of few micron is applied on highly stiff samples and it might resent of some local inhomogeneity of the samples. This hypothesis is supported by the low E' modulus (14 GPa) of the Re-DGEVA-C composite which has an estimated fiber content of about 70%. Instead, the temperature at the E' onset of the different composites displays the same behaviour found in the plain resins in *Chapter 3*: in the DGEVA-based composite the E' modulus drops down at about 115 °C, in the other ones at about 160 °C. The $\tan \delta$ and the E'' curves are plotted as a function of temperature in Figure 51. All the analysed composites show a main relaxation process (α) whose position depends on the type of epoxy resin systems and their T_g s after the curing; only a lower β relaxation peak, centred at 55 °C was detected for the DGEVA-based composite, as observed for the plain DGEVA based resin¹³². Although a shorter cure cycle was used to cure the composites (Figure 46), their T_g s (Table 15), are considerably higher than those obtained for the corresponding plain resins in *Chapter 3*, except for the EPON 828 based composite where a slight decrease in viscoelastic properties was observed. The DGEVA-based composite confirms what already observed in the plain DGEVA resin, i.e. the β relaxation peak that is ascribed to the methyl group in the aromatic ring of the VA and a lower the T_g due to the presence of the methoxy in meta-position that increases the free volume within the polymer network¹³². Noteworthy are the increases in the resins' T_g

which are as high as +8°C and + 10 °C for the DGEVA and DGEGD-based composite, respectively. These positive increases are usually observed in heterogeneous materials and can be ascribed to the hindered chain mobility due to the intimate contact between the crosslinked polymer backbone and the carbon fibers surface.

Table 15. DMA data of all produced SCFRP composites.

Sample	E' (GPa) ^a	E'_{onset} (°C)	T_g (°C) ^b	T_g (°C) ^c
Vi-EPON828-C	17	157	171	175
Re-EPON82-C	16	157	170	174
Re-DGEVA-C	14	114	128	130
Re-DGEGD-C	16	160	181	185

^a E' measured at 25 °C

^b T_g measured as the temperature at the peak maximum of the loss modulus (E'') curve.

^c T_g measured as the temperature at the peak maximum of the tan δ curve.

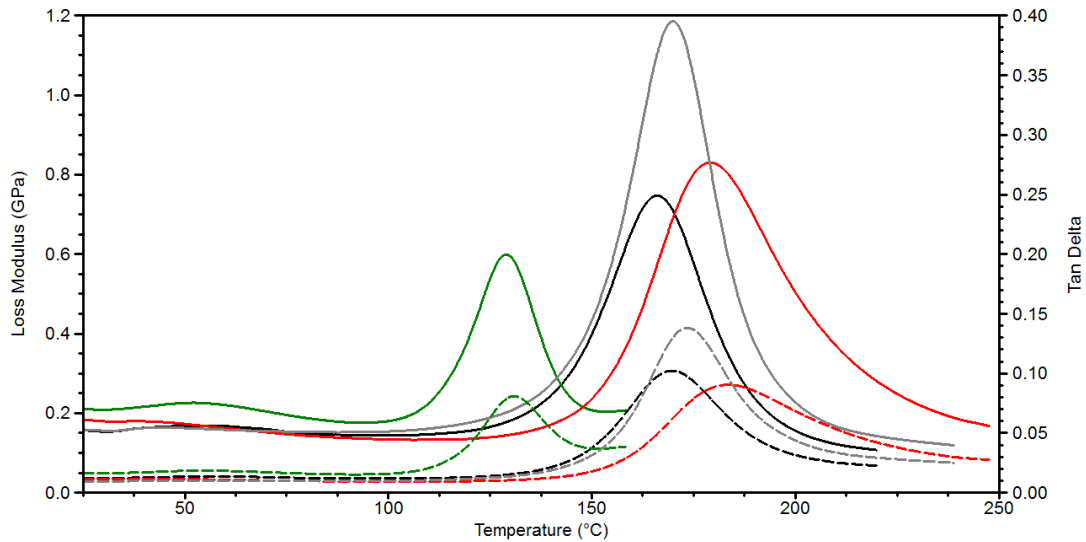


Figure 51. E'' (solid line) and tan δ (broken line) DMA curves of Vi-EPON828-C (—), Re-EPON828-C (—), Re-DGEGD-C (—) and Re-DGEVA-C (—).

The mechanical proprieties of all the composites were also investigated by tensile tests. The Young's modulus and the tensile strength and strain at break were collected and reported in Table 16.

Table 16. Tensile mechanical properties of all produced SCFRP composites.

Sample	Young's modulus (GPa)	σ_b (MPa)	ϵ_b (%)
Vi-EPON828-C	6.4±0.3	190±38	4.3±0.8
Re-EPON82-C	5.8±0.8	132±13	2.9±0.9
Re-DGEVA-C	5.8±0.7	124±26	2.6±0.3
Re-DGEGD-C	5.7±0.5	126±12	2.3±0.5

Figure 52 shows some curves of the tensile stress versus strain, representative of the tests performed on each different composite. The EPON828 based composites, made of virgin (Vi-EPON828-C) and recycled (Re-EPON828-C) carbon fibers, display different remarkable mechanical tensile properties: Re-EPON828-C lost about a 10% in the Young's modulus and a 30% in their properties at break, with respect to Vi-EPON828-C.

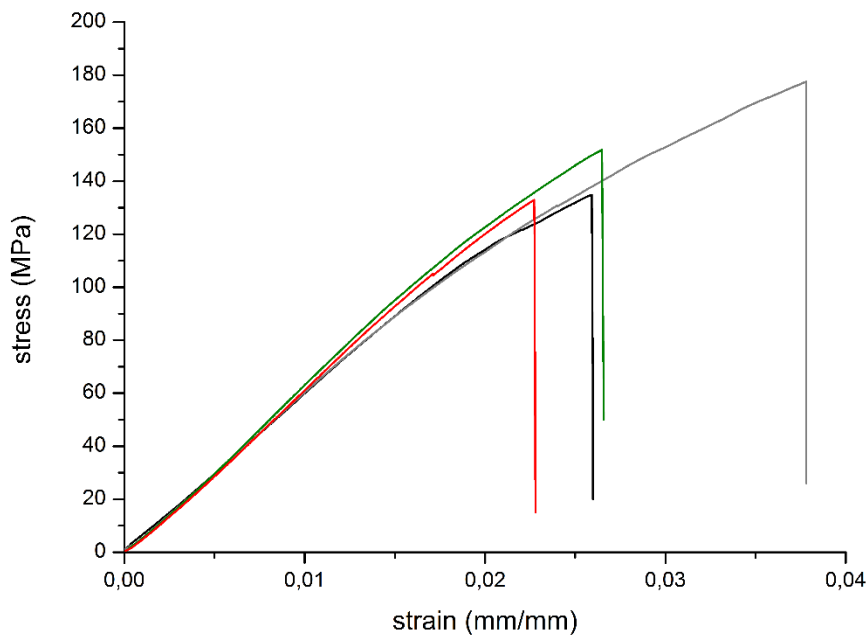


Figure 52. Representative stress versus strain curves of the obtained SCFRPs: Vi-EPON828-C (—), Re-EPON828-C (—), Re-DGEGD-C (—) and Re-DGEVA-C (—).

These losses in mechanical properties are generally observed in the literature^{64,145,161,163} when carbon fibers reclaimed by pyrolysis are used. Conversely, previous results discussed in *Chapter 4*, showed comparable tensile mechanical properties for both virgin and recycled carbon fiber composites. In this work, the longer carbon fibers length, 30 mm as opposed to 20 mm, might not have promoted the full disentanglement of the virgin carbon fiber bundles during the hand-impregnation, increasing the possibility of encountering aligned bundles along the section of the tensile specimens. Thus, the mechanical properties at break of Vi-EPON828-C might largely be improved by this higher presence of aligned bundles; the discrepancy in Young's moduli can instead be also ascribed to the 10% more of fiber content, which could have highlighted the worsening of recycled carbon fiber performances occurred during the pyrolytic reclamation process^{64,145,161,163}.

However, other factors that do not directly depend on the recycled fiber quality must be considered: the presence of sizing on virgin fibers and the filamentous (no bundles),

random, low-density-packing (fluffy) form of recycled carbon fibers^{62,64,184}. Virgin carbon fibers, coated with a thin film of sizing agent, possess improved surface properties, like handleability, wettability and interfacial adhesion with the polymer matrixes^{3,4,139,184}. Moreover, sizing agents can modify the surface roughness and promote chemical reactions within the interphase region, formed by fiber sizing agent, pre-polymer and hardener¹⁵⁴. The gasification treatments required before reusing recycled carbon fibers^{63,64,149}, as observed in *Chapter 4*, can introduce oxidized groups on the fiber surface, which might promote covalent bonds with the resin components, thus acting as a multifunctional cross-linker. However, the different epoxy systems used in this work as well as the higher fiber fraction within the composites did not lead to take advantage from these oxidized groups. In addition, the almost preserved sized tow (bundle) form of virgin carbon fibers leads to a much better adhesion between the single filaments, which are in contact with others almost continuously along its length¹⁴⁶, as well as a to ensure effective fiber-matrix load transfers. By contrast, the disaggregation of the bundles in recycled carbon fibers after the reclamation treatments may reduce these possibilities of contact between the each single fiber and increase the randomness of the fibers orientation as well as the isotropic character of the final composites. These phenomena were supported by two reported SEM micrographs (Figure 53 A and B) of the fracture surface of virgin (Figure 53A) and recycled based composites (Figure 53 B).

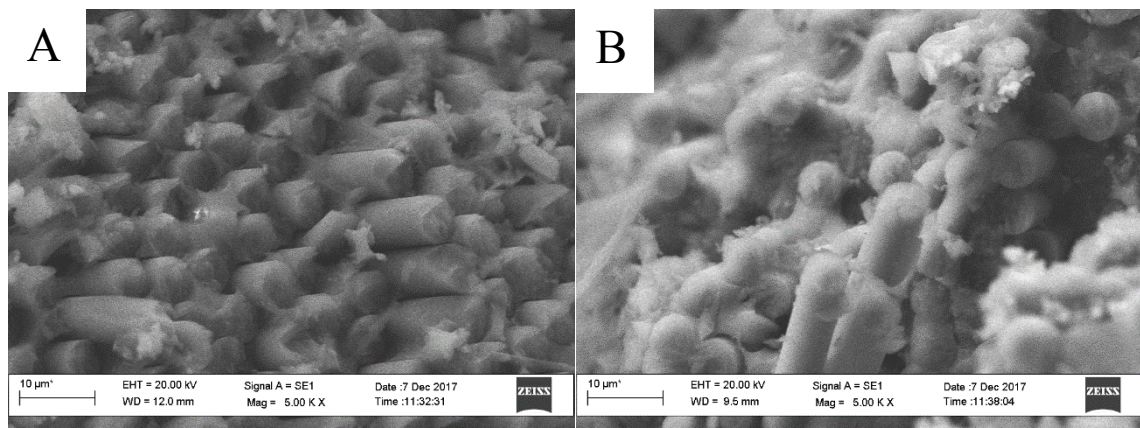


Figure 53. SEM micrographs of fracture surfaces of Vi-EPON828-C (A) and Re-DGEVA-C (B).

In Figure 53A the fracture surface allows to identify a virgin carbon fibers bundle where the resin surrounds every single fiber filaments and the main failure mechanisms is due to the fibers breakage. Instead, Figure 53B shows a fracture zone of recycled carbon fibers composite where the resin is not homogeneously distributed along the single fibers, but it fills the empty space due to the low-density-packing (fluffy) form of recycled fibers.

Debonding and fiber pull-out failure mechanisms occur in recycled carbon fibers based composites.

Interestingly, the mechanical properties of the two bio-based composites, Re-DGEVA-C and Re-DGEGD-C, show the same behaviour than the Re-EPON828-C (Figure 52 and Table 16). On the other hand, when the BPA-petroleum based epoxy pre-polymer EPON828 is replaced by the bio-based DGEVA and DGEGD, the matrix does not seem to contribute to the final properties of the composites that, within the obtained data variability, remain essentially comparable.

5.4. Conclusions

In this work, the possibility to couple recycled carbon fibers with highly bio-based epoxy resins was investigated and new more sustainable bio-based composites were produced. First, the thermo-mechanical properties of SCFRPs made of both virgin and recycled carbon fibers were assessed using a BPA-petroleum resin (EPON828); then two bio-based epoxy pre-polymers, DGEVA and DGEGD, cured with the same commercial curing agent, were used for making SCFRPs with recycled carbon fibers only. All the obtained composites have a high carbon fibers dosage (about the 70 wt%), good thermal stability until 350°C and T_g s greater than 128 °C. In particular, the Re-DGEGD-C composite shows a T_g that is higher than that obtained in Vi- EPON828 and Re-EPON828-C.

The EPON828 based composites, made of virgin (Vi-EPON828-C) and recycled (Re-EPON828-C) carbon fibers, display different mechanical tensile properties: Re-EPON828-C loses about a 10% in the Young's modulus and a 30% in their properties at break, with respect to Vi-EPON828-C. Such a difference in tensile mechanical properties are not only ascribed to the lower properties of the recycled carbon fibers, but also to the lack of sizing and the fluffy form of those.

Interestingly, Re-DGEVA-C and Re-DGEGD-C perform the same tensile mechanical properties of the recycled EPON828 based composites, highlighting the aptitude of these bio-based epoxy prepolymers to replace current BPA- petroleum-based epoxy resins in the future.

This pioneering work could pave the way for the development of more sustainable, high performance CFRP materials and drive toward the increase of polymers and composites

derived from renewable or sustainable resources. In addition, this study represents another example of how to efficiently re-use carbon fibers reclaimed by pyrolysis.

In the future, tensile, flexural, and rheological properties will be explored for all the bio-based prepolymers to gain a complete understanding of the process-structure-property relations of these materials. The bio-based resins will be used to produce SCFRPs also with virgin carbon fibers to confirm their propensity in high performance applications. Furthermore, it will be interesting to evaluate the mechanical properties of SCFRPs made of desized-virgin carbon fiber in order to understand how much really the sizing affects the SCFRPs mechanical properties.

Chapter 6

Conclusions and future works

On epoxy resin modification with improved flame behaviour (Chapter 2)

In the polymer, industry there exists a need for new, more effective, and environmentally friendly flame resistance polymers. The use of some traditional agents, such as halogenated flame retardants, has suffered limitations as possible sources of halogenated dioxins and dibenzofurans, which are extremely toxic compounds. The ecological problem, associated with the low efficiency in terms of the percentages of use of traditional inorganic systems based on $\text{Al}(\text{OH})_3$, $\text{Mg}(\text{OH})_2$, has then pushed towards the search for new flame-retardant systems: recent data show that organoclays intercalated with suitable functional cations can be used for the production of nanocomposites with flame retardant characteristics.

The hydrated cations are ion-exchanged with organic cations such as more bulky alkylammoniums, it usually results in a larger interlayer spacing and in a more lipophilic clay (organoclay). This modification is obviously helpful when these materials have to be used as nano-fillers to promote the intercalation/exfoliation in the composite, for improving thermo-mechanical and flame resistance properties of the starting polymer.

Due to the organic nature of the polymer matrix, CFRPs suffer from poor fire resistance. *Chapter 2* investigated the flame-retardancy effect on a commercial epoxy resin system, commonly used as polymer matrix in CFRPs manufacturing. Two new organoclays were prepared from the modification of bentonite with nitrogen-based organic compounds BFTDA and APUA.

Lower amount of organoclay dispersed into the epoxy resin do not display any detrimental effect on its curing process and thermal properties, but instead they can improve its flame behaviour. In particular, cone-calorimeter measurements show that the addition of pristine bentonite leads to an increased flammability of the modified-epoxy resin with respect to

the plain resin. The bento-BFTDA organoclay leads to a decreased flammability of the composite with respect to the pristine bentonite containing epoxy resin, but its flame behaviour is quite similar to the plain resin. The APUA-containing resin show instead an encouraging decrease of 17% and 29%, in the Peak Heat Release Rate (pHRR) with respect to the plain resin (NEAT) and to the plain R-BENTO-3, respectively, with just a 3 %wt loading level; moreover a reduction of both FPI and FIGRA indexes, an overall sign that the material tends to be less prone to propagating the fire is observed. In this case, it is worth noting that the same amount of nanofillers, which helps improving thermomechanical performances, is the same that provides the best fire behaviour.

These promising preliminary results, showing a potential for the application of the selected APUA-modified organoclays as flame retardants. A well-optimized and scaled-up dispersion method of this new organoclay could be an alternative solution for improving epoxy matrixes flame behaviour before their use in CFRPs manufacturing. In the future, it will be interesting to evaluate the flame CFRPs flame behaviour of composites made of APUA-modified epoxy resin and carbon fiber.

On bio-based epoxy curing agent modification (Chapter 3)

Nowadays, epoxy resins are almost totally petroleum and BPA based and take about the 70 % of the thermosetting polymer market. Due to the BPA environmental and health issues and the global tendencies toward the more sustainable materials, new alternative and bio-based epoxy resins are nowadays a real target and real challenge from future epoxy resins.

Among all the potential bio-based epoxy resins resources, lignocellulosic materials, lignin resulted very interesting because it is one of the most abundant renewable organic resource present on the earth¹²². In particular, some lignin derivatives, the VA and GD allowed to obtain bio-based epoxy resin having good thermal-mechanical properties¹³² which could be potentially improved by replacing aliphatic curing agents with aromatic ones. In fact, in a prospective to replace BPA- and petroleum-based epoxies in composite materials, bio-based epoxy resins having high T_g s (usually greater than 90 °C), relatively short curing times and better physical properties are required.

In *Chapter 3*, two bio-based epoxy-prepolymers, the DGEVA and the DGEDD, were synthesized and characterized. Both the bio-based prepolymers and a commercial BPA-based epoxy one (EPON 828) were cured with an aromatic commercial curing agent,

EPIKURE W. The thermo-mechanical properties for both the bio-based and the commercial based resins are generally improved or never display a worsen behaviour respect with the same resins cured with an aliphatic hardener. Noteworthy are the improvements in the resins' T_g : +20 °C, + 47 °C and + 27 °C for the DGEVA, DGEGD, and EPON 828-based resin, respectively; also, a significant increase of the resins' char yields was obtained.

This different curing agent led to epoxy resins that well match the required properties to a CFRPs epoxy matrix.

These observations show that, depending on the foreseen applications, the bio-based epoxy resins properties can be tuned by simply changing the curing agents. This approach may encourage the commercialization of bio-based epoxies and their application in composite industry or in other sectors.

Further investigations will be attended with new, or already available, bio-based epoxy prepolymers and different curing agents, which should be bio-based as well, in order to obtain a fully bio-based resin.

On reuse of carbon fibers recovered by pyrolysis and their reuse (Chapter 4)

The increasing use of carbon fiber reinforced polymers (CFRPs) raised the interest in the research of new procedures and technologies to separate and recover carbon fibers from industrial scraps and/or end-of-life materials. Accordingly, the demand for carbon fibers, that grew from 27000 tons in 2009 to 53000 tons in 2014, is foreseen to more than double by 2021 with an expected request of 116000 tons¹⁴¹. Such a boost in the CFRP exploitation is now raising the awareness about their fate.

In this regard, the pyrolysis process appears very attractive for recycling of composites, allowing the recovery of short carbon fibers with high added value that can be reintroduced in the production processes; furthermore pyrolysis is also currently considered to be the only process for recycling CFRPs that is available on an industrial scale.

A previous work⁶³ highlighted the importance of removing the carbonaceous layer (char) present on the surface of the carbon fibers recovered via pyrolysis in order to allow their efficient re-use. This proposition was further confirmed in *Chapter 4* where the oxidative treatments were applied both on virgin and on pyrolyzed carbon fibers. It was observed that during these treatments no additional damage comes to the fibers that were already

subjected to high temperature treatment in the pyrolysis batch. On the contrary, the char layer, acts as a protective coating hampering an excessive damage of the fibers. Moreover, when such oxidized fibers are used to produce short fiber reinforced composites upon reduction of their length to 2 cm, their final performances are comparable to those of a pristine fibers composite, where fibers still bear a sizing treatment. This behavior can be ascribed to the formation of oxidized groups on the fiber surface, which can promote chemical adhesion between the graphitic layer and the crosslinking matrix. Hence, while for the pyrolytic fibers to be positively re-used an additional oxidation treatment is necessary, it was demonstrated that such a treatment can be carried out at the same temperature as the pyrolysis process and is able to boost the fiber/matrix adhesion, given that gasification conditions are finely controlled and tuned for application.

These results provided sufficient validation of the pyro-gasified CF quality, which lead to the scale up of the process to produce an integrated pyro-gasification semi-industrial plant. As a result, the pyro-gasification process has the potential to produce carbon fibers as secondary raw materials, and gaseous and liquid by-products that can sustain the process energy requirement or, from which, some molecules platform could be separate.

The main challenge of this project will be to recover high added value carbon fibers by a self-sustainable process. In this way, the CFRPs recycling will be promoted reducing considerably the issue related to the CFRPs waste disposal. Furthermore, the carbon fibers reclaimed by pyrolysis could totally replace virgin short carbon fiber in nowadays composite market, especially in non-structural application, even making the pyro-gasification process remunerative.

On reusing recycled carbon fibers with highly bio-based epoxy resins (Chapter 5)

Currently, carbon fibers are typically made from PAN-fibers (more than 90%) and a small part from peach precursors; consequently their fabrication and price are strongly influenced by the price and availability of fossil fuels and energy required for their manufacturing. Numerous attempts have been making in order to obtain bio-based carbon fibers with comparable tensile strength and modulus from renewable resources. However, there are not bio-based precursors that allow to produce carbon fibers with comparable performances. By contrast, in the last decades, a number of recycling technologies have been proposed and developed to reclaim high-quality recycled carbon fibers from scraps or end of life (EoL) CFRPs, as discussed in *Chapter 4*.

Short recycled carbon fibers, reclaimed by the pyro-gasification of CFRPs waste were coupled with highly bio-based epoxy resins with the aim to produce new more sustainable bio-based composites. First, the thermo-mechanical properties of SCFRPs made of both virgin and recycled carbon fibers were assessed using a BPA-petroleum resin (EPON828); then two bio-based epoxy pre-polymers, DGEVA and DGEGD, cured with the same commercial curing agent, were used for making SCFRPs with recycled carbon fibers only. All the obtained composites have a high carbon fibers dosage (about the 70 wt%), good thermal stability until 350°C and T_g s greater than 128 °C. In particular, the Re-DGEGD-C composite shows a T_g that is higher than that obtained in Vi- EPON828 and Re-EPON828-C.

The EPON828 based composites, made of virgin (Vi-EPON828-C) and recycled (Re-EPON828-C) carbon fibers, display different mechanical tensile properties: Re-EPON828-C loses about a 10% in the Young's modulus and a 30% in their properties at break, with respect to Vi-EPON828-C. Such a difference in tensile mechanical properties are not only ascribed to the lower properties of the recycled carbon fibers, but also to the lack of sizing and the fluffy form of those.

Interestingly, Re-DGEVA-C and Re-DGEGD-C perform the same tensile mechanical properties of the recycled EPON828 based composites, highlighting the aptitude of these bio-based epoxy prepolymers to replace current BPA- petroleum-based epoxy resins in the future.

This pioneering work could pave the way for the development of more sustainable, high performance CFRP materials and drive toward the increase of polymers and composites derived from renewable or sustainable resources. In addition, this study represents another example of how to efficiently re-use carbon fibers reclaimed by pyrolysis.

In the future, tensile, flexural, and rheological properties will be explored for all the bio-based prepolymers to gain a complete understanding of the process-structure-property relations of these materials. The bio-based resins will be used to produce SCFRPs also with virgin carbon fibers to confirm their propensity in high performance applications. Furthermore, it will be interesting to evaluate the mechanical properties of SCFRPs made of desized-virgin carbon fiber in order to understand how much really the sizing affects the SCFRPs mechanical properties.

Bibliography

1. T. Benelli, L. Mazzocchetti, E. D'Angelo, M. Lanzi, F. Saraga, L. Sambri, M. C. Franchini, and L. Giorgini, *Polym. Eng. Sci.*, 2017, **57**, 621–630.
2. T. Benelli, E. D'angelo, L. Mazzocchetti, F. Saraga, L. Sambri, M. C. Franchini, and L. Giorgini, *AIP Conf. Proc.*, 2016, **1736**.
3. S. Mazumdar, *Composites manufacturing: materials, product, and process engineering*, CRC Press, London, 2001.
4. K. K. Chawla, *Composite Materials: Science and Engineering*, Springer, New York, Third Edit., 2012.
5. E. Witten, M. Sauer, and M. Kuhnel, *Composites Market Report 2017*, 2017.
6. H. Lee and K. Neville, *Handbook of epoxy resins*, McGraw-Hill, 1967.
7. E. J. Barbero, *Introduction to Composite Materials Design*, Taylor & Francis, CRC Press., 2011.
8. P. Mallick, *Fiber-reinforced composites: materials, manufacturing, and design*, London, 3 rd., 2008.
9. H. O. Pierson, *Handbook of Carbon, Graphite, Diamond and Fullerenes*, Park Ridge, NJ, USA, NOYES PUBL., 1993.
10. S. Das, J. Warren, D. West, S. M. Schexnayder, S. Das, J. Warren, D. West, and S. M. Schexnayder, *Global Carbon Fiber Composites Supply Chain Competitiveness Analysis Global Carbon Fiber Composites Supply Chain Competitiveness Analysis*, 2016.
11. <http://zoltek.com/carbon-fiber/how-is-carbon-fiber-made/>, Zoltek, Toray Gr.
12. Rocky Mountain Institute, *Carbon fiber cost breakdown*, 2011.
13. F. Hussain, *J. Compos. Mater.*, 2006, **40**, 1511–1575.
14. D. R. Paul and L. M. Robeson, *Polymer (Guildf.)*, 2008, **49**, 3187–3204.
15. A. Geim and K. Novoselov, *Nat. Mater.*, 2007, **6**, 183–191.
16. E. Giannelis, *Adv. Mater.*, 1996, 29–35.
17. M. M. Shokrieh, A. R. Kefayati, and M. Chitsazzadeh, *Mater. Des.*, 2012, **40**, 443–452.
18. M. W. Ho, C. K. Lam, K. tak Lau, D. H. L. Ng, and D. Hui, *Compos. Struct.*, 2006,

- 75, 415–421.
19. F. Laoutid, L. Bonnaud, M. Alexandre, J. M. Lopez-Cuesta, and P. Dubois, *Mater. Sci. Eng. R Reports*, 2009, **63**, 100–125.
 20. M. Alexandre and P. Dubois, *Mater. Sci. Eng. R Reports*, 2000, **28**, 1–63.
 21. A. B. Morgan and C. A. Wilkie, *Flame Retardant Polymer Nanocomposites*, John Wiley & Sons, 2007.
 22. M. M. Schmidt, G.;Malwitz, *Curr. Opin. Colloid Interface Sci.*, 2003, **8**, 103–108.
 23. D. M. Marquis, É. Guillaume, and C. Chivas-joly, in *Nanocomposites and Polymers with Analytical Methods*, ed. J. Cuppoletti, InTech, 2005, p. 261.
 24. G. Mogilevsky, Q. Chen, A. Kleinhammes, and Y. Wu, *Chem. Phys. Lett.*, 2008, **460**, 517–520.
 25. A. Omrani, L. C. Simon, and A. A. Rostami, *Mater. Chem. Phys.*, 2009, **114**, 145–150.
 26. I. A. Rahman and V. Padavettan, *J. Nanomater.*, 2012, **12**, 1–15.
 27. M. S. A. Bhuyan, M. N. Uddin, M. M. Islam, F. A. Bipasha, and S. S. Hossain, *Int. Nano Lett.*, 2016, **6**, 65–83.
 28. C. Lee, X. Wei, J. Kysar, and J. Hone, *Science (80-.)*, 2008, **321**, 385–8.
 29. A. A. Balandin, S. Ghosh, W. Bao, I. Calizo, D. Teweldebrhan, F. Miao, and C. N. Lau, *Nano Lett.*, 2008, **8**, 902–907.
 30. Y. Zhang, Y.-W. Tan, H. L. Stormer, and P. Kim, *Nature*, 2005, **438**, 201–204.
 31. J. S. Bunch, S. S. Verbridge, J. S. Alden, A. M. Van Der Zande, J. M. Parpia, H. G. Craighead, and P. L. McEuen, *Nano Lett.*, 2008, **8**, 2458–2462.
 32. M. D. Stoller, S. Park, Y. Zhu, J. An, and R. S. Ruoff, *Nano Lett.*, 2008, **8**, 3498–502.
 33. A. Oberlin, M. Endo, and T. Koyama, *J. Cryst. Growth*, 1976, **32**, 335–349.
 34. S. Iijima, *Nature*, 1991, **354**, 56–58.
 35. Q. Zhang, J. Q. Huang, W. Z. Qian, Y. Y. Zhang, and F. Wei, *Small*, 2013, **9**, 1237–1265.
 36. J. R. Potts, D. R. Dreyer, C. W. Bielawski, and R. S. Ruoff, *Polymer (Guildf.)*, 2011, **52**, 5–25.
 37. G. Mittal, V. Dhand, K. Y. Rhee, S.-J. Park, and W. R. Lee, *J. Ind. Eng. Chem.*, 2015, **21**, 11–25.
 38. J. Prakash, J. C. Pivin, and H. C. Swart, *Adv. Colloid Interface Sci.*, 2015, **226**, 187–202.
 39. W. Zhang, G. Camino, and R. Yang, *Prog. Polym. Sci.*, 2017, **67**, 77–125.
 40. S. W. Kuo and F. C. Chang, *Prog. Polym. Sci.*, 2011, **36**, 1649–1696.
 41. M. Zammarano, M. Franceschi, S. Bellayer, J. W. Gilman, and S. Meriani, *Polymer*

- (*Guildf*)., 2005, **46**, 9314–9328.
42. G. Camino, G. Tartaglione, A. Frache, C. Manfredi, and G. Costa, *Polym. Degrad. Stab.*, 2005, **90**, 354–362.
 43. Z. Weng, T. Senthil, D. Zhuo, L. Song, and L. Wu, *J. Appl. Polym. Sci.*, 2016, **133**, 1–11.
 44. S. Liu, H. Yan, Z. Fang, and H. Wang, *Compos. Sci. Technol.*, 2014, **90**, 40–47.
 45. X. Wang, L. Song, W. Pornwannchai, Y. Hu, and B. Kandola, *Compos. Part A Appl. Sci. Manuf.*, 2013, **53**, 88–96.
 46. H. Gu, J. Guo, S. Tadakamalla, X. Zhang, Q. He, Y. Huang, H. a. Colorado, S. Wei, Z. Guo, and X. Yan, *Ind. Eng. Chem. Res.*, 2013, 130517061934003.
 47. E. Franchini, J. Galy, J. F. Gérard, D. Tabuani, and A. Medici, *Polym. Degrad. Stab.*, 2009, **94**, 1728–1736.
 48. Q. Wu, C. Zhang, R. Liang, and B. Wang, *J. Therm. Anal. Calorim.*, 2010, **100**, 1009–1015.
 49. C. F. Kuan, W. J. Chen, Y. L. Li, C. H. Chen, H. C. Kuan, and C. L. Chiang, *J. Phys. Chem. Solids*, 2010, **71**, 539–543.
 50. S. S. Rahatekar, M. Zammarano, S. Matko, K. K. Koziol, A. H. Windle, M. Nyden, T. Kashiwagi, and J. W. Gilman, *Polym. Degrad. Stab.*, 2010, **95**, 870–879.
 51. G. Beyer, *Plast. Addit. Compd.*, 2005, **7**, 32–35.
 52. G. Beyer, *Plast. Addit. Compd.*, 2002, **4**, 22–28.
 53. H. Boehm and A. Clauss, *Proc. fifth ...*, 1962, 73–80.
 54. M. C. Franchini, P. Fabbri, A. Frache, G. Ori, M. Messori, C. Siligardi, and A. Ricci, *J. Nanosci. Nanotechnol.*, 2008, **8**, 6316–6324.
 55. A. B. Morgan, *Polym. Adv. Technol.*, 2006, **17**, 206–217.
 56. P. Kiliaris and C. D. Papaspyrides, *Prog. Polym. Sci.*, 2010, **35**, 902–958.
 57. G. Camino, L. Costa, and M. P. Luda di Cortemiglia, *Polym. Degrad. Stab.*, 1991, **33**, 131–154.
 58. H. Ma, P. Song, and Z. Fang, *Sci. China Chem.*, 2011, **54**, 302–313.
 59. B. Schartel and T. R. Hull, *Fire Mater.*, 2007, **31**, 327–354.
 60. R. Francis, *Recycling of polymers: Methods, characterization and applications*, Wiley, 2016.
 61. S. J. Pickering, *Compos. Part A Appl. Sci. Manuf.*, 2006, **37**, 1206–1215.
 62. S. Pimenta and S. T. Pinho, *Waste Manag.*, 2011, **31**, 378–92.
 63. L. Giorgini, T. Benelli, L. Mazzocchetti, C. Leonardi, G. Zattini, G. Minak, E. Dolcini, M. Cavazzoni, I. Montanari, and C. Tosi, *Polym. Compos.*, 2015, **36**, 1084–1095.
 64. G. Oliveux, L. O. Dandy, and G. A. Leeke, *Prog. Mater. Sci.*, 2015, **72**, 61–99.

65. C. Morin, A. Loppinet-Serani, F. Cansell, and C. Aymonier, *J. Supercrit. Fluids*, 2012, **66**, 232–240.
66. I. Okajima, M. Hiramatsu, Y. Shimamura, T. Awaya, and T. Sako, *J. Supercrit. Fluids*, 2014, **91**, 68–76.
67. A. P. Mouritz and A. G. Gibson, *Fire Properties of Polymer Composite Materials*, Springer, 2006.
68. D. Price, G. Anthony, and P. Carty, *Fire Retardant Materials*, Elsevier, Cambridge, 2001.
69. *The Geneva Association - World Fire Statistics Bulletin*, Geneva, 2014, vol. 29.
70. B. Biswas, B. K. Kandola, A. R. Horrocks, and D. Price, *Polym. Degrad. Stab.*, 2007, **92**, 765–776.
71. D. Price, K. J. Bullett, L. K. Cunliffe, T. R. Hull, G. J. Milnes, J. R. Ebdon, B. J. Hunt, and P. Joseph, *Polym. Degrad. Stab.*, 2005, **88**, 74–79.
72. G. E. Zaikov and S. M. Lomakin, *J. Appl. Polym. Sci.*, 2002, **86**, 2449–2462.
73. G. C. Stevens and A. H. Mann, *Risks and benefits in the use of flame retardants in consumer products*, Guildford, University of Surrey, Guildford, 1999.
74. Directive-2006/1907/EC, *Off. J. Eur. Union*, 2006, **396**, 1–849.
75. G. J. van Esch, *Environmental Health Criteria 218 - World health organization (WHO)*, Geneva, 2000.
76. *US Environmental Protection Agency, EPA/600*, Washington: US GPO, 1994, vol. I–III.
77. I. K. Varma and V. B. Gupta, in *Comprehensive Composite Materials*, 2000, pp. 1–56.
78. L. E. Nielsen and R. F. Landel, *Mechanical Properties of Polymers and Composites*, New York, 1994.
79. L. Sisti, J. Belcari, L. Mazzocchetti, G. Totaro, M. Vannini, L. Giorgini, A. Zucchelli, and A. Celli, *Polym. Test.*, 2016, **50**, 283–291.
80. L. Mazzocchetti, T. Benelli, E. D'Angelo, S. Ligi, G. Minak, E. Poodts, F. Tarterini, V. Palermo, and L. Giorgini, *2D Mater.*, 2016, **4**, 15020.
81. L. Giorgini, C. Leonardi, L. Mazzocchetti, G. Zattini, M. Cavazzoni, I. Montanari, C. Tosi, and T. Benelli, *FME Trans.*, 2016, **44**, 405–414.
82. F. Zheng, Q. H. Mi, K. Zhang, and J. Xu, *Polym. Compos.*, 2016, **37**, 21.
83. S. V. Levchik and E. D. Weil, *Polym. Int.*, 2004, **53**, 1901–1929.
84. S. Sinha Ray and M. Okamoto, *Prog. Polym. Sci.*, 2003, **28**, 1539–1641.
85. J. K. Pandey, K. Raghunatha Reddy, A. Pratheep Kumar, and R. P. Singh, *Polym. Degrad. Stab.*, 2005, **88**, 234–250.
86. T. Benelli, E. D'Angelo, L. Mazzocchetti, F. Saraga, L. Sambri, M. C. Franchini, and L. Giorgini, *AIP Conf. Proc.*, 2016, **1736**.

87. A. Blumstein and F. W. Billmeyer, *J. Polym. Sci. Part A-2 Polym. Phys.*, 1966, **4**, 465–474.
88. A. Blumstein, *J. Polym. Sci. Part A Gen. Pap.*, 1965, **3**, 2665–2672.
89. S. Fujiwara and T. Sakamoto, *Japan Kokai Pat. Appl.*, 1976.
90. J. W. Gilman, C. L. Jackson, A. B. Morgan, R. Harris, E. Manias, E. P. Giannelis, M. Wuthenow, D. Hilton, and S. H. Phillips, *Chem. Mater.*, 2000, **12**, 1866–1873.
91. S. Y. Lu and I. Hamerton, *Prog. Polym. Sci.*, 2002, **27**, 1661–1712.
92. B. K. Kandola, a. R. Horrocks, P. Myler, and D. Blair, *J. Appl. Polym. Sci.*, 2003, **88**, 2511–2521.
93. J. Zhang, M. Lewin, E. Pearce, M. Zammarano, and J. W. Gilman, *Polym. Adv. Technol.*, 2008, **19**, 928–936.
94. S. V. Levchik, I. Balabanovich, G. Caminob, and L. Costab, *Polym. Degrad. Stab.*, 1996, **54**, 217–222.
95. H. Horacek and R. Grabner, *Polym. Degrad. Stab.*, 1996, **54**, 205–215.
96. E. D. Weil and V. Choudhary, *J. Fire Sci.*, 1995, **13**, 104–126.
97. T. Kashiwagi, *25th Symp. Combust.*, 1994, **25**, 1423–1437.
98. M. Rakotomalala, S. Wagner, and M. Döring, *Materials (Basel)*, 2010, **3**, 4300–4327.
99. FTT: FIRE TESTING TECHNOLOGY, *Fire Test. Technol. Prod. Cat.*, 2015.
100. C. Huggett, *Fire Mater.*, 1980, **4**, 61–65.
101. W. L. F. Armarego and D. D. Perrin, *Purification of Laboratory Chemicals*, Pergamont Press, Oxford, 1966.
102. B. Aghabarari and N. Dorostkar, *J. Taiwan Inst. Chem. Eng.*, 2014, **45**, 1468–1473.
103. E. Poodts, G. Minak, L. Mazzocchetti, and L. Giorgini, *Compos. Part B Eng.*, 2014, **56**, 673–680.
104. B. K. Kandola and E. Kandare, in *Advances in Fire Retardant Materials*, 2008, pp. 398–442.
105. L. Giorgini, L. Mazzocchetti, T. Benelli, G. Minak, E. Poodts, and E. Dolcini, *Polym. Compos.*, 2013, **34**, 1506–1514.
106. Z. Ying, L. Xianggao, C. Bin, C. Fei, and F. Jing, *Compos. Struct.*, 2015, **132**, 44–49.
107. R. E. Zeebe, *Proc. Natl. Acad. Sci.*, 2013, **110**, 13739–13744.
108. R. Auvergne, S. Caillol, G. David, B. Boutevin, and J. P. Pascault, *Chem. Rev.*, 2014, **114**, 1082–1115.
109. G. R. Palmese and R. L. McCullough, *J. Appl. Polym. Sci.*, 1992, **46**, 1863–1873.
110. F. L. Jin, X. Li, and S. J. Park, *J. Ind. Eng. Chem.*, 2015, **29**, 1–11.

111. Acmite Market Intelligence, *Global Epoxy Resin Market - 3rd June*, 2017.
112. E. C. Dodds and W. Lawson, *Nature*, 1936, **137**, 996–996.
113. J. W. Cook, E. C. Dodds, and C. L. Hewett, *Nature*, 1933, **131**, 56–57.
114. L. N. Vandenberg, R. Hauser, M. Marcus, N. Olea, and W. V. Welshons, *Reprod. Toxicol.*, 2007, **24**, 139–177.
115. C. A. Richter, L. S. Birnbaum, F. Farabollini, R. R. Newbold, B. S. Rubin, C. E. Talsness, J. G. Vandenberg, D. R. Walser-Kuntz, and F. S. vom Saal, *Reprod. Toxicol.*, 2007, **24**, 199–224.
116. NTP, *NTP-CERHR monograph on the potential human reproductive and developmental effects of bisphenol A.*, 2008, vol. 22.
117. Legislature National Conference of State, *NCSL Policy Update: State Restrictions on Bisphenol A (BPA) in Consumer Products*, 2015.
118. S. K. Bobade, N. R. Paluvai, S. Mohanty, and S. K. Nayak, *Polym. - Plast. Technol. Eng.*, 2016, **55**, 1863–1896.
119. S. Kumar, S. K. Samal, S. Mohanty, and S. K. Nayak, *Polym. Plast. Technol. Eng.*, 2016, 03602559.2016.1253742.
120. E. A. Baroncini, S. Kumar Yadav, G. R. Palmese, and J. F. Stanzione, *J. Appl. Polym. Sci.*, 2016, **133**, 1–19.
121. B. M. Bell, J. R. Briggs, R. M. Campbell, S. M. Chambers, P. D. Gaarenstroom, J. G. Hippler, B. D. Hook, K. Kearns, J. M. Kenney, W. J. Kruper, D. James Schreck, C. N. Theriault, and C. P. Wolfe, *Clean - Soil, Air, Water*, 2008, **36**, 657–661.
122. F. Aeschelmann and M. Carus, *Bio-based Building Blocks and Polymers Global Capacities and Trends 2016–2021*, 2017.
123. E. F. Aransiola, T. V. Ojumu, O. O. Oyekola, T. F. Madzimbamuto, and D. I. O. Ikhu-Omoregbe, *Biomass and Bioenergy*, 2014, **61**, 276–297.
124. S. Miao, P. Wang, Z. Su, and S. Zhang, *Acta Biomater.*, 2014, **10**, 1692–1704.
125. M. Stemmelen, F. Pessel, V. Lapinte, S. Caillol, J. P. Habas, and J. J. Robin, *J. Polym. Sci. Part A Polym. Chem.*, 2011, **49**, 2434–2444.
126. T. Saito, R. H. Brown, M. A. Hunt, D. L. Pickel, J. M. Pickel, J. M. Messman, F. S. Baker, M. Keller, and A. K. Naskar, *Green Chem.*, 2012, **14**, 3295.
127. M. C. Monte, E. Fuente, A. Blanco, and C. Negro, *Waste Manag.*, 2009, **29**, 293–308.
128. F. G. Calvo-Flores and J. A. Dobado, *ChemSusChem*, 2010, **3**, 1227–1235.
129. S. Van den Bosch, W. Schutyser, R. Vanholme, T. Driessen, S.-F. Koelewijn, T. Renders, B. De Meester, W. J. J. Huijgen, W. Dehaen, C. M. Courtin, B. Lagrain, W. Boerjan, and B. F. Sels, *Energy Environ. Sci.*, 2015, **8**, 1748–1763.
130. C. Xu, R. A. D. Arancon, J. Labidi, and R. Luque, *Chem. Soc. Rev.*, 2014, **43**, 7485–7500.
131. D. K. Shen, S. Gu, K. H. Luo, S. R. Wang, and M. X. Fang, *Bioresour. Technol.*,

- 2010, **101**, 6136–6146.
132. E. D. Hernandez, A. W. Bassett, J. M. Sadler, J. J. La Scala, and J. F. Stanzione, *ACS Sustain. Chem. Eng.*, 2016, **4**, 4328–4339.
 133. W. De los Santos Ramos, T. Poznyak, I. Chairez, and I. Córdova R., *J. Hazard. Mater.*, 2009, **169**, 428–434.
 134. M. Fache, B. Boutevin, and S. Caillol, *ACS Sustain. Chem. Eng.*, 2016, **4**, 35–46.
 135. J. Hayashi, T. Sekine, S. Deguchi, Q. Lin, and S. Horie, 2002, **59**, 513–519.
 136. M. Fache, R. Auvergne, B. Boutevin, and S. Caillol, *Eur. Polym. J.*, 2015, **67**, 527–538.
 137. J. B. Enns and J. K. Gillham, *J. Appl. Polym. Sci.*, 1983, **28**, 2831–2846.
 138. E. A. Turi, *Thermal characterization of polymeric materials*, Academic Press, New York, 2nd edn., 1997.
 139. D. D. L. Chung, *Mater. Sci. Eng. R Reports*, 2017, **113**, 1–29.
 140. R. J. DIFENDORF, in *Acs Symposium Series*, American Chemical Society, WASHINGTON, D. C., 1976, pp. 315–323.
 141. E. Witten, T. Kraus, and M. Kühnel, *Composites Market Report 2016*, 2016.
 142. E. Zini and M. Scandola, *Polym. Compos.*, 2011, **32**, 1905–1915.
 143. S. Pickering, R. Kelly, and J. Kennerley, *Compos. Sci. ...*, 2000, **60**, 509–523.
 144. G. Jiang, S. J. Pickering, G. S. Walker, K. H. Wong, and C. D. Rudd, *Appl. Surf. Sci.*, 2008, **254**, 2588–2593.
 145. G. Jiang, S. J. Pickering, E. H. Lester, T. A. Turner, K. H. Wong, and N. A. Warrior, *Compos. Sci. Technol.*, 2009, **69**, 192–198.
 146. D. A. Baker and T. G. Rials, *J. Appl. Polym. Sci.*, 2013, **130**, 713–728.
 147. Y. S. Song, J. R. Youn, and T. G. Gutowski, *Compos. Part A Appl. Sci. Manuf.*, 2009, **40**, 1257–1265.
 148. S. Job, *Reinf. Plast.*, 2014, **58**, 32–38.
 149. F. A. López, O. Rodríguez, F. J. Alguacil, I. García-Díaz, T. A. Centeno, J. L. García-Fierro, and C. González, *J. Anal. Appl. Pyrolysis*, 2013, **104**, 675–683.
 150. R. A. Witik, R. Teuscher, V. Michaud, C. Ludwig, and J. A. E. Månson, *Compos. Part A Appl. Sci. Manuf.*, 2013, **49**, 89–99.
 151. L. O. Meyer, K. Schulte, and E. Grove-Nielsen, *J. Compos. Mater.*, 2009, **43**, 1121–1132.
 152. M. Bortolani, G; Giorgini, L; Tosi, C; Bianchi, *Plant for disposing of used tyres*, WO20140574., 2014.
 153. L. Giorgini, T. Benelli, C. Leonardi, L. Mazzocchetti, G. Zattini, M. Cavazzoni, I. Montanari, and C. Tosi, *Environ. Eng. Manag. J.*, 2015, **14**, 1611–1622.
 154. L. Yao, M. Li, Q. Wu, Z. Dai, Y. Gu, Y. Li, and Z. Zhang, *Appl. Surf. Sci.*, 2012,

- 263**, 326–333.
155. Y. Zhou, Y. Wang, Y. Xia, and S. Jeelani, *Mater. Lett.*, 2010, **64**, 246–248.
 156. Y. Yin, J. G. P. Binner, T. E. Cross, and S. J. Marshall, *J. Mater. Sci.*, 1994, **29**, 2250–2254.
 157. S. Pimenta and S. T. Pinho, *Compos. Struct.*, 2012, **94**, 3669–3684.
 158. A. C. Ferrari, *Solid State Commun.*, 2007, **143**, 47–57.
 159. P. Lespade, R. Al-Jishi, and M. S. Dresselhaus, *Carbon N. Y.*, 1982, **20**, 427–431.
 160. J. Meredith, S. Cozien-Cazuc, E. Collings, S. Carter, S. Alsop, J. Lever, S. R. Coles, B. M. Wood, and K. Kirwan, *Compos. Sci. Technol.*, 2012, **72**, 688–695.
 161. M. H. Akonda, C. A. Lawrence, and B. M. Weager, *Compos. Part A Appl. Sci. Manuf.*, 2012, **43**, 79–86.
 162. K. Stoeffler, S. Andjelic, N. Legros, J. Roberge, and S. B. Schougaard, *Compos. Sci. Technol.*, 2013, **84**, 65–71.
 163. L. O. Meyer, K. Schulte, and E. Grove-Nielsen, *J. Compos. Mater.*, 2009, **43**, 1121–1132.
 164. E. Frank, L. M. Steudle, D. Ingildeev, J. M. Spörl, and M. R. Buchmeiser, *Angew. Chem. Int. Ed. Engl.*, 2014, **53**, 5262–98.
 165. Y. Liu and S. Kumar, *Polym. Rev.*, 2012, **52**, 234–258.
 166. X. Huang, *Materials (Basel)*, 2009, **2**, 2369–2403.
 167. A. A. Ogale, M. Zhang, and J. Jin, *J. Appl. Polym. Sci.*, 2016, **133**, 1–13.
 168. Y. Liu, M. Farnsworth, and A. Tiwari, *J. Clean. Prod.*, 2017, **140**, 1775–1781.
 169. J. Yang, J. Liu, W. Liu, J. Wang, and T. Tang, *J. Anal. Appl. Pyrolysis*, 2015, **112**, 253–261.
 170. J. Shi, L. Bao, R. Kobayashi, J. Kato, and K. Kemmochi, *Compos. Sci. Technol.*, 2012, **72**, 1298–1303.
 171. K. L. Goh, *Discontinuous-Fibre Reinforced Composites: Fundamentals of Stress Transfer and Fracture Mechanics*, Springer, London, 2017.
 172. W. Carberry, *Boeing AERO Mag. QRT*, 2008, 6–13.
 173. M. J. John and S. Thomas, *Carbohydr. Polym.*, 2008, **71**, 343–364.
 174. T. Gurunathan, S. Mohanty, and S. K. Nayak, *Compos. Part A Appl. Sci. Manuf.*, 2015, **77**, 1–25.
 175. F. P. La Mantia and M. Morreale, *Compos. Part A Appl. Sci. Manuf.*, 2011, **42**, 579–588.
 176. S. Rwawiire, B. Tomkova, J. Militky, A. Jabbar, and B. M. Kale, *Compos. Part B Eng.*, 2015, **81**, 149–157.
 177. A. K. Mohanty, M. Misra, and L. T. Drzal, *J. Polym. Environ.*, 2002, **10**, 19–26.

178. T. Flemming, G. Kress, and M. Flemming, *Adv. Compos. Mater.*, 1996, **5**, 151–159.
179. P. Feraboli, E. Peitso, F. Deleo, and T. Cleveland, *J. Reinf. Plast. Compos.*, 2009, **28**, 1191–1214.
180. M. L. Longana, N. Ong, H. N. Yu, and K. D. Potter, *Compos. Struct.*, 2016, **153**, 271–277.
181. P. Amuthakkannan, V. Manikandan, J. T. W. Jappes, and M. Uthayakumar, *Mater. Phys. Mech.*, 2013, **16**, 107–117.
182. H. Yu, K. D. Potter, and M. R. Wisnom, *Compos. Part A Appl. Sci. Manuf.*, 2014, **65**, 175–185.
183. C. Capela, S. E. Oliveira, and J. A. M. Ferreira, *Fibers Polym.*, 2017, **18**, 1200–1207.
184. Q. Wu, M. Li, M. M. Zhu, Y. Z. Gu, Y. X. Li, and Z. G. Zhang, *19Th Int. Conf. Compos. Mater.*, 2013.